

AD-A031 494

REGIS COLL RESEARCH CENTER WESTON MASS

F/G 8/14

GEOPOLE OBSERVATORY DATA SUMMARY 1 JULY 1974-31 MARCH 1976.(U)

AUG 76 D.F. KORFF

F19628-73-C-0259

UNCLASSIFIED

SCIENTIFIC-2

AFGL-TR-76-0197

NL

1 OF 1  
ADA031494



END

DATE  
FILMED  
12 - 76

AD A031494

AFGL-TR-76-0197

GEOPOLE OBSERVATORY DATA SUMMARY

01 JULY 1974 - 31 MARCH 1976

D. F. KORFF

Regis College Research Center  
Regis College  
235 Wellesley Street  
Weston, Massachusetts 02193

31 August 1976

Scientific Report - Final

Approved for public release; distribution unlimited

AIR FORCE GEOPHYSICS LABORATORY  
AIR FORCE SYSTEMS COMMAND  
UNITED STATES AIR FORCE  
HANSCOM AIR FORCE BASE, MASSACHUSETTS 01731





Qualified requestors may obtain additional copies from the Defense Documentation Center. All others should apply to the National Technical Information Service.

SECURITY CLASSIFICATION OF THIS PAGE (When Data Entered)

DD FORM 1473 EDITION OF 1 NOV 65 IS OBSOLETE

SECURITY CLASSIFICATION OF THIS PAGE (When Data Entered)

→ next  
page

Unclassified

SECURITY CLASSIFICATION OF THIS PAGE(When Data Entered)

CONT.

Five energetic particle events are examined in greater detail. An analysis of the 5577<sup>8</sup> night airglow in the northern Polar Cap is discussed.

ACCESSION BY	
NTIS	White Section <input checked="" type="checkbox"/>
DTIC	Black Section <input type="checkbox"/>
UNANNOUNCED	<input type="checkbox"/>
JUSTIFICATION	
BY	
DISTRIBUTION/AVAILABILITY CODES	
Dist.	AVAIL. and/or SPECIAL
A	

Unclassified

SECURITY CLASSIFICATION OF THIS PAGE(When Data Entered)



## PREFACE

The author is grateful to Dr. Sam Silverman for discussions regarding Polar Cap atmospheric processes; to Mr. E. G. Mullen for discussions concerning the Geopole Observatory sensors, the digital data recording systems, and the software development for handling the data; and to Dr. Tai Fu Tuan for discussions regarding magnetic substorms. Thanks are extended to the project scientists named in Section 2.1 for answering questions pertaining to their instruments and data gathering procedures. The author is grateful to Dr. Leif Svalgaard for providing a magnetic tape containing inferred sectors and sector boundaries, and for the accompanying "Atlas of Interplanetary Sector Structure 1957-1974". The assistance of the systems programmers and computer operators at the AFGL Computer Center where the data processing was carried out is gratefully acknowledged. Thanks are also extended to Sister Leonarda Burke for her understanding and encouragement, and to the student members of the Regis College Research Center staff who assisted with the data processing.

Special credit is to be given to the observers at the AFCRL Geopole Observatory whose dedicated efforts have made these data possible: Mr. James Blodgett (station leader), Mr. Robert Schroeder, and Mr. Francis Hart.

## TABLE OF CONTENTS

i.	Report Documentation Page	1
ii.	Preface	3
iii.	Table of Contents	4
iv.	List of Figures	6
v.	List of Tables	6
1.	INTRODUCTION	7
2.	GEOPOLE OBSERVATORY INSTRUMENT DESCRIPTION AND BASIC DATA SUMMARY FOR THE PERIOD 1JULY1974- 31MARCH1976.	7
2.1.	Instrument Description	7
2.1.1.	General	7
2.1.2.	VLF/LF	8
2.1.3.	Magnetometer	9
2.1.4.	Riometer	9
2.1.5.	Neutron Monitor	10
2.1.6.	Photometer	10
2.1.7.	Electric Field Mill	11
2.1.8.	Polarimeter	11
2.2.	Data Summary 1July74-31March76.	12
3.	ENERGETIC PARTICLE EVENTS-WINTER SEASONS OF 1973-1974, 1974-1975, and 1975-1976.	12
3.1.	Definition	12
3.2.	18 Events	13
3.2.1.	Basic Summary	13

3.2.2.	Occurrence Relative to Bartel's Rotation and IMF Sector	16
3.2.3.	Occurrence Relative to Godhavn 30MHz Riometer Absorption	17
3.2.4.	Extended Coverage for Five of the Eighteen Events	23
4.	MAGNETIC DISTURBANCE EVENTS	24
4.1.	Definition	24
4.2.	Identification and Occurrence Relative to Interplanetary Magnetic Field Sectors	25
4.3.	Statistical Analysis of the Z-Magnetometer Disturbances-Separation by Sector	26
4.4.	Magnetic Disturbance Examples and Discussion	30
4.5.	Relation to Godhavn 30MHz Riometer and Absorption	31
4.5.1.	Superposed Epoch Analysis	31
4.5.2.	30-second Data Plots	
5.	<sup>O</sup> 5577Å NIGHT AIRGLOW IN THE CENTRAL POLAR CAP	34
vi.	REFERENCES	36
vii.	Figures for Section 2	38
viii.	Figures for Section 3	60
ix.	Figures for Section 4	83



### LIST OF FIGURES

Figures 2.1 - 2.21:	Plots of edited ten-minute averaged Thule data month by month from July 1974 to March 1976.	39
Figures 3.1 - 3.19:	Plots of thirty-second Thule data for the eighteen energetic particle events.	61
Figures 3.20 - 3.21:	Plots of thirty-second Thule data for two quiet days.	80
Figure 3.22:	Godhavn 30 MHz riometer traces	82
Figures 4.1 - 4.8:	Plots of thirty-second Thule data for selected magnetic disturbance events.	84

### LIST OF TABLES

3.1	Energetic Particle Events - Winter Seasons 1973-1974, 1974-1975, and 1975-1976.	14
4.1	Z-Magnetometer Disturbance Indicator W(T) for 1973-1974 and 1974-1975 Winter Quarters.	28

## 1. INTRODUCTION

This report comprises (i) a summary of data recorded on the 40-channel digital recording systems at the AFGL Geopole Observatory, Thule Air Base, Greenland during the period 1 July 1974-31 March 1976; (ii) a study of energetic particle events which occurred during the winter seasons of 1973-1974, 1974-1975, and 1975-1976; and (iii) an analysis of 5577<sup>0</sup>Å night airglow in the northern Polar Cap. Some of the data presented herein has appeared previously in the Geophysics and Space Data Bulletin<sup>1</sup>. and in the reports "AFCRL Scientific Research in Greenland - 1974"<sup>2</sup>. and "AFGL Scientific Research in Greenland - 1975"<sup>3</sup>.

The description of the Geopole Observatory instrumentation and the summary of the data recorded on the 40-channel system is given in Section 2., following the format of Ref. 1. Section 3. contains a discussion of the energetic particle events, Section 4. the magnetic disturbance events, and Section 5. the 5577<sup>0</sup>Å night airglow in the central Polar Cap.

## 2. GEPOLE OBSERVATORY INSTRUMENTATION DESCRIPTION AND BASIC DATA SUMMARY FOR THE PERIOD 1 JULY 1974 - 31 MARCH 1976.

### 2.1. Instrument Description

#### 2.1.1. General

The geographic coordinates of the AFGL Geopole Observatory at Thule Air Base, Greenland are 76°36'N latitude, and 68°48'W longitude; geomagnetic coordinates are 88°11'N lati-

tude, and 1°8' E longitude; and the elevation is 260 meters.

Instrumentation operated at the observatory has included 5 VLF phase tracking receivers, 3 LF receivers, a 3-component fluxgate magnetometer, 4 riometers, a cosmic ray neutron monitor, 3 two channel photometers, an electric field mill, and a polarimeter. 30-second samples of the data from these sensors were routinely recorded on magnetic tape by two 40-channel digital recording systems, the first of which became fully operational on 9 April 1973, the second on 1 August 1974.

#### 2.1.2. VLF/LF

The VLF/LF program was directed by Mr. John P. Turtle, Project Scientist, formerly of the Space Physics Division of AFGL. Five VLF phase tracking receivers were used to record the phase and the amplitude of the signal from transmitters in Yosami, Japan (NDT, 18.4kHz); Norway (NOVIK, 16.4kHz); Jim Creek, Washington (NLK, 18.6kHz); Rugby, England (GBR, 16.0kHz); and Cutler, Maine (NAA, 17.8kHz). The phase measurements were referred to a rubidium frequency standard at the observatory. Three LF receivers were used to record the amplitude of the signal from transmitters in Fort Collins, Colorado (WWBV, 60.0kHz); Silver Creek, Nebraska (34.5kHz); and Hawes, California (37.2kHz).

Ten-minute averages of VLF phase and VLF/LF amplitude data were plotted versus universal time (UT). Phase data were plotted in micro seconds and amplitude data were plotted in relative decibels (dB).



#### 2.1.3. Magnetometer

The magnetometer data were taken by a Schonstedt HMS-1 three component fluxgate magnetometer provided by the 12th Weather Squadron/AL, Ent Air Force Base, Colorado Springs, Colorado. The three components recorded were the orthogonal X, Y, and Z components. The X-component sensor was oriented approximately  $70^{\circ}15'$  W of geographic North, the approximate direction of the magnetic pole. The Z-component is the vertical component.

Ten-minute averages of the horizontal (H) and vertical (Z) components of the magnetic field were plotted as a relative deflection in gammas versus UT.

#### 2.1.4. Riometer

The riometer program was directed by Mr. John W. F. Lloyd of the Space Physics Division of AFGL. Riometer data were taken by 4 riometer, one each at the frequencies 26.3MHz, 30.0MHz, 40.0MHz, and 50.0MHz.

Because of the inherent noise characteristics of the riometer system, only one data point per 10-minute interval was routinely reduced, that point being the minimum value in the interval. Ten-minute values of 10 times the logarithm to the base 10 of the riometer output current in milliamperes ( $10 \log_{10} I$ ) were plotted versus UT. The difference of the value of  $10 \log_{10} I$  from a quiet-day curve in sidereal time is a direct measure of the cosmic noise absorption in dB.

#### 2.1.5. Neutron Monitor

The cosmic ray neutron monitor at the AFGL Geopole Observatory was sponsored by the Bartol Research Foundation of the Franklin Institute (see Section 2.3 of Ref. 1. for more information on this sensor).

Ten minute averages of the pressure corrected data of the nucleonic intensity were plotted as percent variations versus UT.

#### 2.1.6. Photometer

The two-channel photometer programs were directed by Mr. John W. F. Lloyd and Mr. James Moore, both of the Space Physics Division of AFGL.

The three two-channel interference-filter photometers, with each of the two channels collimated to include the same  $5^\circ$  field of view, were used for making observations of the  $3914\overset{\circ}{\text{\AA}}$  (0,0) band of the  $\text{N}_2^+$  First Negative transition and the atomic oxygen lines  $5577\overset{\circ}{\text{\AA}}$   $(\text{OI})_{3,2}$  and  $6300\overset{\circ}{\text{\AA}}$   $(\text{OI})_{2,1}$  in the zenith night sky. The interference filters of 4 inch diameter were centered at  $\lambda 3914\overset{\circ}{\text{\AA}}$ ,  $\lambda 3960\overset{\circ}{\text{\AA}}$ ,  $\lambda 5525\overset{\circ}{\text{\AA}}$ ,  $\lambda 5577\overset{\circ}{\text{\AA}}$ ,  $\lambda 6230\overset{\circ}{\text{\AA}}$ , and  $\lambda 6300\overset{\circ}{\text{\AA}}$  and had half bandwidths of  $30\overset{\circ}{\text{\AA}}$ ,  $30\overset{\circ}{\text{\AA}}$ ,  $23\overset{\circ}{\text{\AA}}$ ,  $11\overset{\circ}{\text{\AA}}$ ,  $11\overset{\circ}{\text{\AA}}$ , and  $11\overset{\circ}{\text{\AA}}$ , respectively.

Ten-minute averages of the intensities of the lines  $5577\overset{\circ}{\text{\AA}}$ ,  $6300\overset{\circ}{\text{\AA}}$ , and  $3914\overset{\circ}{\text{\AA}}$  in Rayleighs and of the continuum  $5525\overset{\circ}{\text{\AA}}$ ,  $6230\overset{\circ}{\text{\AA}}$ , and  $3960\overset{\circ}{\text{\AA}}$  in Rayleighs/Angstrom were plotted versus UT. Data dropouts are due to the sun being above a  $9^\circ$  solar depression angle, instrumental calibrations, or

malfunctions.

#### 2.1.7. Electric-Field Mill

An electric-field mill was routinely operated at the AFGL Geopole Observatory under the direction of Mr. Donald Olsen of the University of Minnesota at Duluth. The field mill measured changes in the near-earth atmospheric electric field, which at Thule correlated well with world-wide thunderstorm activity as well as auroral effects. However, care must be taken in interpreting the data as the instrument is very wind sensitive and no corrections for wind have been made.

Ten-minute averages of the field in volts/meter were plotted versus UT.

#### 2.1.8. Polarimeter

The polarimeter program was directed by Mr. J. Klobuchar of the Space Physics Division of AFGL. A two-channel polarimeter with its channels set  $180^\circ$  out of phase measured the Faraday Rotation of linearly polarized radio signals transmitted from a satellite. The amount of rotation (Faraday Rotation) of the resultant plane of polarization of the planes of polarization of the ordinary and extra-ordinary modes of the signal is proportional to the total electron content (integrated electron number density) along the path from the satellite to the receiver.

The 30-second data from one of the polarimeter channels were reduced to obtain the total electron content (TEC). The second polarimeter channel was used to reduce the data for



those time intervals for which the determination of the Faraday Rotation by the first polarimeter channel was ambiguous due to noise or scale shifts. Ten-minute averages of the TEC in electrons/(square meter) were plotted versus UT.

## 2.2 Data Summary 1 July 74 - 31 March 76

Ten-minute average plots of the reduced data for the operating sensors were routinely generated each time a digital system tape was received at AFGL from the Geopole Observatory. Based on these plots and accompanying printouts of the data, plots of edited VLF (GBR, NLK, and/or NAA) phase and amplitude, H (or X and Y) and Z-magnetometer, 26.3MHz and 30.0MHz riometer, and 5577<sup>0</sup>Å photometer data were normally made. Time prohibited the editing of all of the data for all of the sensors. The data presented in Figures 2.1 - 2.21 is sufficient to give a general picture of the polar atmosphere at Thule, Greenland for the time period 1 July 74 - 31 March 76.

Requests for data for sensors not shown in Figures 2.1 - 2.21 as well as for 30-second resolution data should be made to Mr. E. G. Mullen, AFGL (PHD), Hanscom Air Force Base, MA 01731.

## 3. ENERGETIC PARTICLE EVENTS - WINTER SEASONS OF 1973-1974, 1974-1975, AND 1975-1976.

### 3.1 Definition

The term energetic particle event as used herein refers to a period of time of usually less than one hour duration

during which one or more of the riometers shows some absorption. During these times the other sensors usually also record disturbances: one or more of the VLF receivers may show significant absorption, the X(H), Y, and Z-magnetometer data may undergo fluctuations exceeding 250 gammas, and the  $5577\text{\AA}^{\circ}$  line intensity may exceed 1000 Rayleighs. These events may be preceded or followed by periods of one to two hour duration during which the VLF, magnetometer, and/or  $5577\text{\AA}^{\circ}$  data may be significantly disturbed. Those events which are accompanied by significant magnetic field fluctuations may also be referred to as Polar Cap magnetic substorms.

### 3.2 18 Events

#### 3.2.1. Basic Summary

The 18 (eighteen) energetic particle events which occurred at Thule, Greenland during the winter seasons (October through February) of 1973-1974, 1974-1975, and 1975-1976 are shown in Figure 3.1-3.19. Figure 3.13 is an expanded version of Figure 3.1, the exceptionally strong event of 7 January 1975. Each figure consists of plots of unedited VLF, magnetometer, riometer, and  $5577\text{\AA}^{\circ}$  photometer data. As a reference, Figures 3.20 and 3.21 show the behavior of the data under very quiet conditions early in the winter season and in the middle of the winter season.

Table 3.1 contains a summary for each event of the time of occurrence, the approximate strength (based on 26.3MHz riometer absorption), and the position in a Bartel's rotation

TABLE 3.1

Energetic Particle Events - Winter Seasons 1973-1974, 1974-1975, and 1975-1976

Date	Times (UT)	26.3 MHz Rio. Abs. (dB)	Bartel's Rotation	Day in Rotation	Sector*	Distance* into Sector (°)
30 Oct 73	0100-0140	1.25	1918	6	+	28
22 Dec 73	0100-0140	2.00	1920	5	+	50
12 Feb 74	0600	0.25	1922	3	+	50
01 Jan 74	0200-0220	1.00	1920	15	-	33
26 Jan 74	0035	0.25	1921	13	-	13
27 Jan 74	0300-0330	1.75	1921	14	-	20
12 Nov 74	0205-0230	0.25	1932	6	+	40
13 Nov 74	0005-0025	0.25	1932	7	+	50
14 Nov 74	0535-0610	1.25	1932	8	+	60
07 Jan 75	0040-0120	5.25	1934	8	+	50
01 Feb 75	2350-0005	1.50	1935	6	+	28
18 Jan 75	0130-0145	0.75	1934	19	-	60
04 Nov 75	0225-0300	1.50	1946	15	+	
03 Dec 75	0110-0140	0.50	1947	17	+	
22 Dec 75	0810	0.25	1948	9	-	



TABLE 3.1 (CONTINUED)

<u>Date</u>	<u>Times (UT)</u>	<u>26.3MHz Rio. Abs. (dB)</u>	<u>Bartel's Rotation</u>	<u>Day in Rotation</u>	<u>Sector*</u>	<u>Distance* into Sector (%)</u>
28 Dec 75	0310	0.25	1948	15		
28 Dec 75	2010-2040	0.50	1948	15		
23 Jan 76	0215-0245	0.75	1949	14	+	

---

\* + = away, - = toward; sector assignments and distances are based on data in Refs. 4 & 5.

and in an interplanetary magnetic field (IMF) sector.<sup>4,5</sup> All but 4 of the events occurred between 2350 and 0330 UT. The events of 12 February 1974 and 14 November 1974 which occurred near 0600 UT appear to be of the same type as those which occurred between 2350 and 0330 UT based on the disturbances of the riometer, VLF, magnetometer, and 5577Å data. The only difference appears to be the displacement in time. However, for the other two events 22 December 1975 (0810 UT) and 28 December 1975 (2010 UT) not only is there an even greater displacement in time of occurrence but there is also little or no disturbance of the VLF and magnetometer data, only the riometer absorption and 5577Å enhancements appear to be similar to the other events. This suggests that these latter two events may be of a different origin than the others which are related to substorm expansion from the Auroral Oval (see Sections 3.2.3. and 3.3. below).

### 3.2.2. Occurrence Relative to Bartel's Rotation and IMF Sector

With reference to Table 3.1., the events within a given IMF sector occur at approximately 27-day intervals, or multiples of the 27-day interval, the solar rotation period. This periodicity is most clearly illustrated by the events of 4 November 1975, 3 December 1975, 28 December 1975, and 23 January 1976 which, except for 3 December 1975, occur at exactly the same position in four successive Bartel's rotations. 3 December 1975 is two days out of position. The 27-day periodicity suggests, if only indirectly, the solar origins and/or control

of these events, with the possible exception of the 22 and 28 December 1975 events mentioned previously.

In addition to the 27-day periodicity within a given sector, Column 7 of Table 3.1. also shows that the events are observed to occur in the early to middle part of a sector, with no events occurring late in the sector. The early part of a sector is the magnetically active part, as indicated by superposed epoch analyses of  $\Sigma K_p$ ,<sup>6</sup>  $K_p$  being the planetary magnetic index. These analyses show that  $\Sigma K_p$  has a maximum early in the sector and a minimum near the end of a sector. For all of the events  $\Sigma K_p$ ,  $A_p$ , and  $C_p$  all show local (in time) maxima on or near the event day.<sup>7</sup> Since these indices are sub-auroral zone in origin, they are not necessarily indicative of the state of the earth's magnetic field of Thule. However, inspection of the ten-minute average plots (Figures 2.1-2.21) shows that at Thule the magnetic activity is at or near a local maximum on the event days.

### 3.2.3. Occurrence Relative to Godhavn 30MHz Riometer Absorption

The occurrence of the energetic particle events at Thule during days of significant global magnetic activity has been pointed out in Section 3.2.2.. To get an idea of how widespread the particle precipitation in the Polar Cap might be, the 30MHz riometer measurements<sup>8</sup> at Godhavn, Greenland (69.3 N, 306.5 E geographic; 80.1 N, 50.2 E magnetic) were examined. Table 3.2. shows the approximate onset times of 30 MHz absorption (if present) at Godhavn and 26.3 MHz absorption at Thule



TABLE 3.2.

30 MHz Riometer Absorption at Godhavn for the  
18 Energetic Particle Events Observed at Thule

Date	Thule	Godhavn	
	26.3 MHz Onset (UT)	30 MHz Onset (UT)	Abs. (milliamps)
30 Oct 73	0100	0030	2.6
22 Dec 73	0100	0050	2.4
01 Jan 74	0200	0130	2.8
26 Jan 74	0035	0015	1.5
27 Jan 74	0300	0205	3.5
12 Feb 74	0600	data not available	
12 Nov 74	0205	0130	2.1
13 Nov 74	0005	2340	1.9
14 Nov 74	0535	0530	1.6
07 Jan 75	0040	data not available	
18 Jan 75	0130	0055	0.6
01 Feb 75	2350	2335	3.3
04 Nov 75	0225	0150*	2.3
03 Dec 75	0110	0050*	1.8
22 Dec 75	0810	--	0.0
28 Dec 75	0310	0235*	0.5
28 Dec 75	2010	--	0.0
23 Jan 76	0215	0150*	2.4

\* See Figure 3.22

for the 18 energetic particle events. The strength of absorption at Godhavn is given in milliamperes in Column 4. For the times of the events shown in Table 3.2., the unabsorbed current level is about 5 milliamps. Therefore, a 2.5 milliamp absorption corresponds to about  $10 \log_{10} \frac{5.0}{2.5} = 3$  dB absorption. The absorption at Godhavn precede those at Thule by times of from 10 minutes to an hour. These time differences are consistent with what would be expected from a poleward expanding substorm which reaches both Godhavn and Thule. Also note that the two events (22 and 28 December 1975) which do not show the same characteristics as the others are also not preceded by 30 MHz absorption at Godhavn.

In order to get a better idea of the relation between disturbances at Thule and 30 MHz absorption at Godhavn, consider Figures 3.14, 3.15, 3.17, 3.19, and 3.22. Figure 3.22 contains Godhavn 30 MHz chart reproductions corresponding to the same times as the data in Figures 3.14, 3.15, 3.17, and 3.19, as well as data for a few other days.

First compare the 3-4 November 1975 Thule data with Figure 3.22 (third chart from the top). Since the riometer charts are arranged so that time increases to the right, absorptions appear as positive deflections rather than negative. The 3-4 November 1975 Godhavn 30 MHz record shows two distinct absorptions, a weak one with a gradual onset commencing at about 2340 UT on 3 November and a strong one with a sharp onset commencing at 0150 UT on 4 November. The only Thule

sensor (Figure 3.14) showing any disturbance near the time of the weak absorptions is the VLF sensor NAA whose amplitude shows a very sharp absorption at about 2330 UT. All three magnetic field components seem to be very quiet during this hour. The 5577<sup>0</sup>Å airglow shows an enhancement beginning at about 2300 UT.

The response of the Thule sensors near the time of the second strong, sharp-onset event at Godhavn is much different. At the 0150 onset time at Godhavn, the NAA VLF sensor is undergoing appreciable absorption, the X-component of the earth's magnetic field is beginning a positive bay, the Y-component is beginning a negative bay, and the Z-component is in the midst of a positive bay. By 0230 UT the main event is over at Godhavn, but the main event at Thule is just getting underway as indicated by the intense disturbances on the VLF, magnetic field, and 5577<sup>0</sup>Å sensors. This sequence of events is consistent with the picture of a poleward expanding substorm which reaches Godhavn at 0150 UT producing an N-type<sup>9</sup> riometer absorption and then 20-30 minutes later reaches the vicinity of Thule.

Now consider the 2-3 December 1975 event at Thule (Figure 3.15) and the corresponding Godhavn riometer record shown in Figure 3.22 (fourth chart from top). The Godhavn 30 MHz riometer shows two sharp-onset absorptions, the stronger one commencing at 2200 UT on 2 December, the weaker one commencing at 0050 UT on 3 December. Corresponding to the first event, the GBR phase and NAA amplitude VLF sensors show absorptions



commencing just prior to 2200 UT. The X-magnetic field shows a weak positive bay centered at about 2200 UT, the Y-component is in the midst of a very broad positive bay extending from 2000~0030 UT, and the Z-component as well as the 5577A<sup>0</sup> intensity show sharp onsets commencing at 2200 UT. Corresponding to the second event at Godhavn, the GBR phase and NAA amplitude VLF sensors show absorptions commencing at about 0050 UT, an X-component positive bay began earlier at about 0020 UT, and the Y and Z-components positive bays began gradually at about 0030 UT. The 5577A<sup>0</sup> intensity has a sharp onset at 0100 UT. As with the 3-4 November 1975 event, by the time the second Godhavn event is over at 0130 UT, the main magnetic and riometer events are underway at Thule. The earlier event is apparently a lower-latitude substorm which does not expand into the Polar Cap any further than the vicinity of Godhavn.

The comparison of the next event 27-28 December 1975 (Figure 3.17) with the Godhavn 30 MHz absorptions (Figure 3.22, second chart from the bottom) is interesting because of the highly structured nature of the absorptions. The event at Godhavn commences at 0030 UT with a sharp absorption, followed by successive sharp absorptions. The Thule VLF absorptions, Y and Z magnetic field positive bays, and 5577A<sup>0</sup> intensity enhancement all have onsets at about 0030 UT. The X-magnetic field positive bay onset begins earlier near 0015 UT. In particular, the Z-magnetic field component and 5577A<sup>0</sup> intensity show structure which coincides quite closely with the

Godhavn 30 MHz absorption structures. This event does not show riometer absorption at Thule, instead it appears that the weak riometer absorption at Thule at about 0310 UT is preceded at Godhavn by the weak absorption commencing at 0230 UT. The Thule sensors, in particular, the Z magnetic field component and the  $5577\overset{\circ}{\text{Å}}$  line show enhancements commencing at about this same time. The X and Y component disturbances are not as pronounced in this case.

At 0530 UT there is a weak absorption at Godhavn. This occurs approximately coincident in time with NAA absorption, X-component negative onset, Y and Z-component positive bay onsets, and  $5577\overset{\circ}{\text{Å}}$  line onset. The  $5577\overset{\circ}{\text{Å}}$  line shows extensive auroral activity commencing with this weak event and continuing until the event of 2020 UT on 28 December 1975 (Figure 3.18). As discussed earlier this latter event does not exhibit the same characteristics as the majority of the energetic particle events. It may be that the auroral activity commencing with the 0530 UT event on 28 December was principally a Polar Cap disturbance and did not grow out of a lower-latitude substorm expanding into the Polar Cap. Further research will be necessary in order to clarify this situation.

The fourth event in the 1975-1976 27-day sequence is the event of 22-23 January 1976 (Figure 3.19). The Godhavn 30MHz riometer (Figure 3.22, bottom chart) shows a weak absorption with onset at 2020 UT on 22 January. The GBR phase, Z magnetic field component, and the  $5577\overset{\circ}{\text{Å}}$  line all show disturbances at

about the same time. The Y-component is in the midst of a broad positive bay which commenced at 1930 UT. At this same time the Z-component shows the onset of a weak negative bay which at the time of the Godhavn absorption at 2020 UT then becomes a positive bay onset. The fact that the GBR VLF receiver shows absorption but the NAA does not suggests that the principle substorm disturbance is probably well to the east of the west coast of Greenland. This is also consistent with where the magnetic substorm would be, namely in the magnetic midnight sector. In addition the X-component does not show a disturbance comparable to the Y-component. This also is consistent with the substorm disturbance being to the east since the substorm enhanced auroral electrojet will lead to across-the-cap equivalent return currents which would be close to being parallel to the X-component direction; hence no X-disturbance, but a significant Y-disturbance at Thule.

At 0150 UT on 23 January the Godhavn 30 MHz riometer shows another sharp onset and strong absorption. The principal absorption event is over at about 0230, which is the time of the main absorption event at Thule. All of the Thule sensors show significant disturbances during the 0200-0300 UT hours.

#### 3.2.4. Extended Coverage for Five of the Eighteen Events

For the five energetic particle events 20 October 1973 (Figure 3.1), 22 December 1973 (Figure 3.2), 1 January 1974 (Figure 3.3), 12 November 1974 (Figure 3.7), and 13 November



1974 (Figure 3.8) the author has been cooperating with three other researchers in an effort to get extended coverage of magnetospheric and auroral oval conditions in order to better understand the nature of these energetic particle events. The other cooperating researchers are Dr. Sam Silverman, formerly of AFGL, Dr. Tai Fu Tuan of the University of Cincinnati, and Mr. E. G. Mullen of AFGL. Dr. Silverman has previously collected magnetometer and riometer data for some of these events, in particular, riometer data from the Danish Greenland network. Dr. Tuan has collected magnetometer network data from the World Data Center and is providing the theoretical expertise in the area of substorm formation and interaction between the earth's near and far magnetosphere. Mr. Mullen has examined DMSP satellite data which are available for these events. While the final results of this research are not available at this writing, the principal preliminary result based on examining the Geopole data, the magnetometer and riometer network data, and the satellite data is that these five energetic particle events result from the poleward expansion of substorms from the auroral oval.

#### 4. MAGNETIC DISTURBANCE EVENT.

##### 4.1. Definition

The magnetic disturbance events of interest here are those Z-magnetometer positive bays of magnitude approximately 100 gammas or more occurring in the midnight sector, 1800 UT-0600 UT. These disturbances occur principally during the first

half of an interplanetary magnetic field sector and are the largest Z-magnetometer disturbances occurring during the winter season. These disturbances occur separate from as well as preceding, coinciding with, and/or following energetic particle events. They are accompanied by one or more of the following X(H)-component magnetic field positive and/or weak negative bays, Y-component positive bays, VLF absorptions, and 5577Å<sup>0</sup> enhancements. In many cases the Z-positive bay onset coincides with the onset of 30 MHz riometer absorption at Godhavn, this is especially true if the riometer onset is of the sharp N-type. Since these events exhibit all of the characteristics of the energetic particle event with the exception of riometer absorption at Thule these events are most likely responses to expanding substorms which in many cases reach as far as Godhavn, but whose precipitating particles do not reach Thule.

#### 4.2. Identification and Occurrence Relative to Interplanetary Magnetic Field Sectors

The principal Z-magnetometer winter season disturbances are relatively easy to identify on the ten-minute average plots where they show up as sharp spikes at the end of one day or at the beginning of another day. As an illustration of the identification of these spikes as well as of the influence of the interplanetary magnetic field sectors, consider the Z-magnetometer data in Figure 2.7, the data for the month of January 1975. 3 January is a (-,+) sector boundary day. The magnetic activity of 1 and 2 January, the last two days of a

toward sector, is visibly much less than that of the early days of the away sector which immediately follow 3 January. At the end of 4, 5, and 6 January there are sharp Z-magnetic field spikes. At the beginning of 7 January there is one large spike, the strong energetic particle event. 8 January contains a rather unusual mid-day spike. 9-12 January, the end of the away sector, is magnetically quiet. 13 January is the beginning of a toward sector and the magnetic activity picks up again. With the exception of the two spikes at the beginning of 19 and 20 January, the magnetic activity settles down again during the end of the sector, 19-22 January. The beginning of days 13-15 and 18-20 January show Z-magnetic field spikes. 16 and 17 January show significant enhancements with the end of 17 January showing a spike which precedes the 18 January morning spike (energetic particle event).

#### 4.3. Statistical Analysis of the Z-magnetometer Disturbances - Separation by Sector

The time of day of the occurrence of the principal Z-magnetometer disturbance may be analyzed by the following method. Let  $Z(T,D)$  denote the ten-minute average of the Z-magnetometer data for the ten-minute interval  $T(1 \leq T \leq 144)$  and the day  $D$ . By fixing  $T$  and averaging over  $D$  for some specified number of days, the mean level for ten-minute interval  $T$  and the variance  $V(T)$  with respect to this mean can be easily computed.



Define  $W(T)$  as follows:

$$W(T) = (V(T) - \bar{V}) / \sigma(V)$$

where

$$\bar{V} = \frac{1}{144} \sum_{T=1}^{144} V(T)$$

and

$$\sigma^2(V) = \frac{1}{144} \sum_{T=1}^{144} (V(T) - \bar{V})^2.$$

$W(T)$  measures the fluctuations of  $V(T)$  about the mean,  $\bar{V}$ , in units of the root mean square of  $V$  about  $\bar{V}$ ,  $\sigma(V)$ . Time intervals during which  $W(T)$  is large are the times of day during which the Z-magnetometer is most disturbed relative to the mean disturbance level,  $\bar{V}$ , for the number of days taken in the sample. It should be noted that  $W(T)$  contains diurnal variation influences. For the winter season these diurnal effects may be neglected relative to the disturbance effects of interest here. For the other seasons of the year the diurnal effect on  $V(T)$  should be removed before  $W(T)$  is computed.

Table 4.1 summarizes the largest values of  $W(T)$  for the winter quarters (November, December, and January) of 1973-1974 and 1974-1975. A B C denotes taking all days D of available data during the quarter, A denotes taking away sector days, and C denotes taking toward sector days<sup>10</sup>. For each day-type the table gives the time TMAX of the local maximum in  $W(T)$ ,  $W(TMAX)$ , and the duration DUR of the disturbance in minutes. The duration is defined as the time period about the local maximum starting with the time preceding the maximum when  $W(T)$  becomes greater than 1 and ending with the time following the maximum when  $W(T)$  becomes less than 1.

Table 4.1. Z-magnetometer Disturbance Indicator W(T)  
for the 1973-1974 and 1974-1975 Winter Quarters\*

Winter Quarter	ABC			A		C		
	TMAX	W(TMAX)	DUR	TMAX	W(TMAX)	DUR	TMAX	W(TMAX)
73-74	0035	3.1	30	0445	2.2	70	0035	3.2
	0305	5.8	90	0815	4.3	110	0305	5.6
	$\bar{V} = 789(\text{gamma})^2$			$\bar{V} = 224(\text{gamma})^2$		$\bar{V} = 1238(\text{gamma})^2$		
74-75	2235	3.4	20	2235	8.9	30		
	0105	6.3	90				0105	7.0
	$\bar{V} = 858(\text{gamma})^2$			$\bar{V} = 781(\text{gamma})^2$		$\bar{V} = 936(\text{gamma})^2$		

\* ABC denotes all days of available data in the quarter, A denotes away sector days, C denotes toward sector days; see Ref. 6. TMAX, W(T), DUR, and  $\bar{V}$  are respectively, the universal time of the local maximum of W(T), the Z-magnetometer disturbance indicator, the disturbance duration in minutes, and the daily average of the Z-magnetometer variances V(T); see text for additional details.

When all the days (ABC) are used, both quarters show two principal disturbance maxima in the midnight sector. The separation into A- and C-type days shows that for the 1973-74 quarter the maxima are associated with the C-days and for the 1974-75 quarter the first maximum is associated with A-days, the second with C-days. For both quarters the first maximum is of short duration ( $\approx 30$  minutes) and the second is of longer duration ( $\approx 90$  minutes) and is probably the resultant of two or more shorter disturbances.

The appearance of the A-day 1973-74 principal maxima at later times than the other cases is explainable on the basis of sample bias. In the case of the 1973-74 quarter there are only 38 days of available data and these days are biased toward the end of away sectors and the beginning of toward sectors. The A-day average variance of 224 (gamma) compared with the C-day average variance of 1238 (gamma) reflects the lower magnetic activity of the end of a sector versus the higher activity of the earlier part of a sector. Thus the 1973-1974 A-day quarter maxima in W(T) are indicative of the disturbances during the magnetically less active part of the sector. This suggests that another analysis with the separation of sector into active and quiet parts would probably be informative. The 1974-1975 quarter had only three missing days.



#### 4.4. Magnetic Disturbance Examples and Discussion

In addition to the magnetic disturbances accompanying the energetic particle events shown in Figures 3.1 - 3.19, a sample of eight disturbances taken from the 1973-1974, 1974-1975, and 1975-1976 winter seasons is shown in Figures 4.1 - 4.8. During the time interval shown there are one or more significant positive bay Z-magnetometer disturbances of one to two hour duration. Superposition of the VLF and 5577 $\text{\AA}$  graphs over the Z-magnetometer graphs reveals the following:

1. The principal Z-magnetometer positive bays occur coincident with GBR (England-Thule path) and NAA (Maine-Thule path) VLF absorptions. The NLK (Washington-Thule path) VLF absorptions occurring coincident with Z-magnetometer positive bays are identifiable at times but occur less often and are not as pronounced as those for GBR and NAA. The onset of the VLF absorptions coincides to within about five minutes with the weak negative bay or minimum in the Z-magnetometer data which immediately precedes the positive bay. In many cases the VLF absorptions occurring coincident with the Z-magnetometer positive bays are not only limited to the stronger disturbances, but also occur for very weak absorptions and slight positive bay enhancements.
2. Many of the Z-magnetometer positive bays are coincident with 5577 $\text{\AA}$  intensity enhancements, see especially Figure 4.4

at 0020 UT and Figure 4.5 at 0340 UT. Many 5577A<sup>0</sup> enhancements however do not accompany Z-magnetometer positive bays; this is particularly true for times after 0600 UT. The coincident positive bay - 5577A<sup>0</sup> enhancements also show coincident features of finer structure, see again Figure 4.4 at 0000 UT - 0040 UT and Figure 4.6 at 0520 UT and Figure 4.7 at 0220 UT.

In connection with the discussion in Section 4.2, the VLF absorptions coincident with the Z-magnetometer positive bays appear as sharp cuts (inverted spikes) in the VLF ten-minute average plots and are also easy to identify, see again Figure 2.7. Turtle<sup>11</sup> has previously pointed out that there is an increase in these absorptions when the magnetometers show increased activity. From previous discussion (Section 4.2) it is clear that both of these disturbances are associated with sector boundary passages.

#### 4.5. Relation to Godhavn 30 MHZ Riometer Absorption

4.5.1 Superposed epoch analyses of the GBR phase, NAA amplitude and phase, X, Y, and Z magnetic field data, and 5577A<sup>0</sup> data were carried out using the Godhavn 30 MHZ absorption onset as the key time. The data base used consisted of the ten-minute averaged Thule data covering the period 1 October 1973 - 23 January 1975. There were 48 key times and only those times were used for which the Godhavn 30 MHZ absorption exceeded 0.5 milliamps.

The epoch analysis of the Z-magnetic field component

reveals that on the average the Z-positive bay onset is sharp and precedes the Godhavn 30 MHz onset by 10-20 minutes. The X-component positive bay onset is found to be gradual and precedes the Godhavn 30 MHz onset by as much as an hour. The Y-component behavior is like that of the X-component when the key times in the epoch analyses are restricted to the pre-UT midnight times. For the post-UT midnight times the Y-component behavior is similar to the Z-component, except that the onset time is more nearly coincident with the Godhavn 30 MHz onset. The X and Z-components did not show any significant difference when the key times in the epoch analyses were separated into pre and post-UT midnight groups.

The epoch analyses for the GBR and NAA VLF phase both show sharp onsets 10 minutes before the Godhavn 30 MHz onset and maximum absorption about 30 minutes after the Godhavn 30 MHz onset. When a harmonic analysis is used to remove the diurnal component from the GBR and NAA phase data the GBR phase shows the presence of absorptions 2 to 3 hours before the Godhavn 30 MHz onset while the NAA phase data shows the presence of absorptions 2 to 3 hours after the Godhavn 30 MHz onset. These two phase responses are undoubtedly due to earlier (GBR path east of Greenland) and later (NAA path west of Greenland) substorms which disturb the ionosphere and produce the GBR and NAA absorptions. The NAA amplitude epoch analysis shows an absorption onset about 20 minutes before the 30 MHz onset. As with the NAA phase, maximum absorption occurs about 30



minutes after the Godhavn 30 MHz onset. The NAA amplitude also shows the presence of absorptions 2 to 3 hours after the 30 MHz onset.

The 5577A<sup>0</sup> line epoch analysis shows a sharp onset at the time of the onset at Godhavn. The fact that the Thule sensors have onsets preceding or coinciding with the Godhavn 30 MHz onset indicates that the Thule ground-based sensors are responding to the ionospheric and magnetospheric disturbances before the principal particle precipitation has reached Godhavn.

4.5.2. For the months of October, November, and December plots of 30 second Thule data, a day at a time have been made. The onset time of the Godhavn 30 MHz absorption has been noted on these plots. Figure 3.22 (second chart from top) shows the Godhavn 30 MHz absorption corresponding to the magnetic disturbance of 8-9 October 1975 shown in Figure 4.8. The X, Y, and Z positive bays, VLF absorptions, and 5577A<sup>0</sup> line enhancements occurring in conjunction with the two 30 MHz absorption events at Godhavn stand out quite distinctly in this case.

In connection with this work a log of Godhavn 30 MHz absorptions has been made for the following months: October, November, December 1973; January, November, and December 1974; 16-31 January, February, March, October, November, December 1975; and January 1976. The log includes onset time, maximum absorption in milliamps, and a sketch of the absorption profile.

This log is in note form and has been delivered along with the 40 channel plot data.

5. <sup>0</sup>  
5577A NIGHT AIRGLOW IN THE CENTRAL POLAR CAP

In addition to the <sup>0</sup>5577A line emission results which have been presented as part of the energetic particle and magnetic disturbance events, the <sup>0</sup>5577A night airglow in the Central Polar Cap has also been studied in collaboration with two other researchers. This work is summarized in the paper "557.7 nm [OI] Night Airglow in the Central Polar Cap", by E.G. Mullen, S. Silverman, and D.F. Korff<sup>12</sup>. The content of this paper is summarized in the abstract given as follows:

"The 557.7 nm [OI] night airglow emission was measured in the central polar cap by ground-based photometric systems at Thule Air Base, Greenland during the winter seasons from 1972-1973 and 1974-1975 and at Thule-Qanaq, Greenland during the winter season of 1973-1974. The behavior of the 557.7 nm [OI] night airglow emission in the polar cap was found to be quite different from that observed at mid and low latitudes. No diurnal variation greater than  $\pm 5\%$  exist in the data. Large amplitude variations in 557.7 nm [OI] daily average emission intensities can change by up to a factor of approximately 8 over periods ranging from 4 to 19 days. These long-term airglow variations cover at least a 100 km horizontal range as determined by a correlation coefficient of .94

between daily average 557.7 nm [OI] airglow intensities observed at Thule Air Base and Thule-Qanaq. An inter-planetary magnetic field sector related behavior is evident in the daily average intensities which shows an increase of intensity in a + sector and decrease of intensity in a - sector. No significant correlation was found between the 557.7 nm [OI] daily average intensities and Zurich sunspot number  $R_z$ , although a season to season positive trend was evident. Correlations between the 557.7 nm [OI] daily average intensities and planetary magnetic indices  $K_p$  and  $A_p$  were found to be inconclusive due to sector related effects. The Barth and Chapman mechanisms are discussed as possible source mechanisms for the 557.7 nm [OI] airglow in the central polar cap, and a hypothesis is presented to explain the airglow variations."



## REFERENCES

1. Carrigan, Anne L., ed., Geophysics and Space Data Bulletin (AFCRL-TR-74-0608 Special Reports, No. 186, Vol. XI, No. 3, Third Quarter 1974), Section 4, p. 43; (AFCRL-TR-75-0160 Special Reports, No. 190, Vol. XI, No. 4, Fourth Quarter 1974) Section 4, p. 89.
2. Mullen, E. G. and Silverman, S. M., "AFCRL Research in Greenland-1974", Air Force Cambridge Research Laboratories inhouse report.
3. Mullen, E. G., "AFGL Scientific Research in Greenland-1975", AFGL inhouse report.
4. Svalgaard, L., Preliminary draft of "An Atlas of Interplanetary Sector Structure, 1957-1974", SUIPR Report No. 629(1975), private communication.
5. Solar-Geophysical Data, Prompt Reports(World Data Center A for Solar Terrestrial Physics, National Oceanic and Atmospheric Administration, Boulder, Colorado 80302), March, 1976.
6. Wilcox, J. M. and Colburn, D. S., J. Geophys. Res. 77, 751 (1972); Shapiro, R., Geophys. Res. 79, 289 (1974).
7. IUGG: Association of Geomagnetism and Aeronomy preliminary geomagnetic planetary indices.
8. Godhavn charts furnished by E. G. Mullen, AFGL.
9. Akasofu, S. -I., Polar and Magnetospheric Substorms, D. Reidel, Dordrecht, Netherlands, 1968.

10. Sector assignments prior to 6 March 74 and after 1 January 75 are those inferred by L. Svalgaard, private communication via J. Wilcox. Sector assignments from 6 March 74 to 1 January 75 were taken from the Solar-Geophysical Data, Prompt Reports (World Data Center A for Solar Terrestrial Physics, National Oceanic and Atmospheric Administration, Boulder, Colorado 80302), No. 365-Part I, p. 21 (1975).
11. Turtle, J. P. in "AFCRL Research in Greenland - 1974", Air Force Cambridge Research Laboratories inhouse report compiled by E. G. Mullen and S. M. Silverman, p. 4.
12. Mullen, E. G., Silverman, S. M., Korff, D. F., Planetary and Space Science, in press.

FIGURES FOR SECTION 2



# THULE VLF, MAGNETOMETER & RIOMETER DATA

JULY 1974

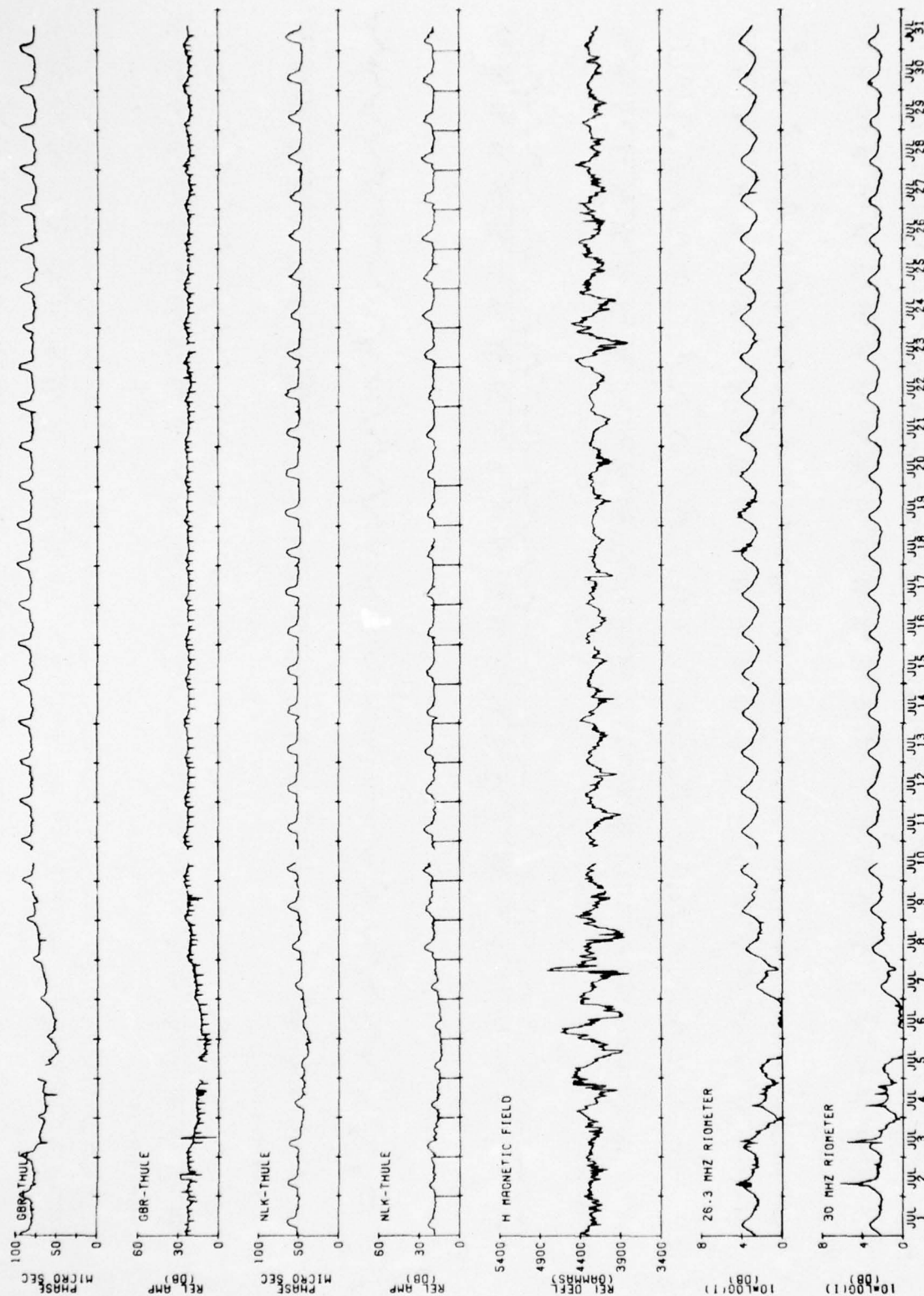


Figure 2.1. Ten-minute average plots of edited Thule VLF, magnetometer, and riometer data versus universal time for July 1974.

# THULE VLF, MAGNETOMETER & RIOMETER DATA

AUGUST 1974

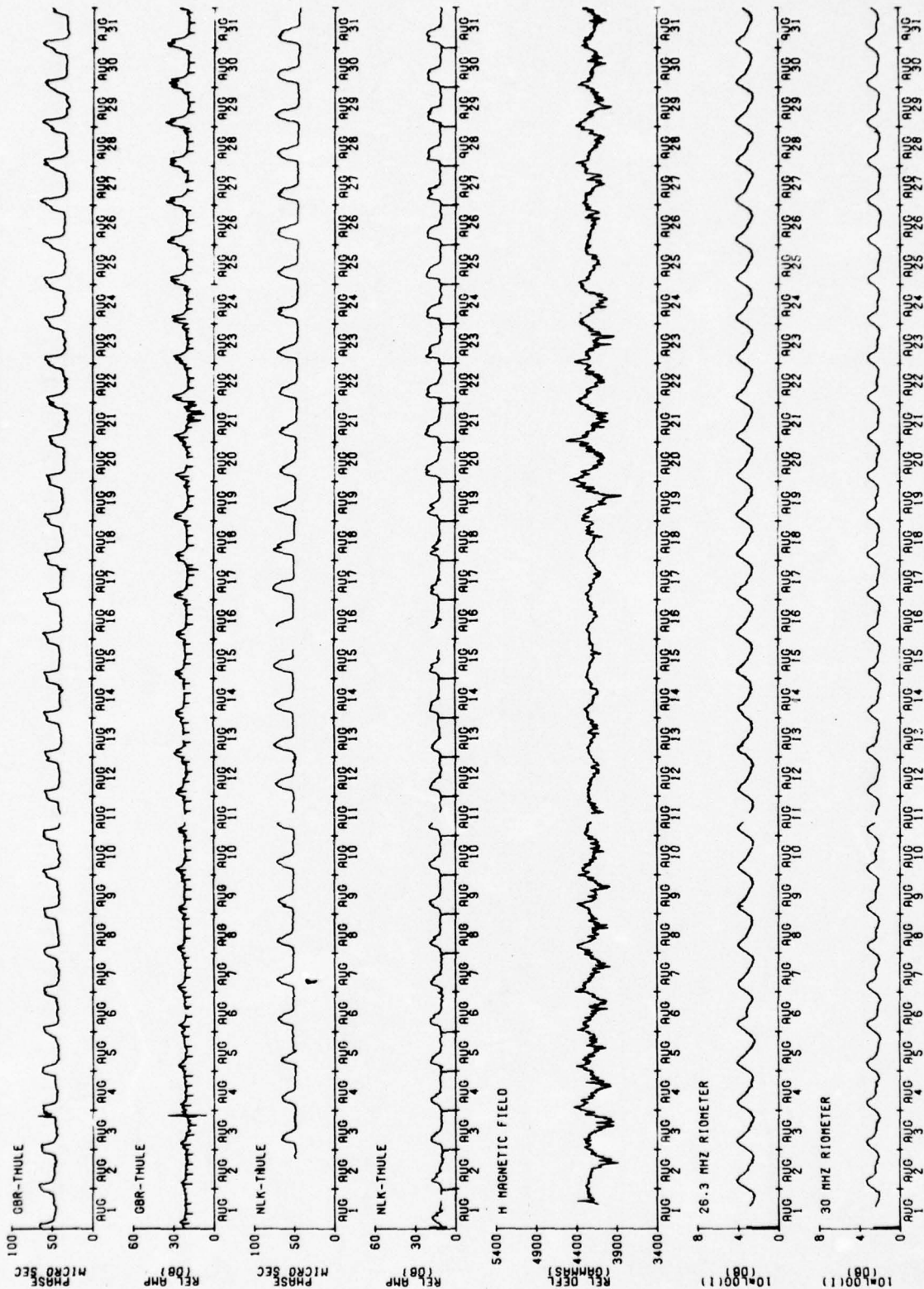


Figure 2.2. Ten-minute average plots of edited Thule VLF, magnetometer, and riometer data versus universal time for August 1974.

# THULE VLF, MAGNETOMETER & RIOMETER DATA

SEPTEMBER 1974

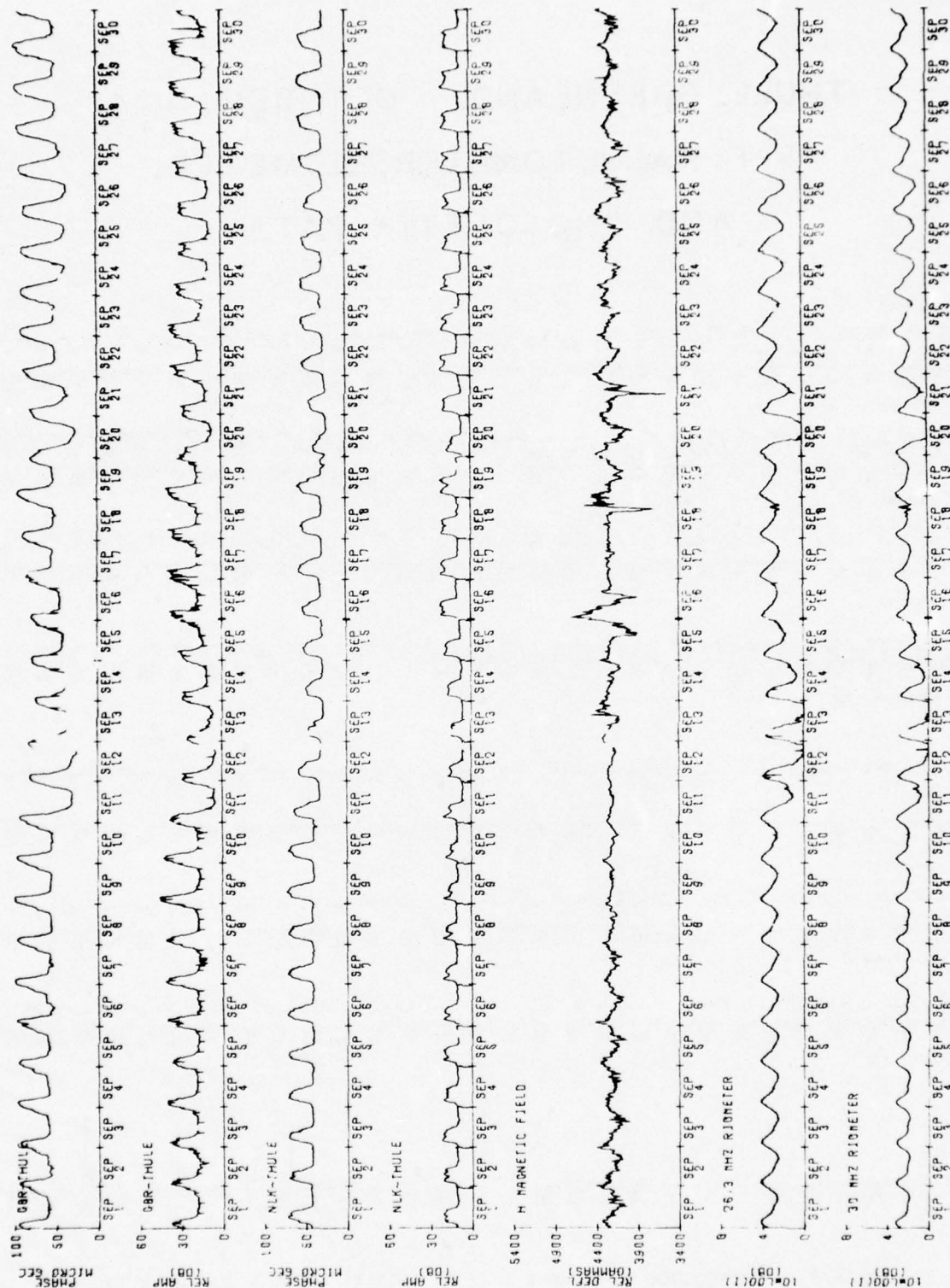


Figure 2.3. Ten-minute average plots of edited Thule VLF, magnetometer, and riometer data versus universal time for September 1974.



# THULE, GREENLAND      OCTOBER, 1974

## VLF, MAGNETOMETER, RIOMETER, AND PHOTOMETER DATA

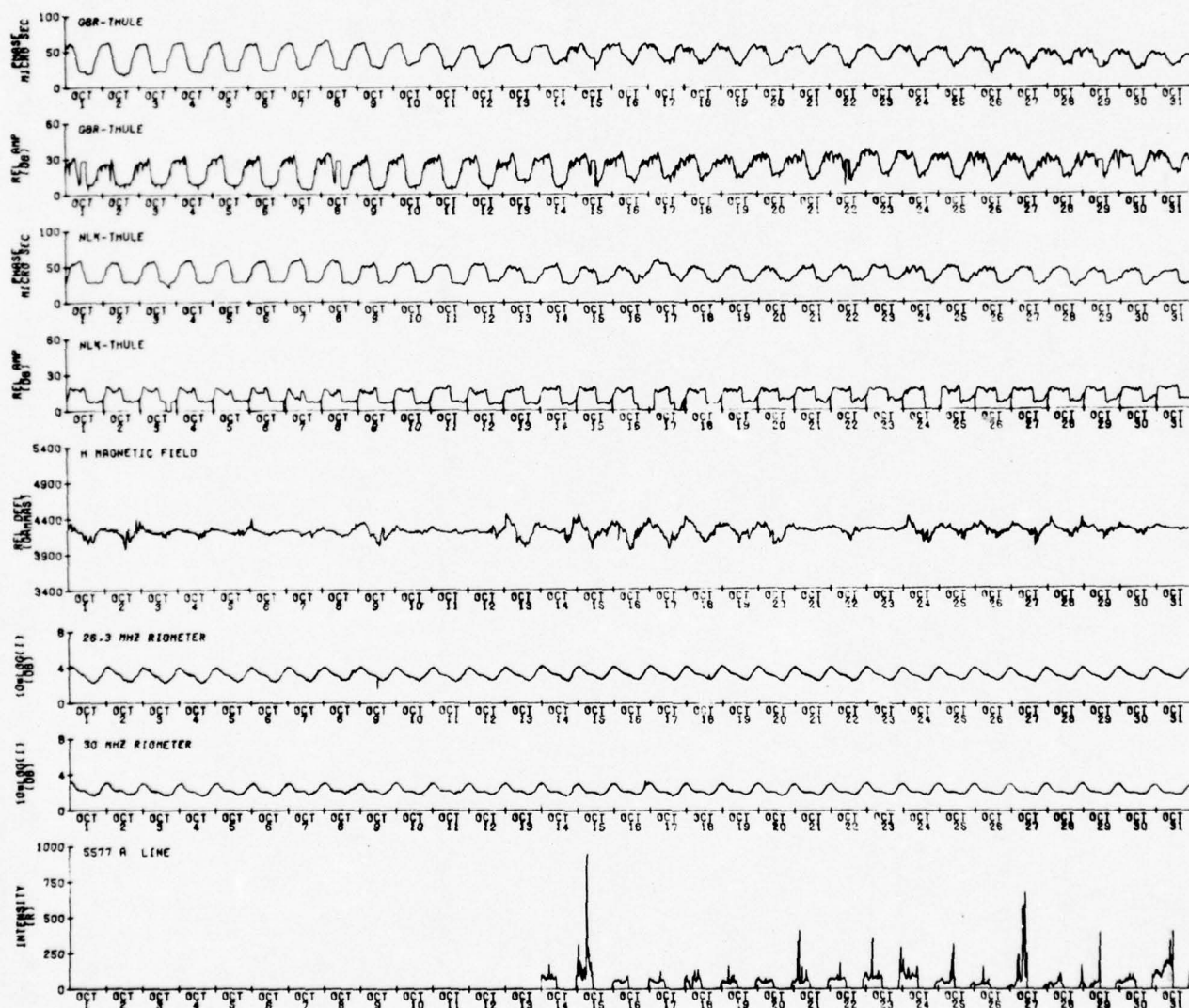


Figure 2.4. Ten-minute average plots of edited Thule VLF, magnetometer, riometer, and 5577 Å photometer data versus universal time for October 1974.

# THULE, GREENLAND NOVEMBER, 1974

## VLF, MAGNETOMETER, RIOMETER, AND PHOTOMETER DATA

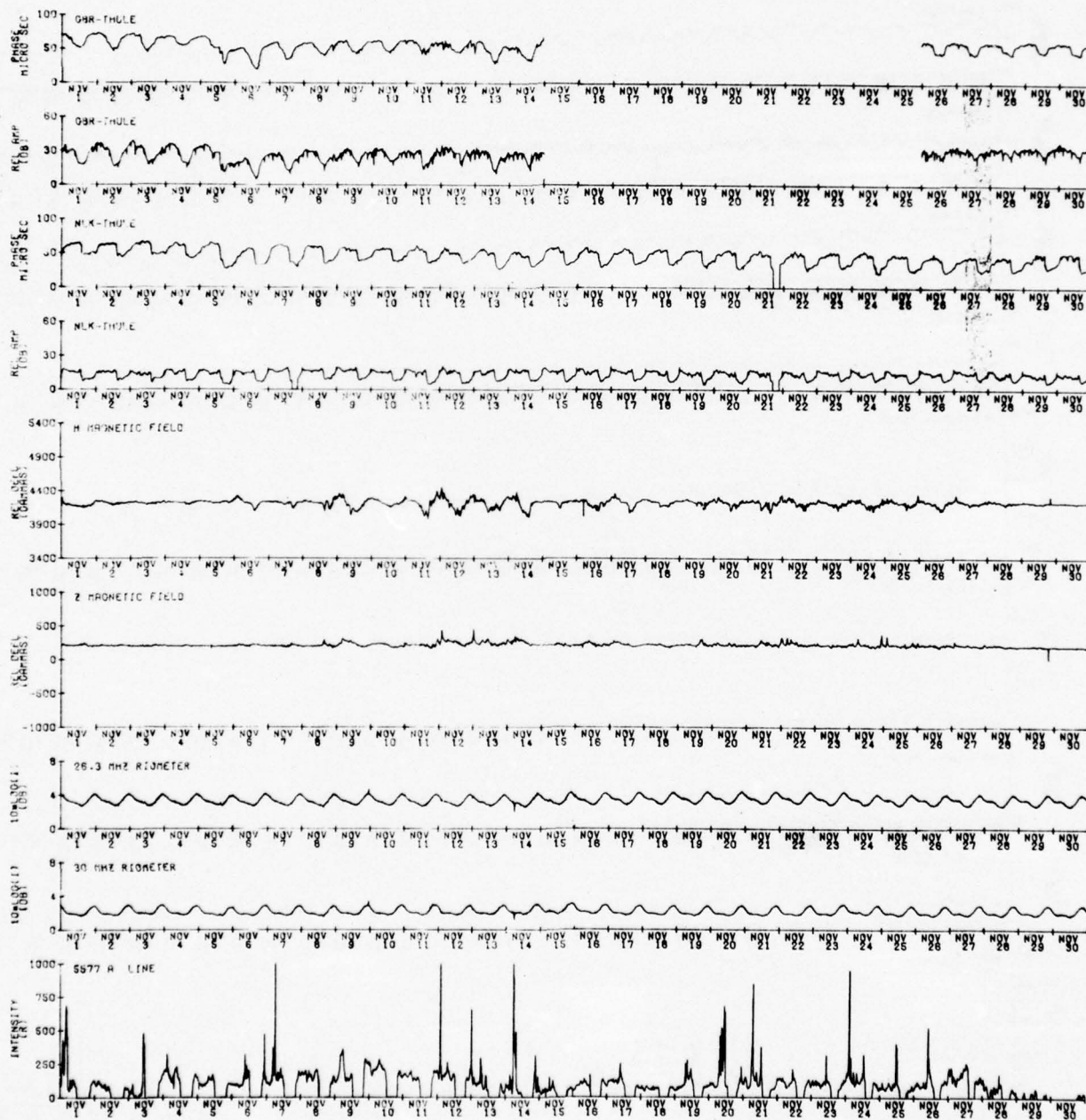


Figure 2.5. Ten-minute average plots of edited Thule VLF, magnetometer, riometer, and 5577 Å photometer data versus universal time for November 1974.

# THULE, GREENLAND DECEMBER, 1974

## VLF, MAGNETOMETER, RIOMETER, AND PHOTOMETER DATA

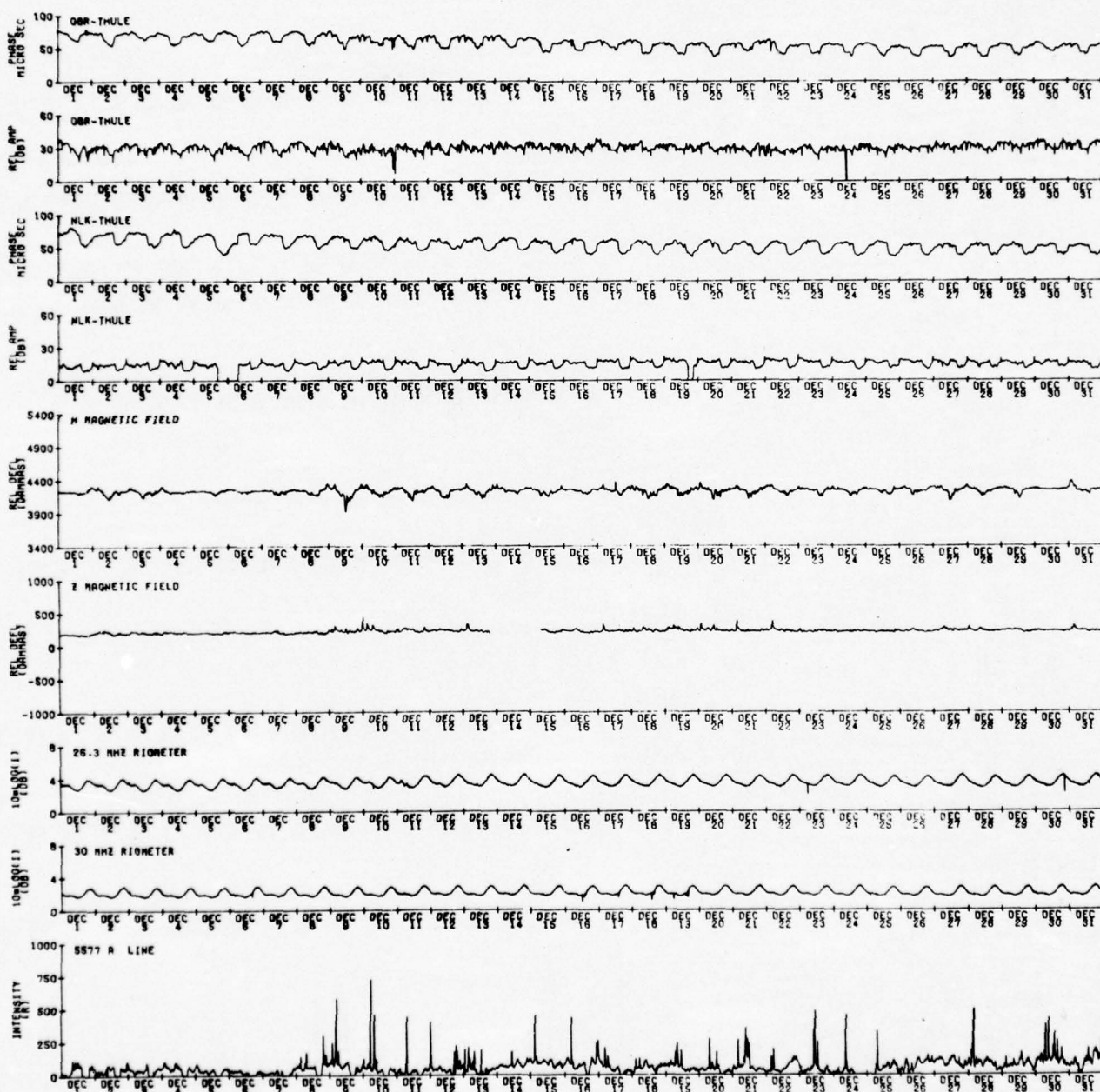


Figure 2.6. Ten-minute average plots of edited Thule VLF, magnetometer, riometer, and 5577A photometer data versus universal time for December 1974.



# THULE, GREENLAND JANUARY, 1975

## VLF, MAGNETOMETER, AND RIOMETER DATA

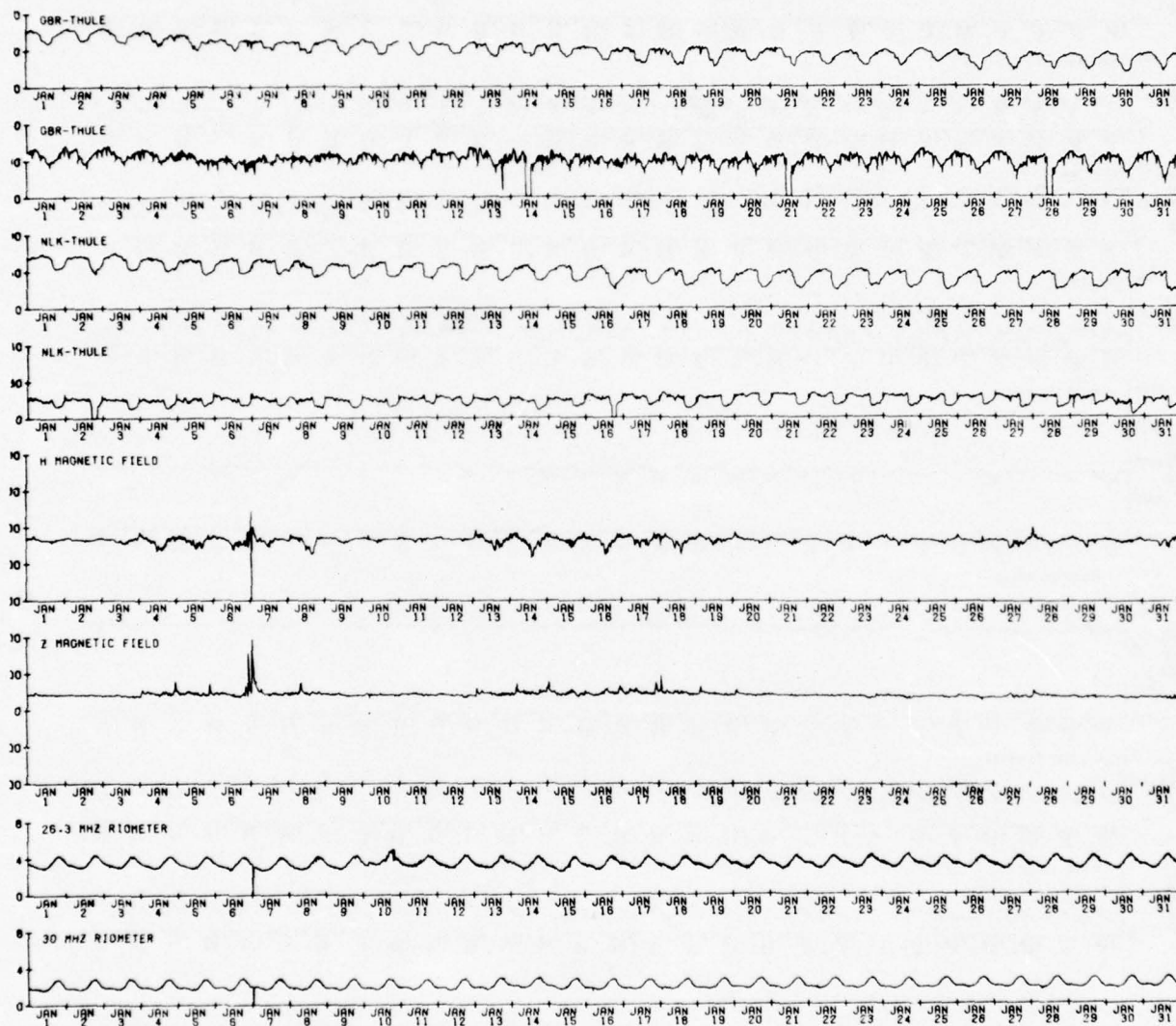


Figure 2.7. Ten-minute average plots of edited Thule VLF, magnetometer, and riometer data versus universal time for January 1975.

# THULE, GREENLAND      FEBRUARY, 1975 VLF, MAGNETOMETER, AND RIOMETER DATA

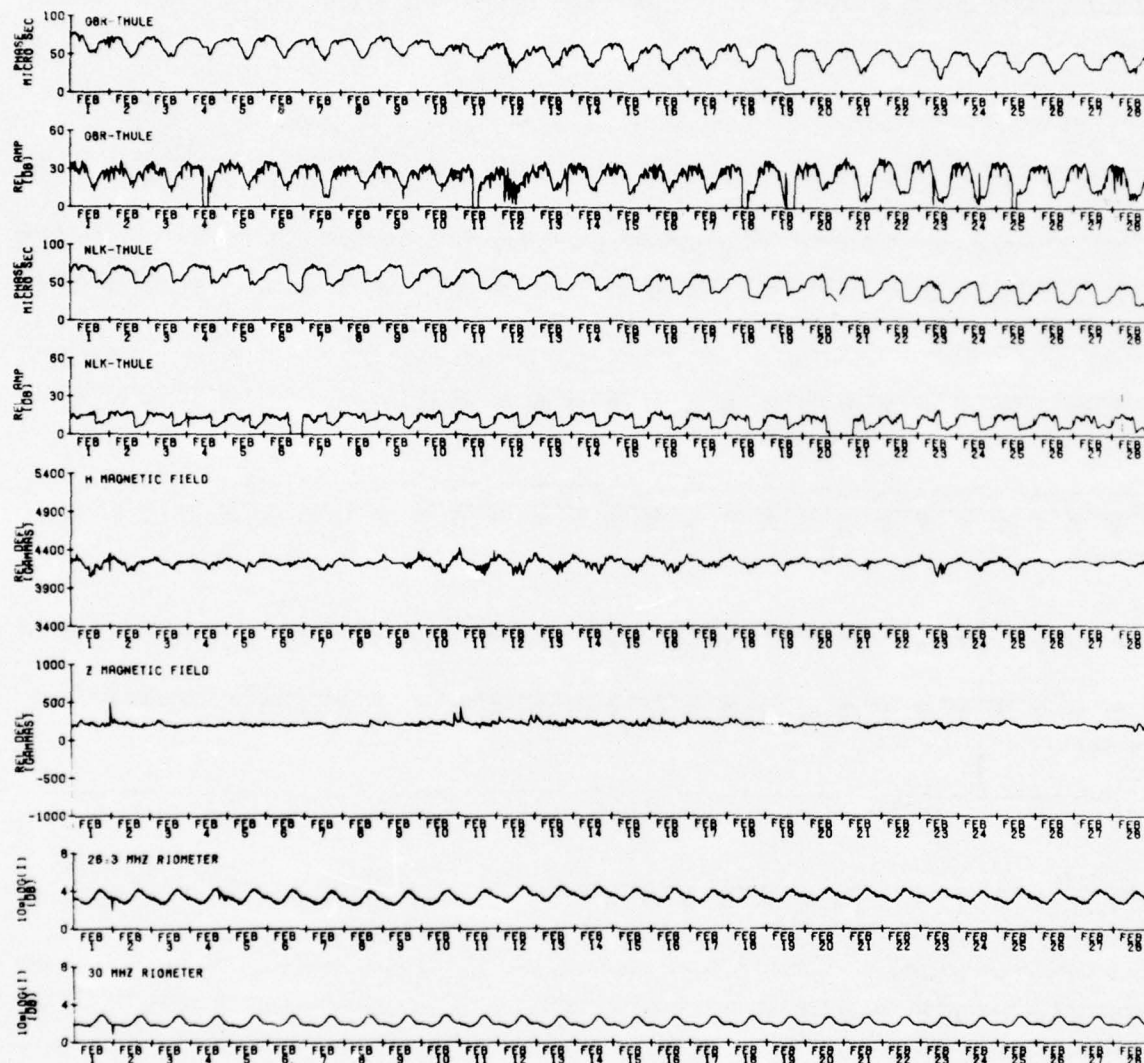


Figure 2.8. Ten-minute average plots of edited Thule VLF, magnetometer, and riometer data versus universal time for February 1975.

# THULE, GREENLAND MARCH, 1975

## VLF, MAGNETOMETER, AND RIOMETER DATA

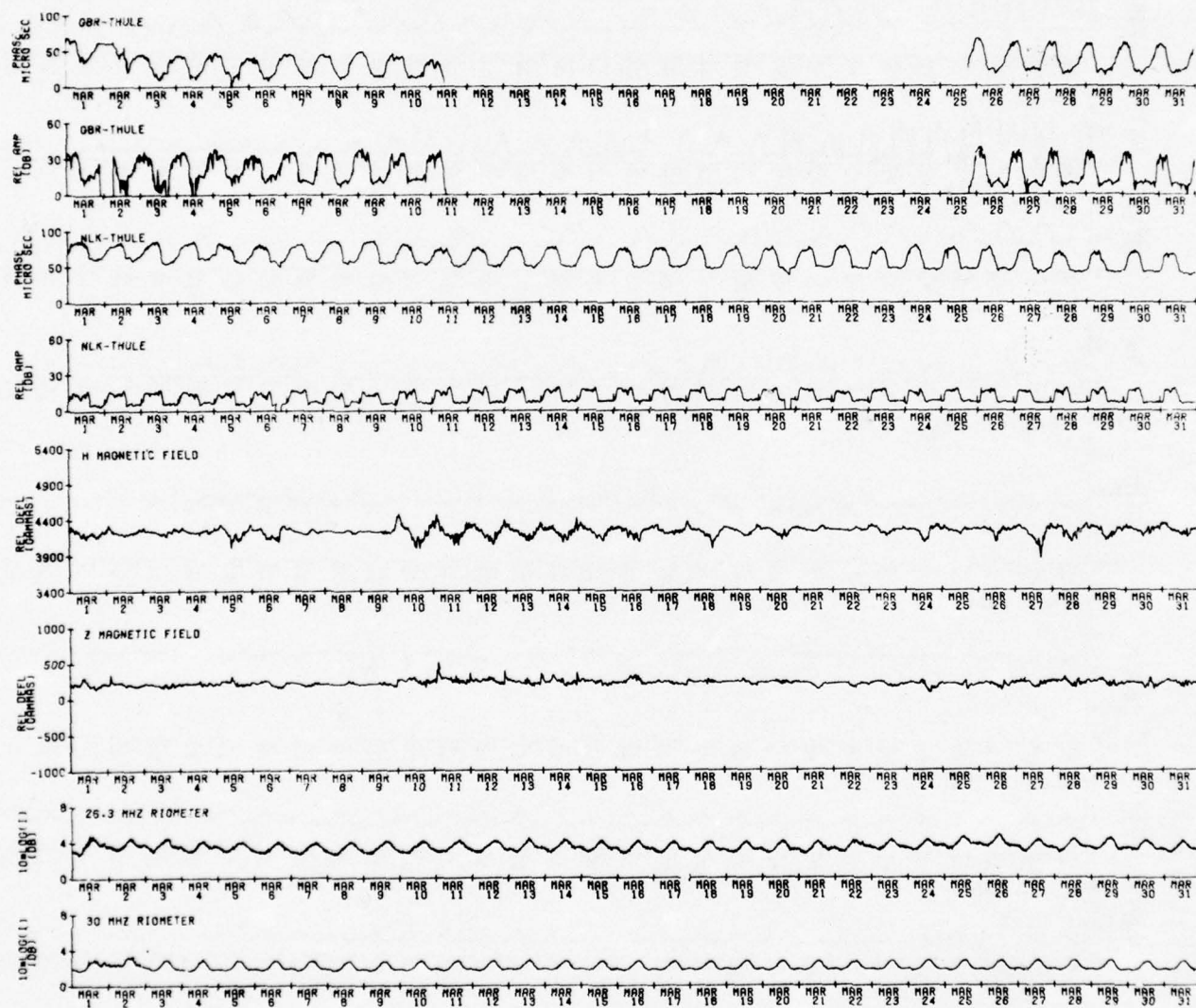


Figure 2.9. Ten-minute average plots of edited Thule VLF, magnetometer, and riometer data versus universal time for March 1975.



# THULE, GREENLAND APRIL, 1975

## VLF, MAGNETOMETER, AND RIOMETER DATA

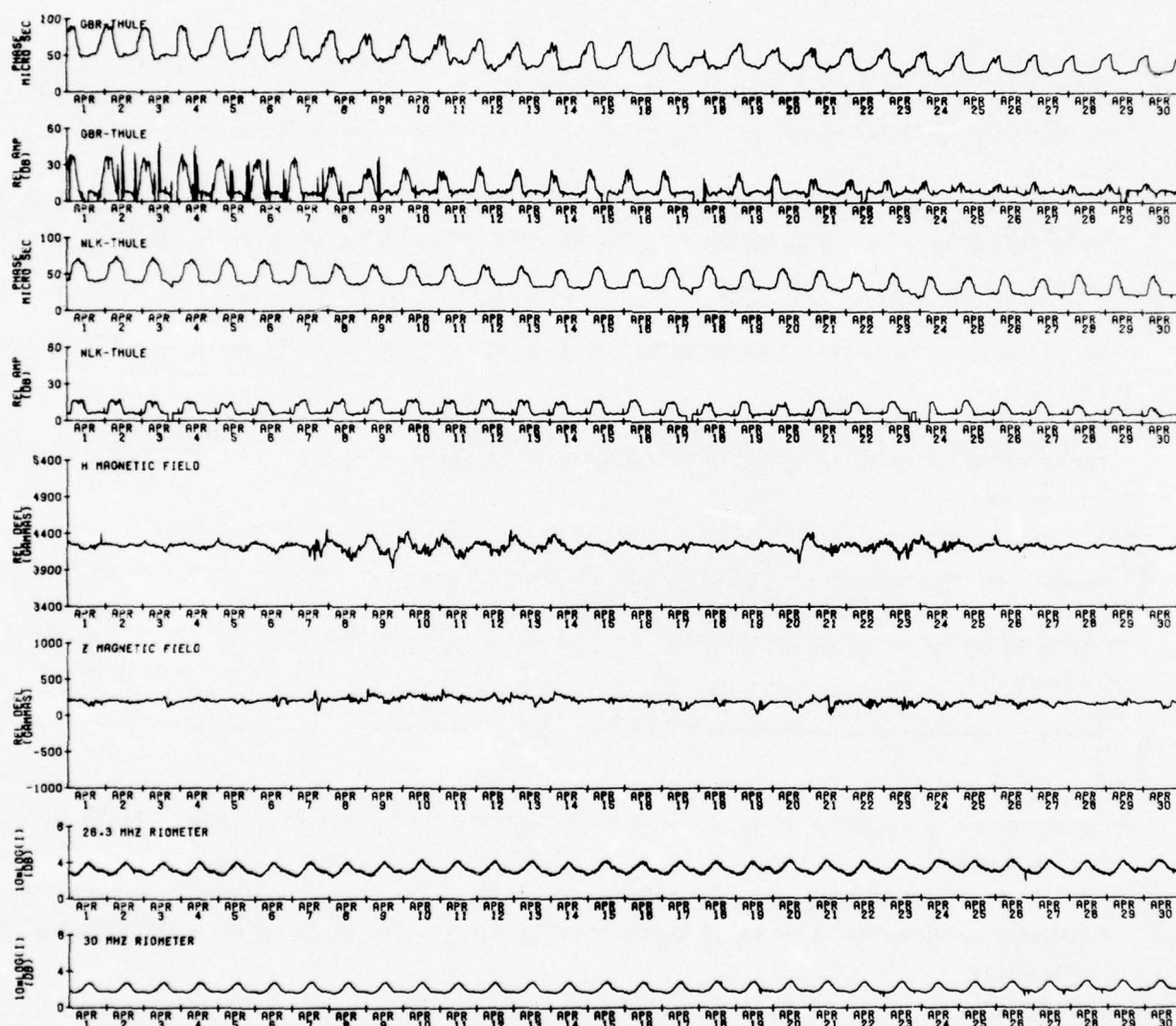


Figure 2.10. Ten-minute average plots of edited Thule VLF, magnetometer, and riometer data versus universal time for April 1975.

# THULE, GREENLAND

## MAY, 1975

### VLF, MAGNETOMETER, AND RIOMETER DATA

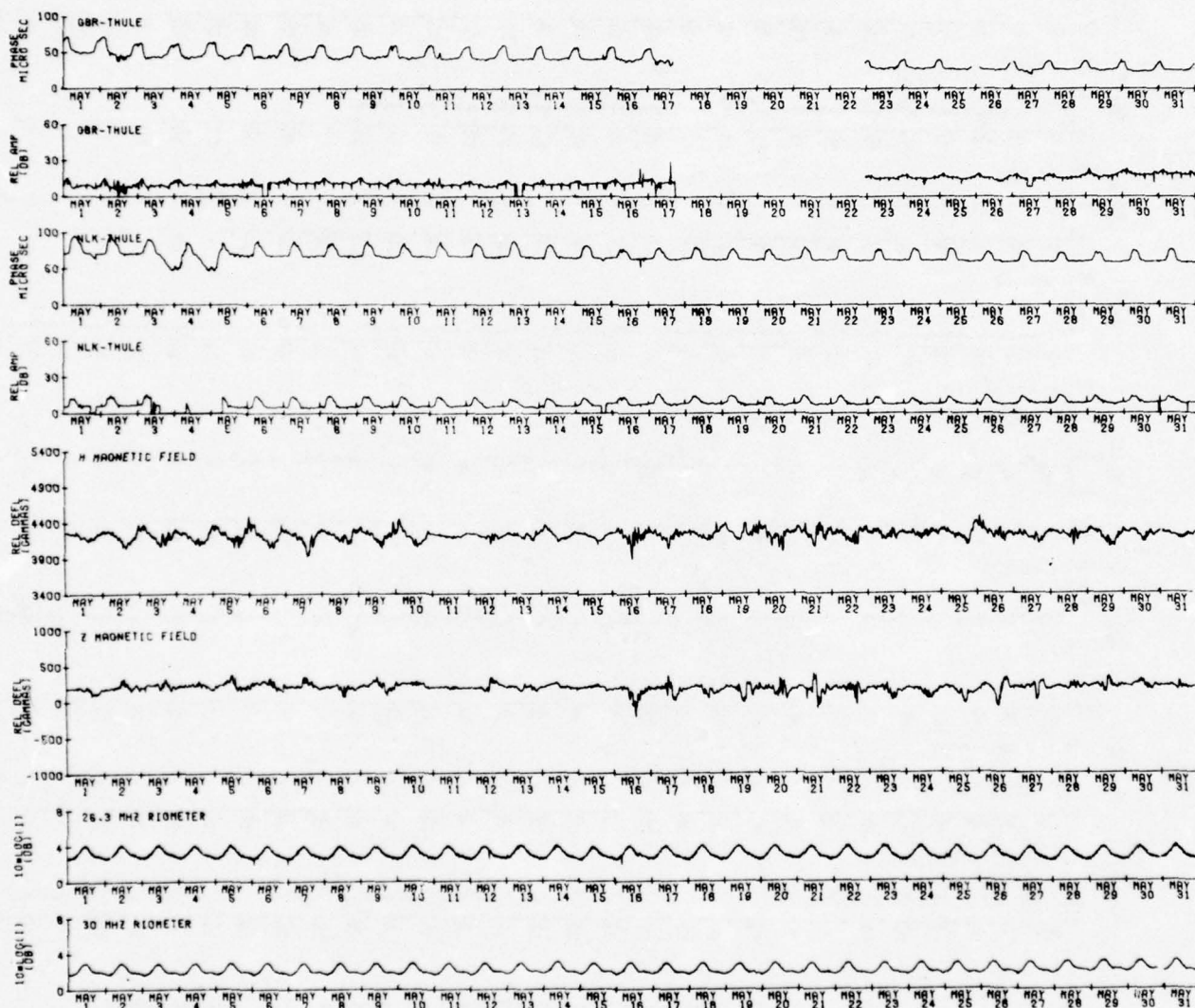


Figure 2.11. Ten-minute average plots of edited Thule VLF, magnetometer, and riometer data versus universal time for May 1975.

# THULE, GREENLAND JUNE, 1975

## VLF, MAGNETOMETER, AND RIOMETER DATA

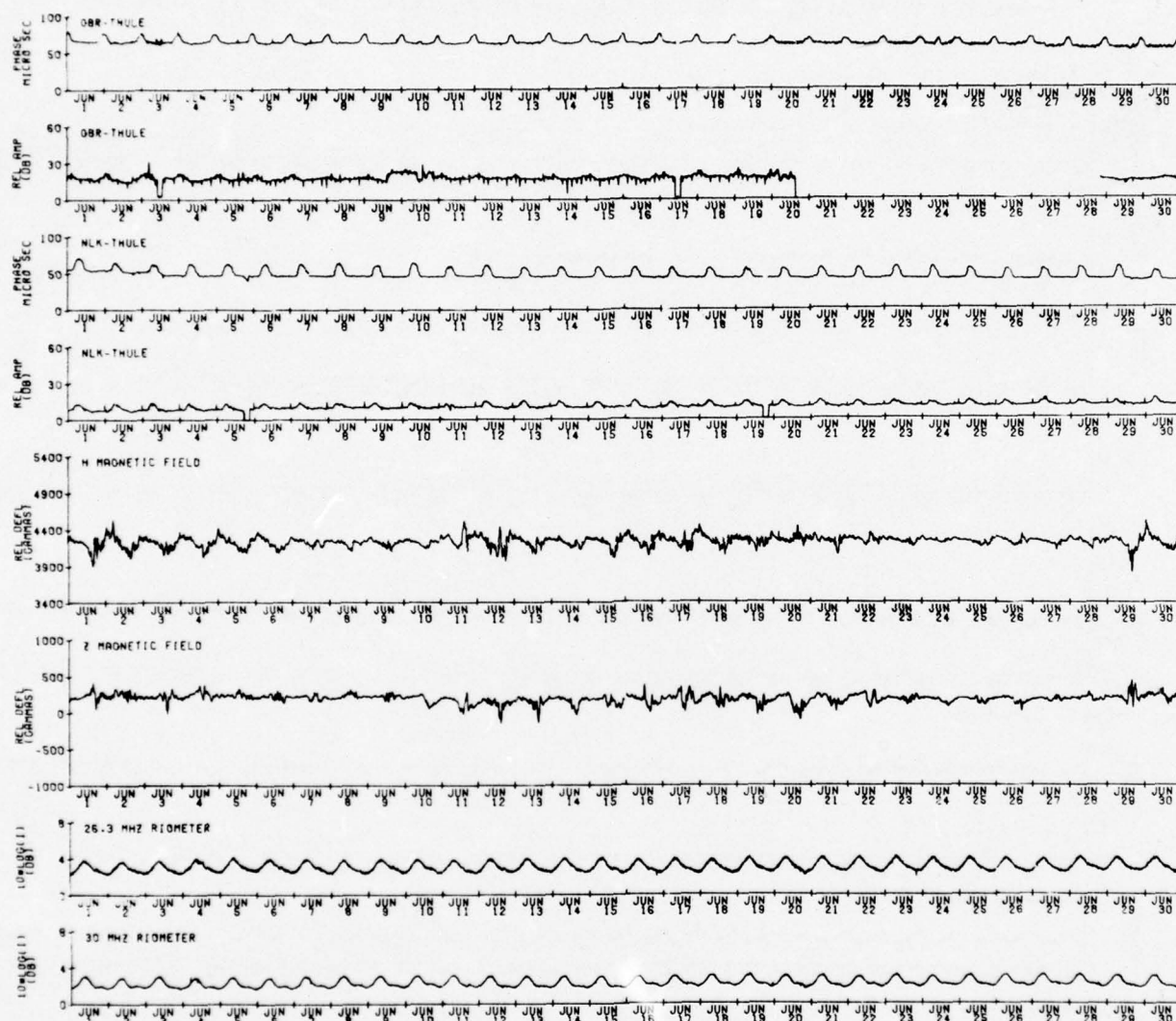


Figure 2.12. Ten-minute average plots of edited Thule VLF, magnetometer, and riometer data versus universal time for June 1975.



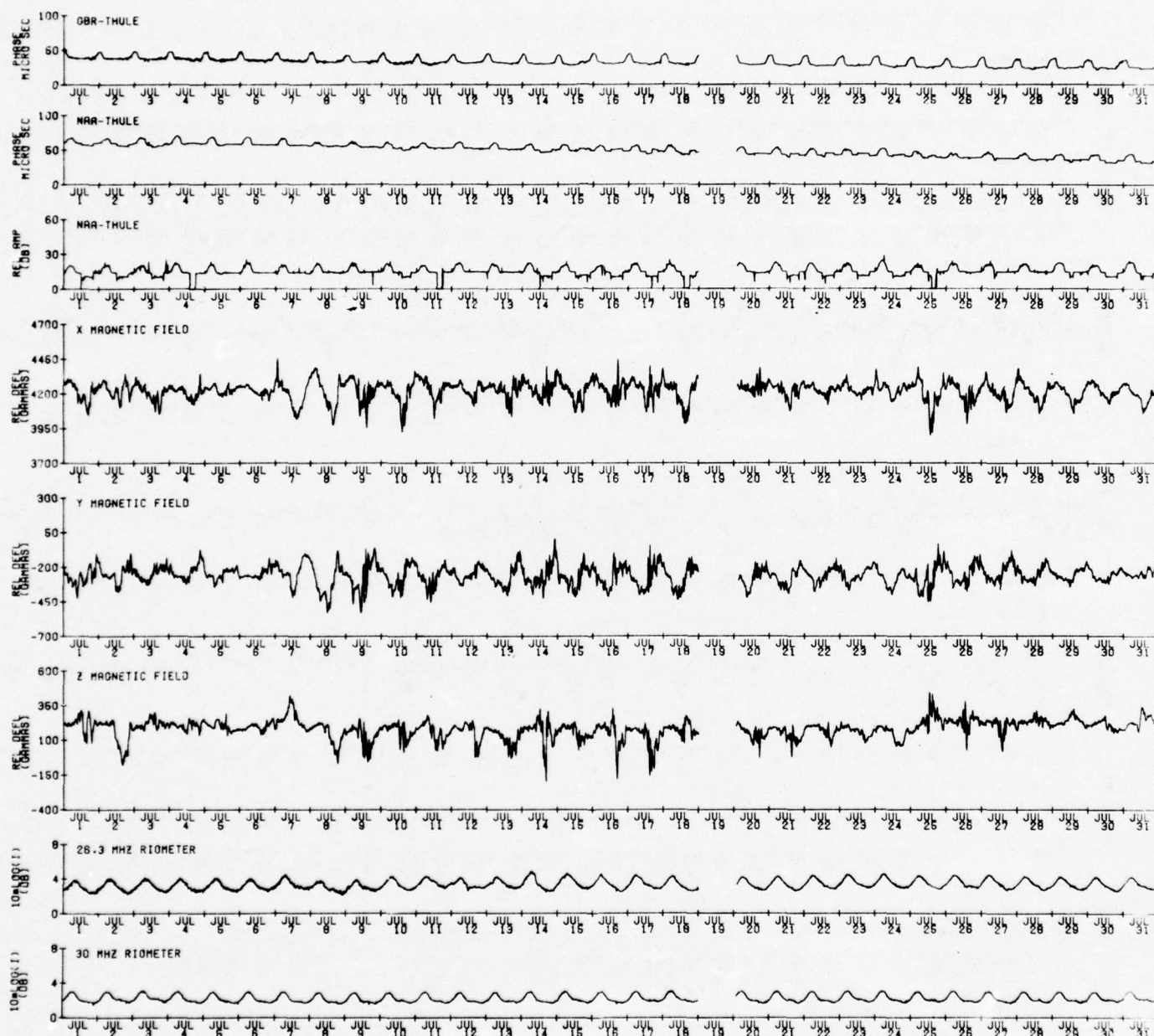


Figure 2.13. Ten-minute average plots of edited Thule VLF, magnetometer, and riometer data versus universal time for July 1975.

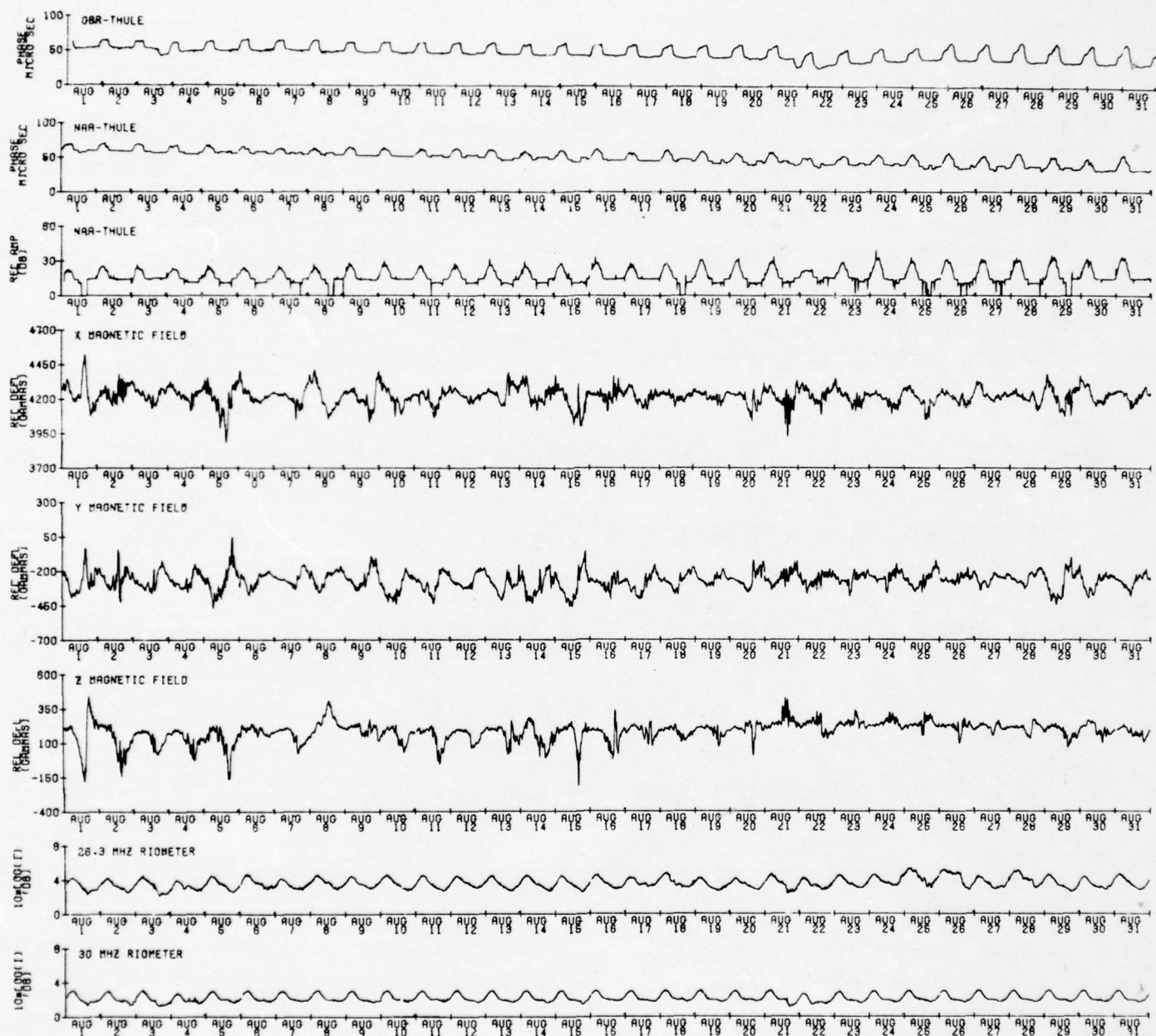


Figure 2.14. Ten-minute average plots of edited Thule VLF, magnetometer, and riometer data versus universal time for August 1975.

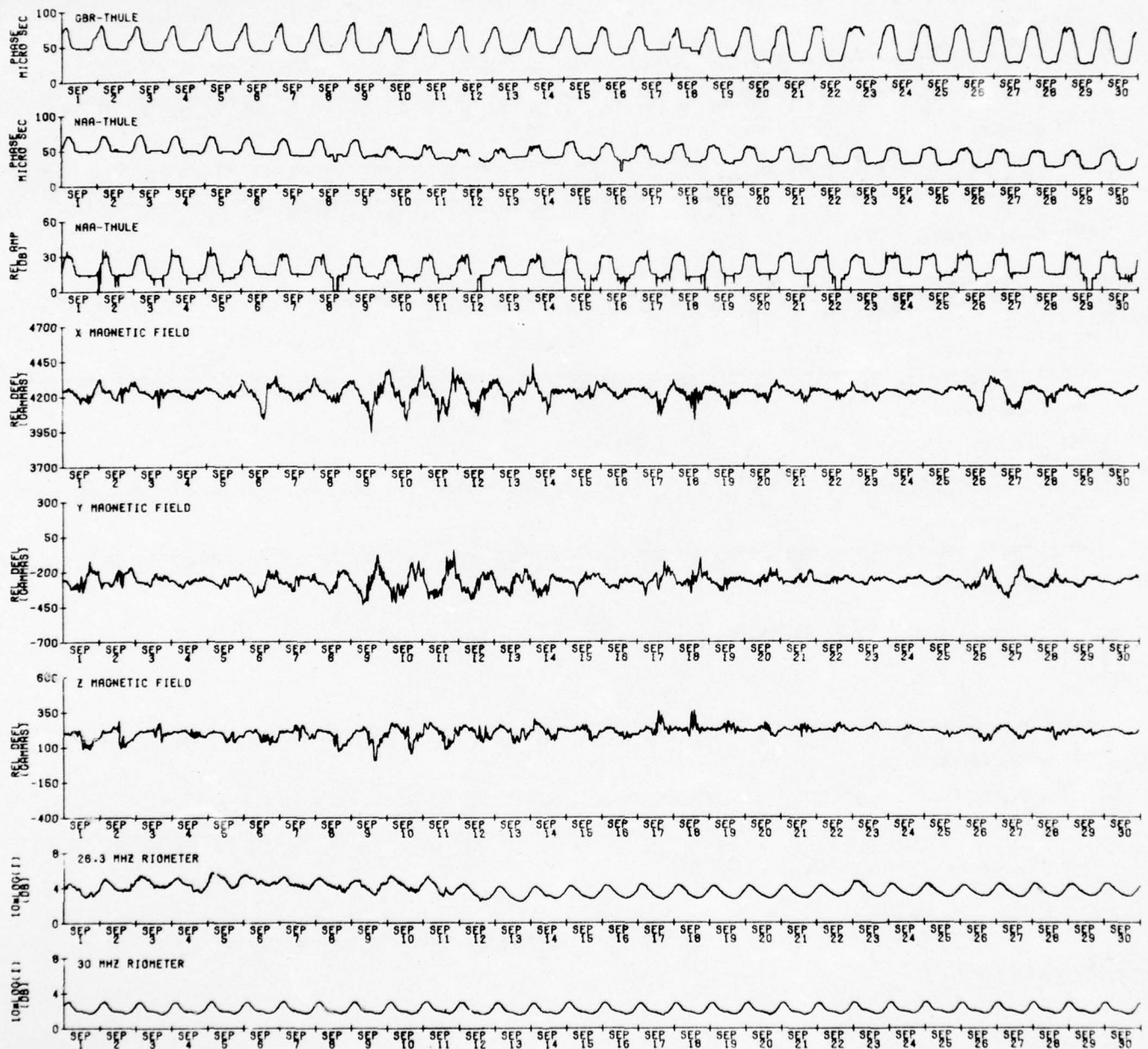


Figure 2.15. Ten-minute average plots of edited Thule VLF, magnetometer, and riometer data versus universal time for September 1975.



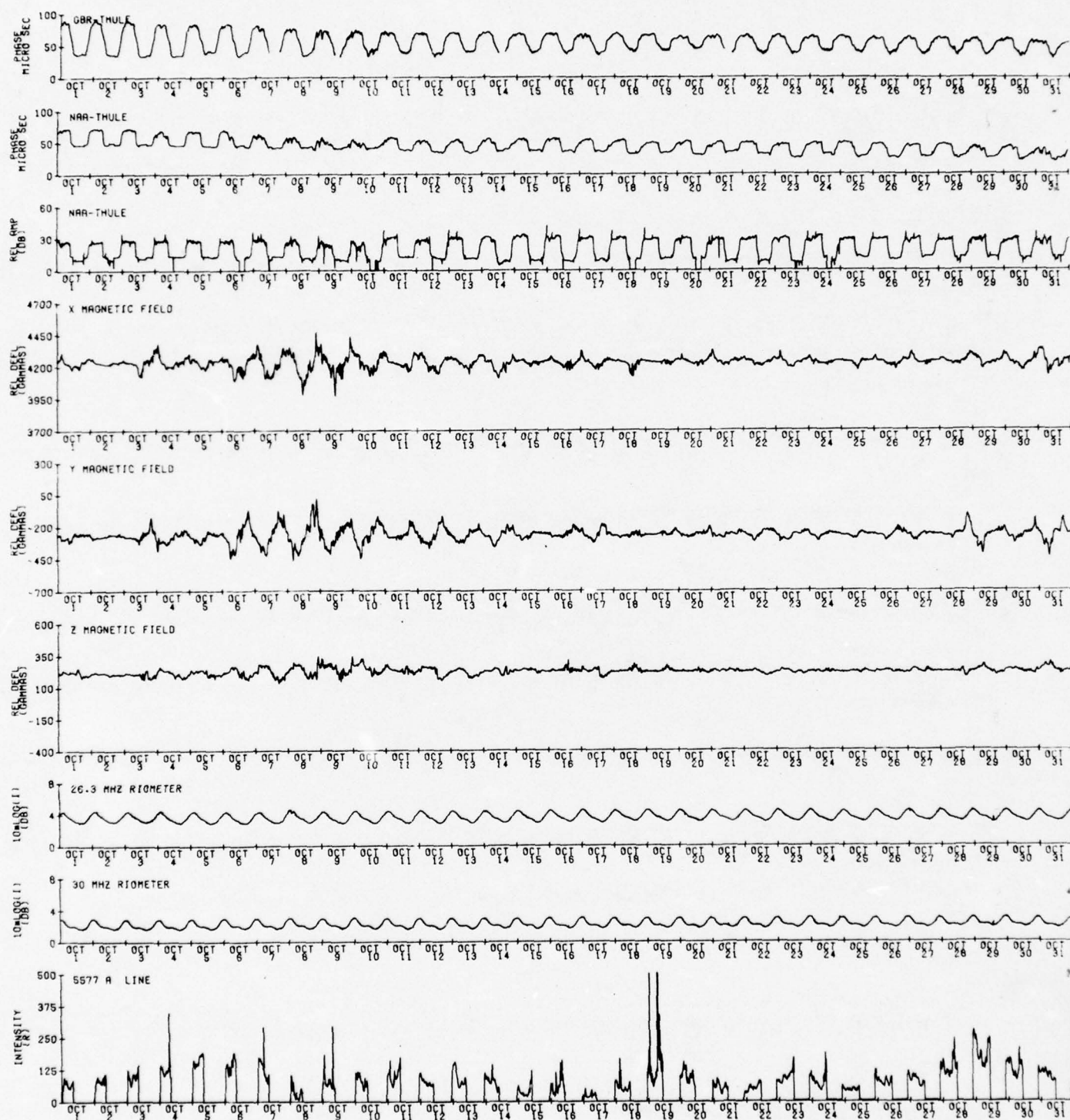


Figure 2.16. Ten-minute average plots of edited Thule VLF, magnetometer, riometer, and 5577 Å photometer data versus universal time for October 1975.

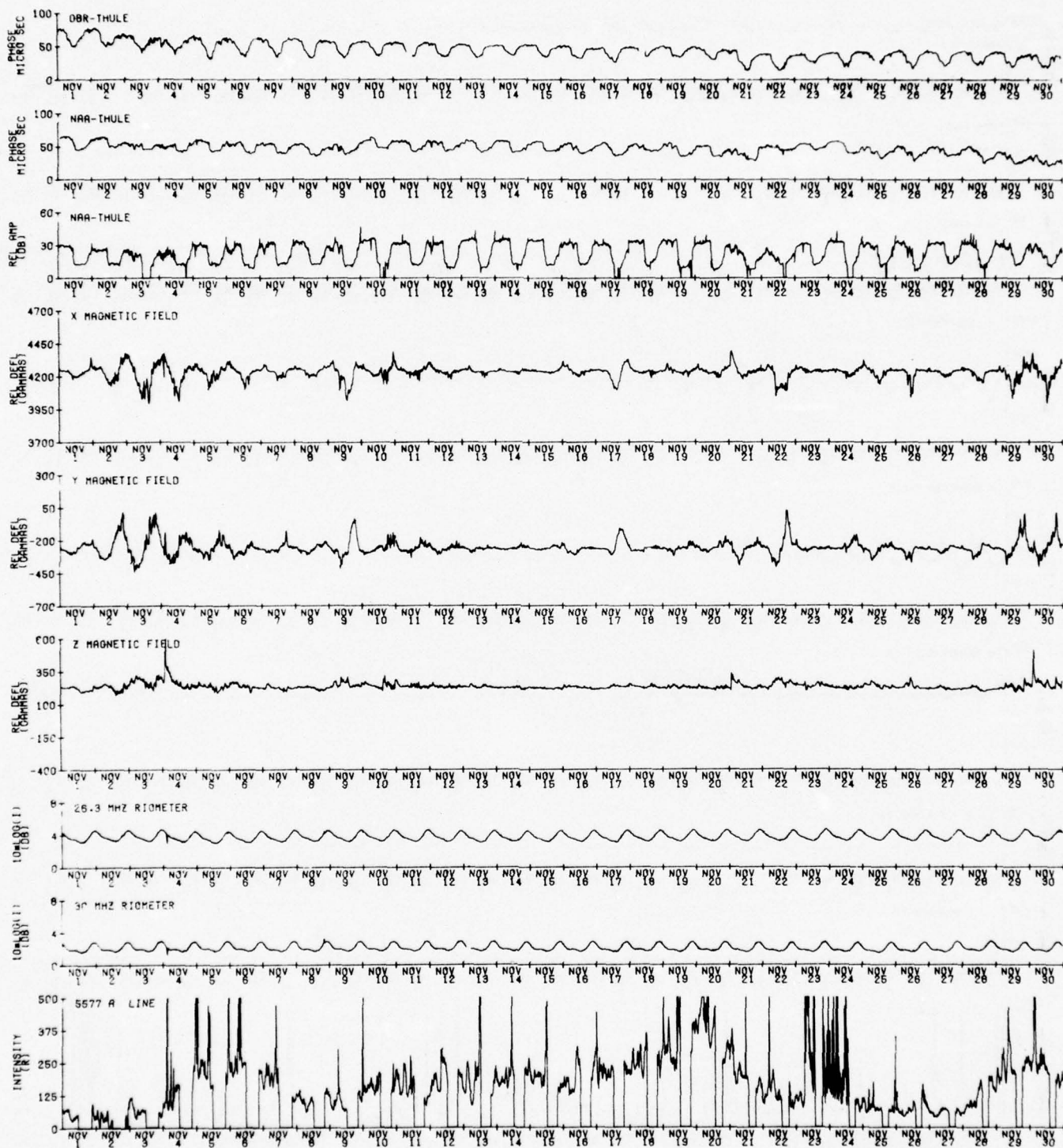


Figure 2.17. Ten-minute average plots of edited Thule VLF, magnetometer, riometer, and 5577 Å photometer data versus universal time for November 1975.

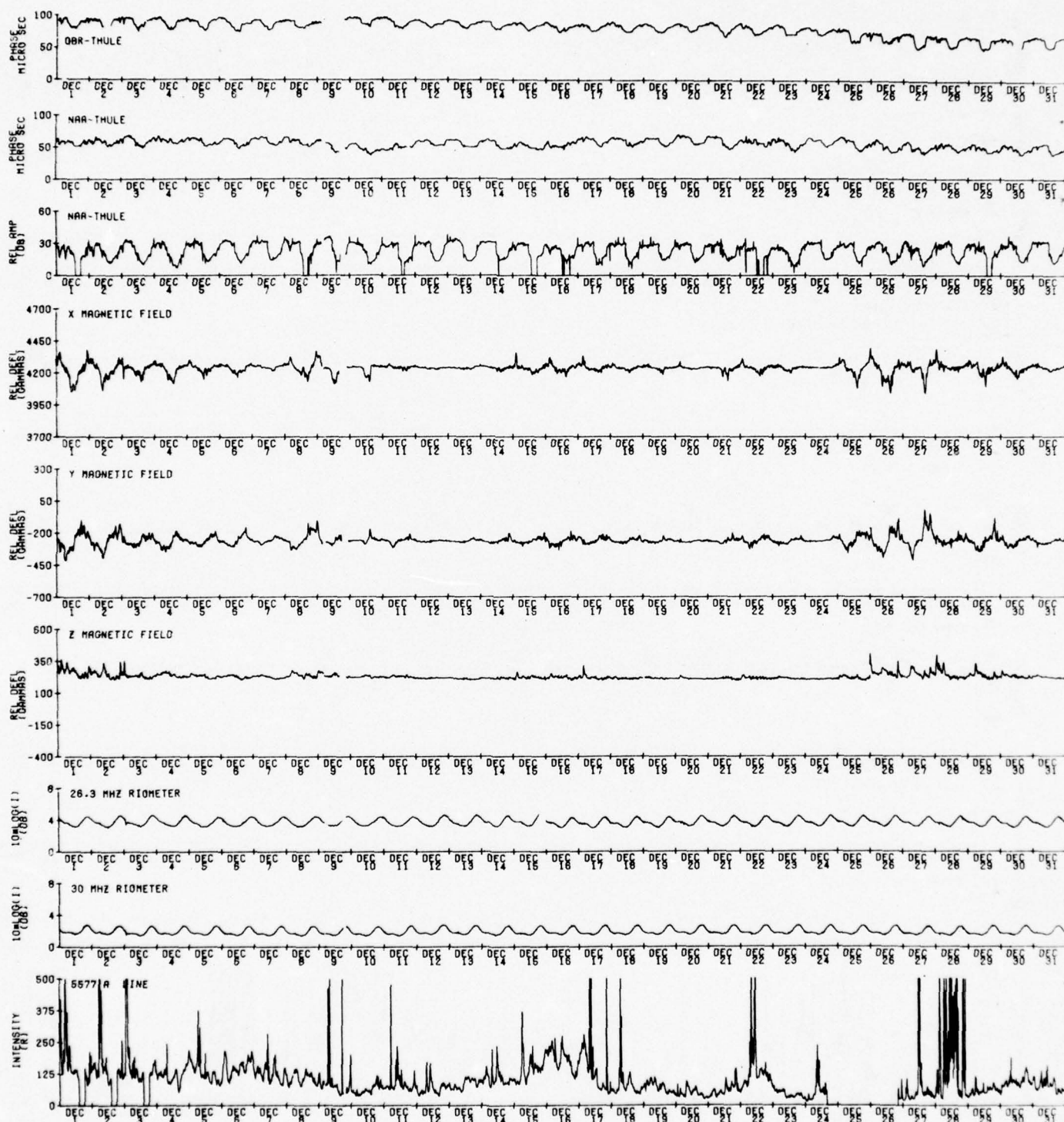


Figure 2.18. Ten-minute average plots of edited Thule VLF, magnetometer, riometer, and 5577A photometer data versus universal time for December 1975.



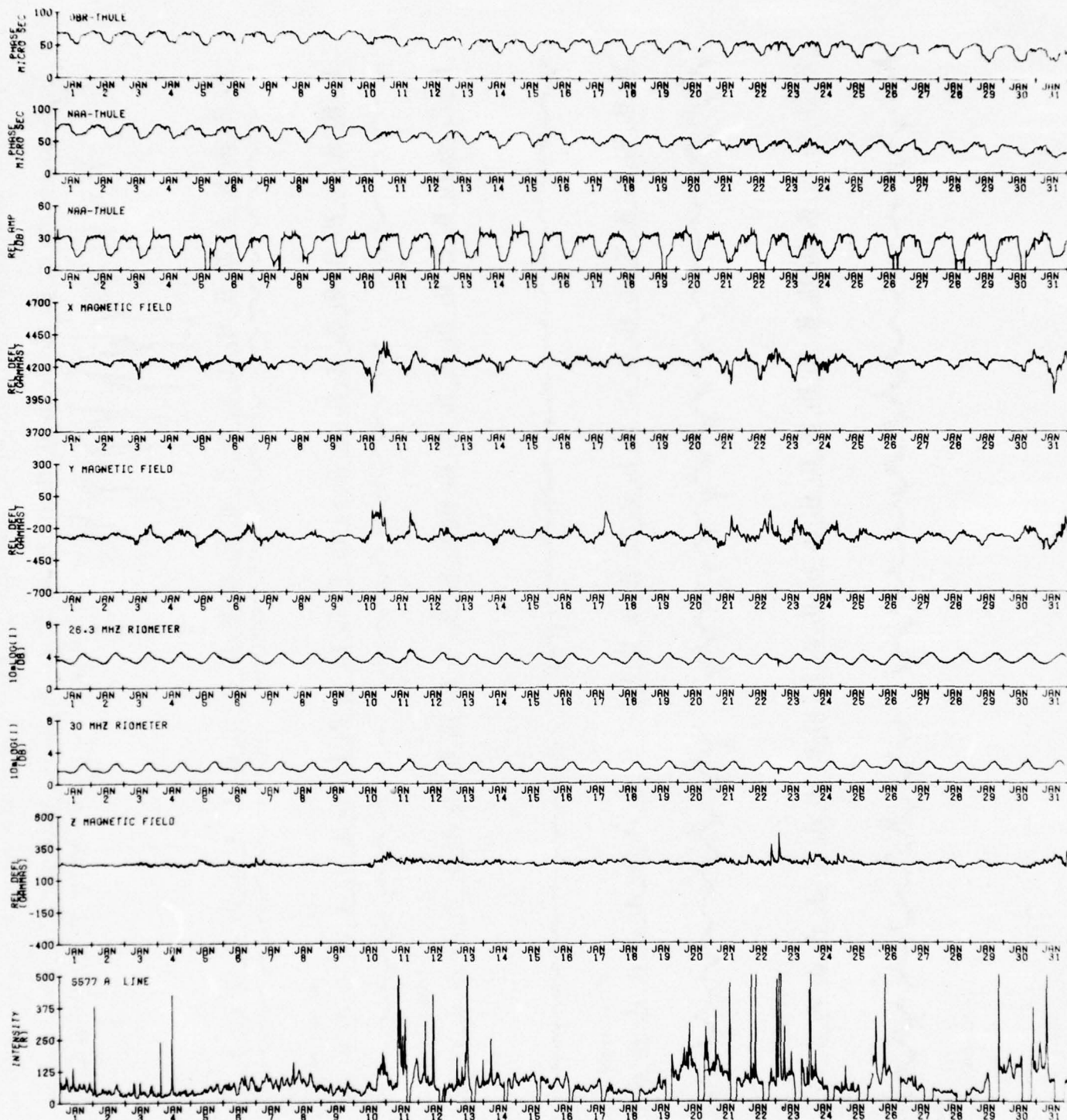


Figure 2.19. Ten-minute average plots of edited Thule VLF, magnetometer, riometer, and 5577 Å photometer data versus universal time for January 1976.

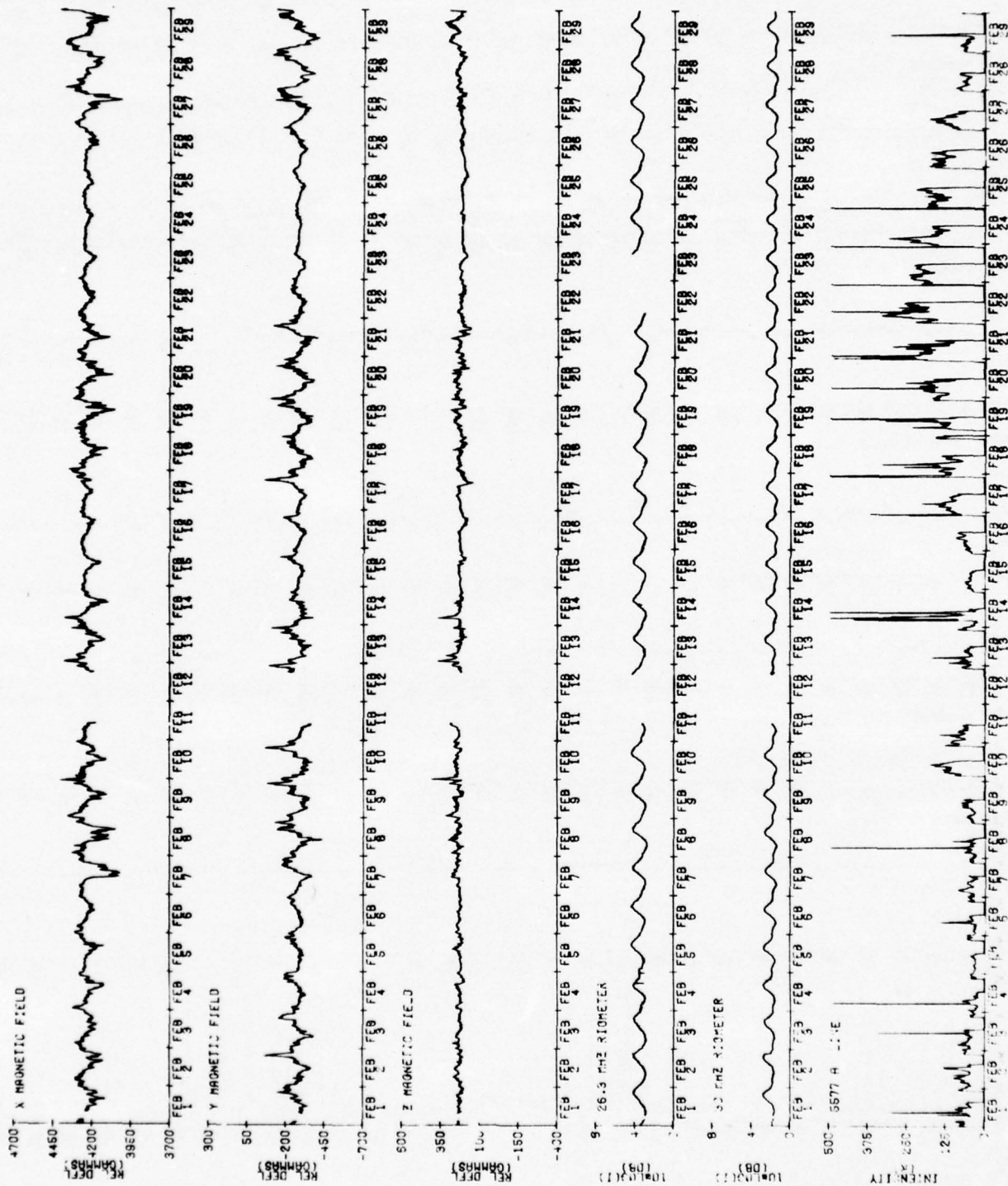


Figure 2.20. Ten-minute average plots of edited Thule VLF, magnetometer, riometer, and 557A photometer data versus universal time for February 1976.

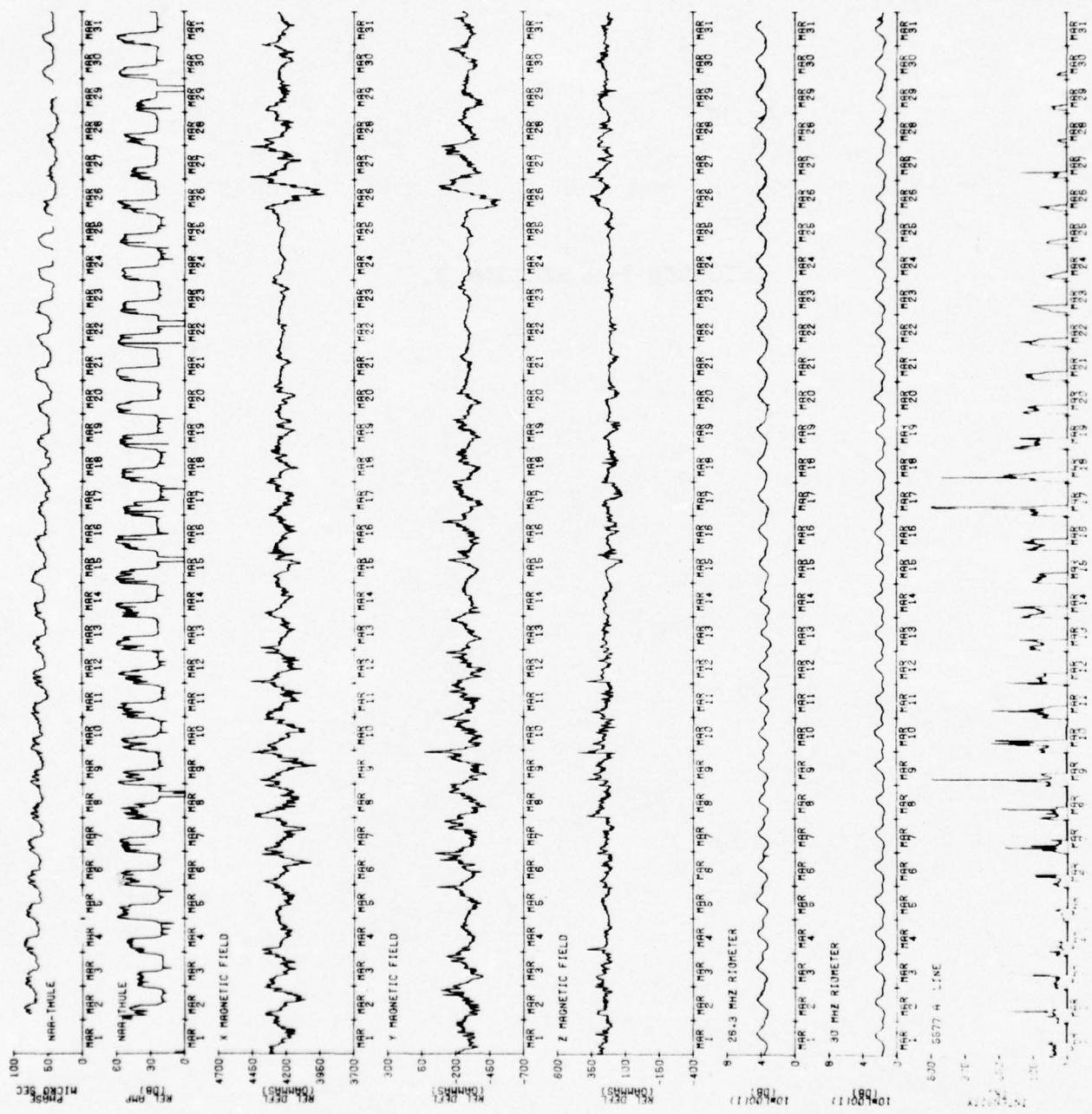


Figure 2.21. Ten-minute average plots of edited Thule VLF, magnetometer, riometer, and 557A photometer data versus universal time for March 1976.



FIGURES FOR SECTION 3.

# ENERGETIC PARTICLE EVENT 29OCT 73-30OCT 73 THULE, GREENLAND

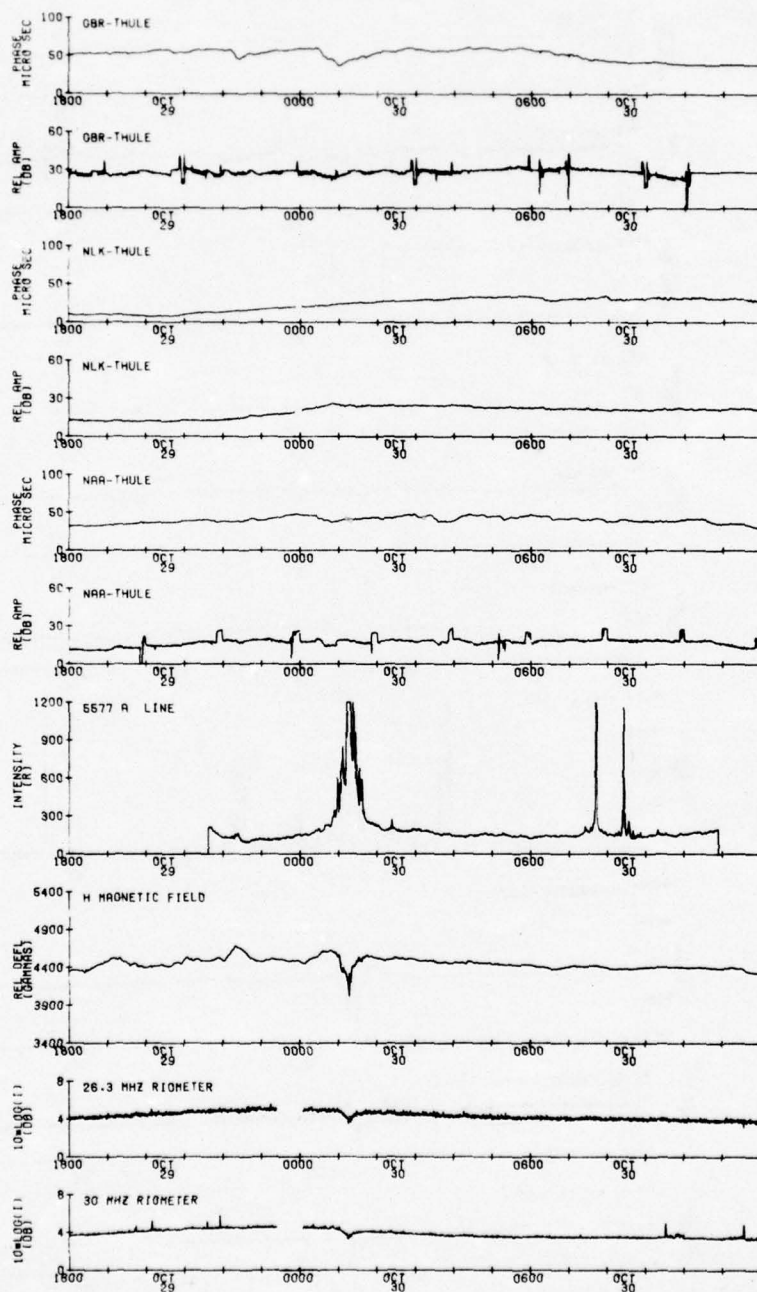


Figure 3.1. 30-second Thule VLF, magnetometer, riometer, and 5577A photometer data: 1800 UT 29OCT73 - 1200 UT 30OCT73.

# ENERGETIC PARTICLE EVENT 21DEC73-22DEC73 THULE, GREENLAND

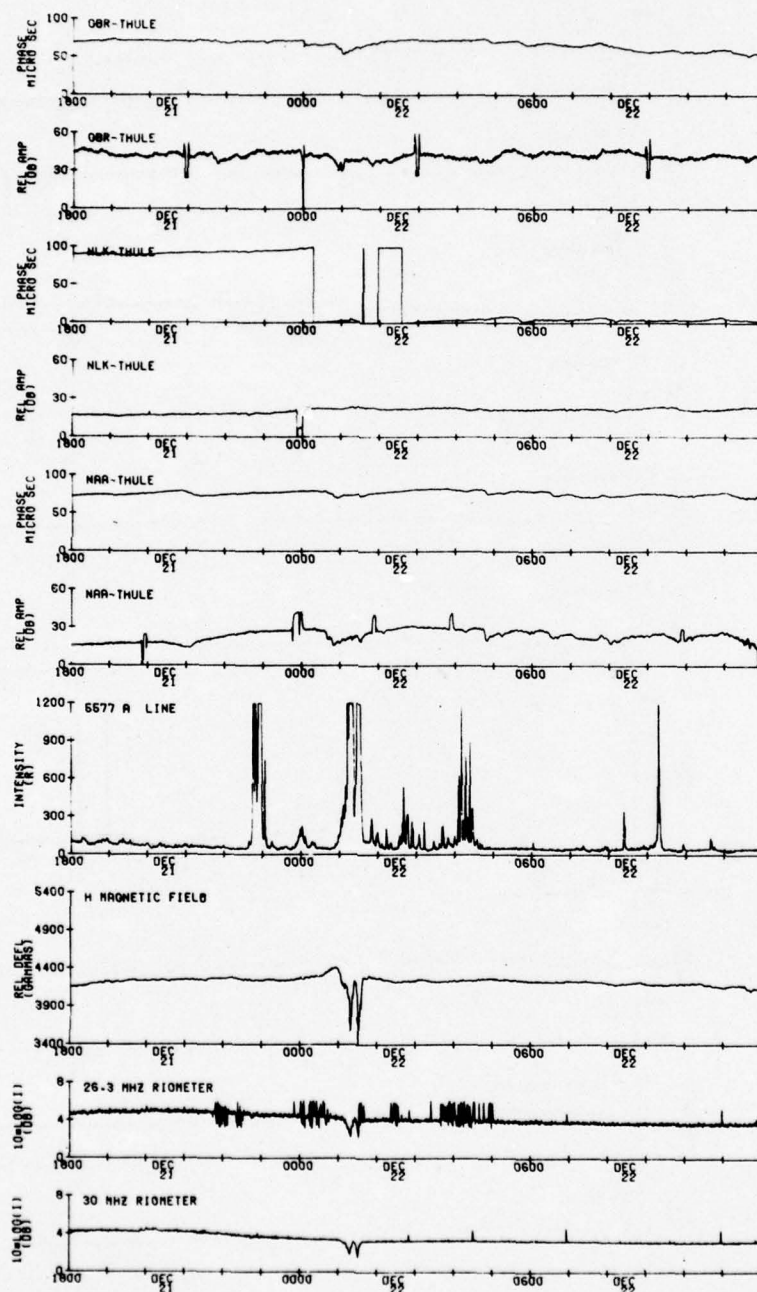


Figure 3.2. 30-second Thule VLF, magnetometer, riometer, and 5577A photometer data: 1800 UT 21DEC73 - 1200 UT 22DEC73.



# ENERGETIC PARTICLE EVENT 31DEC73-1JAN74 THULE, GREENLAND

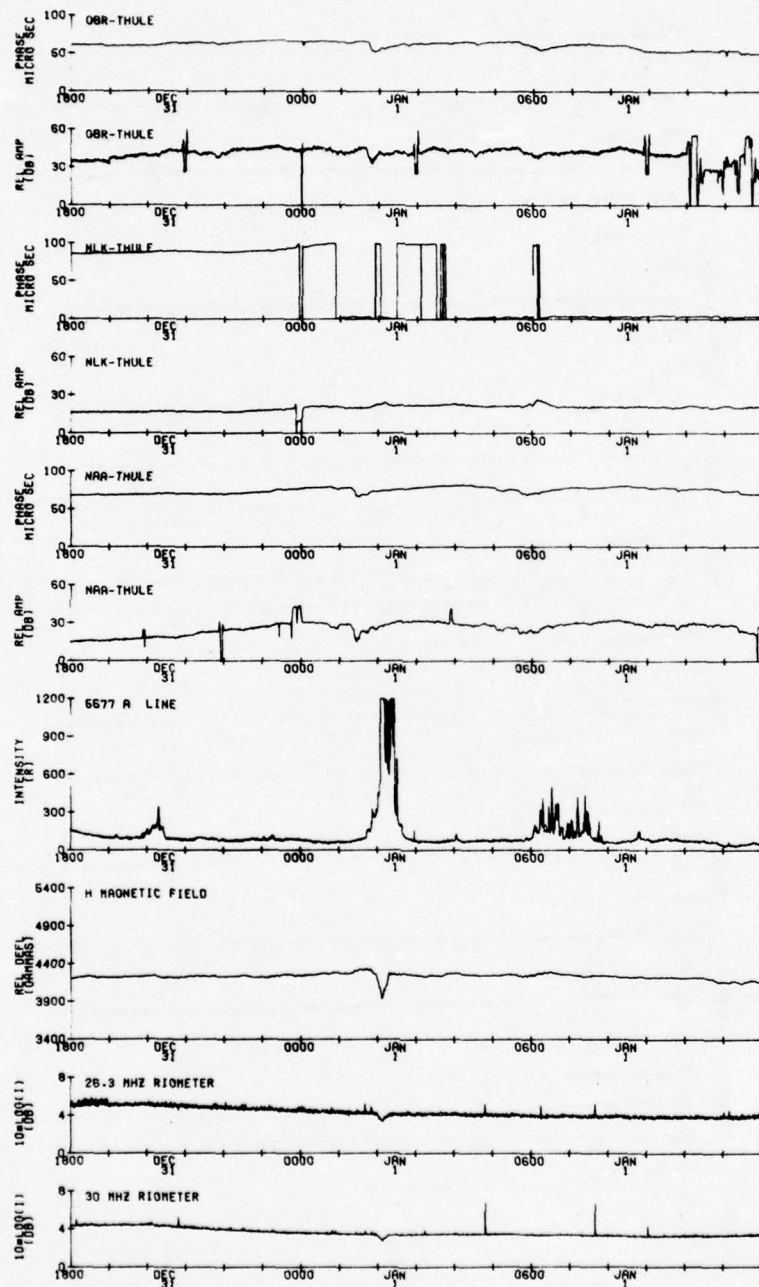


Figure 3.3. 30-second Thule VLF, magnetometer, riometer, and 5577A photometer data: 1800 UT 31DEC73 - 1200 UT 1JAN74.

# ENERGETIC PARTICLE EVENT 25JAN74-26JAN74 THULE, GREENLAND

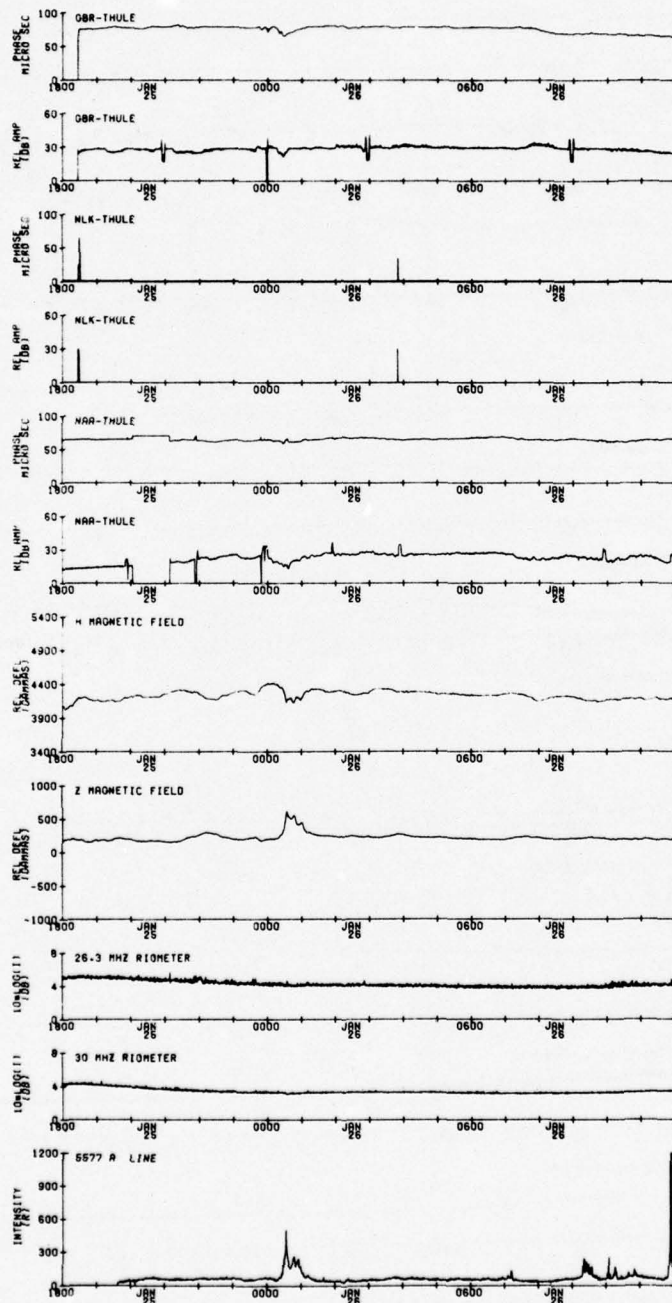


Figure 3.4. 30-second Thule VLF, magnetometer, riometer, and 5577A photometer data: 1800 UT 25JAN74 - 1200 UT 26JAN74.

ENERGETIC PARTICLE EVENT  
26JAN74-27JAN74  
THULE, GREENLAND

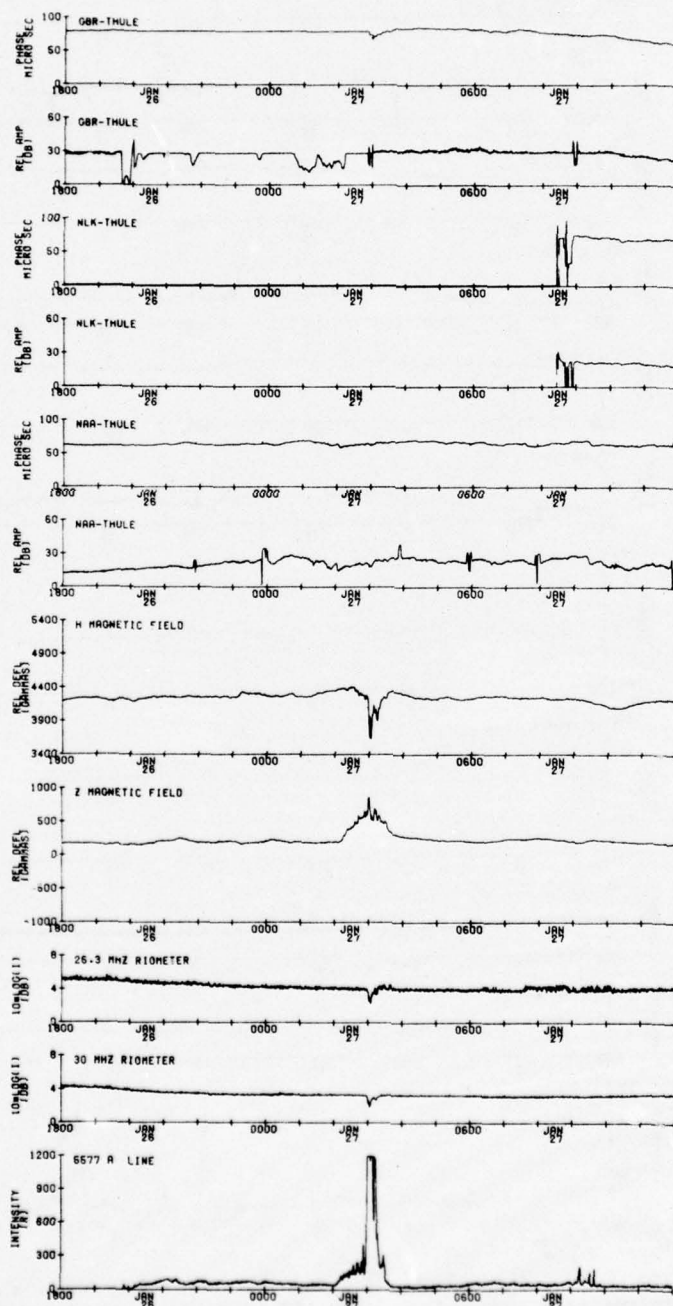


Figure 3.5. 30-second Thule VLF, magnetometer, riometer, and 5577Å photometer data: 1800 UT 26JAN74 - 1200 UT 27JAN74



ENERGETIC PARTICLE EVENT  
11FEB74-12FEB74  
THULE, GREENLAND

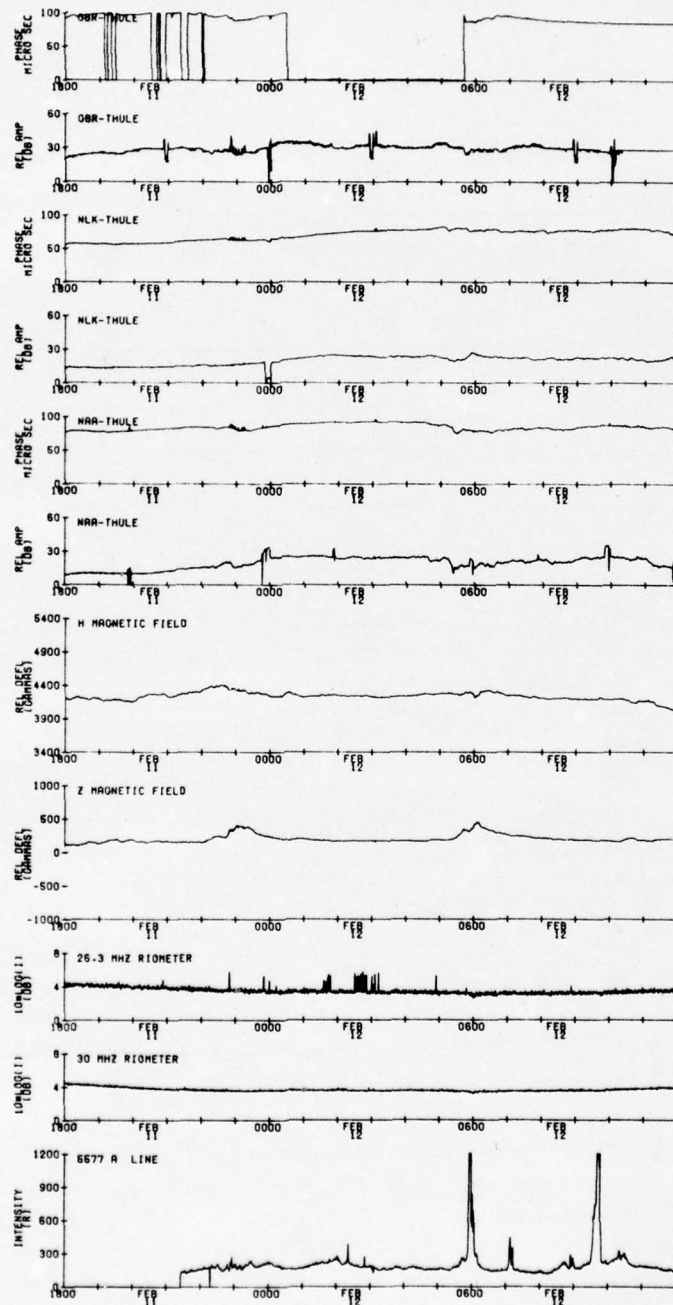


Figure 3.6. 30-second Thule VLF, magnetometer, riometer, and 5577A photometer data: 1800 UT 11FEB74 - 1200 UT 12FEB74.

ENERGETIC PARTICLE EVENT  
11 NOV 74-12 NOV 74  
THULE, GREENLAND

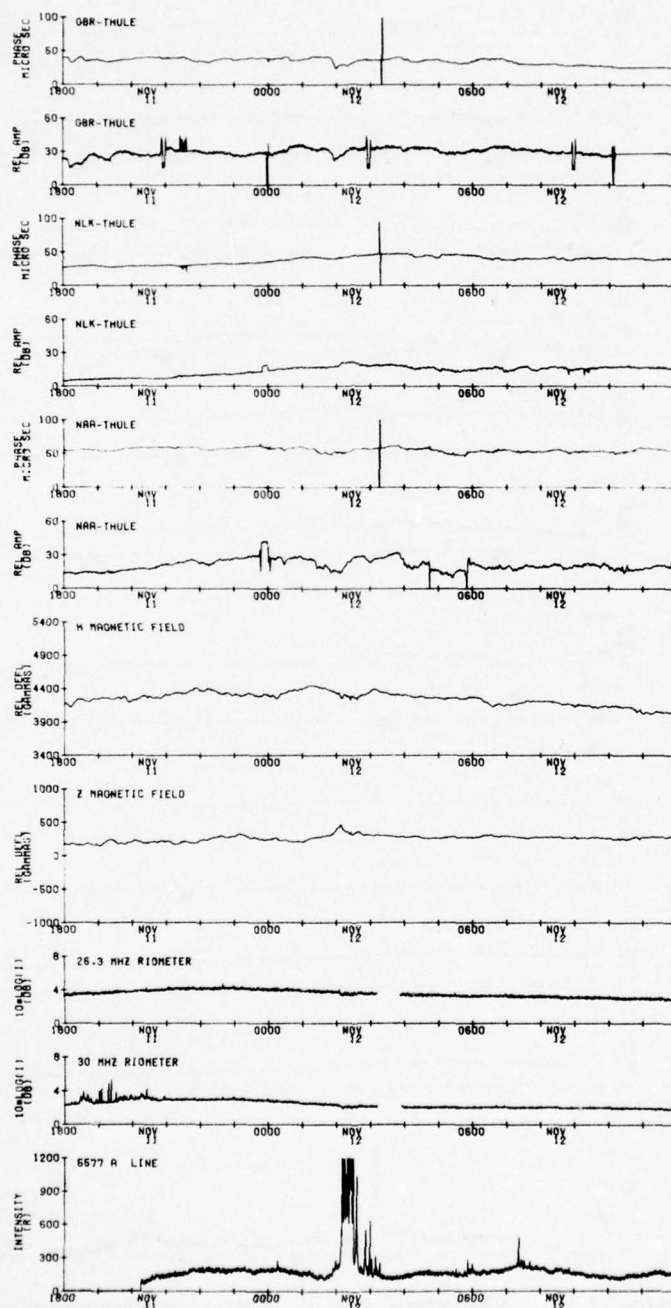


Figure 3.7. 30-second Thule VLF, magnetometer, riometer, and 5577A photometer data: 1800 UT 11NOV74 - 1200 UT 12NOV74.

# ENERGETIC PARTICLE EVENT 12NOV74-13NOV74 THULE, GREENLAND

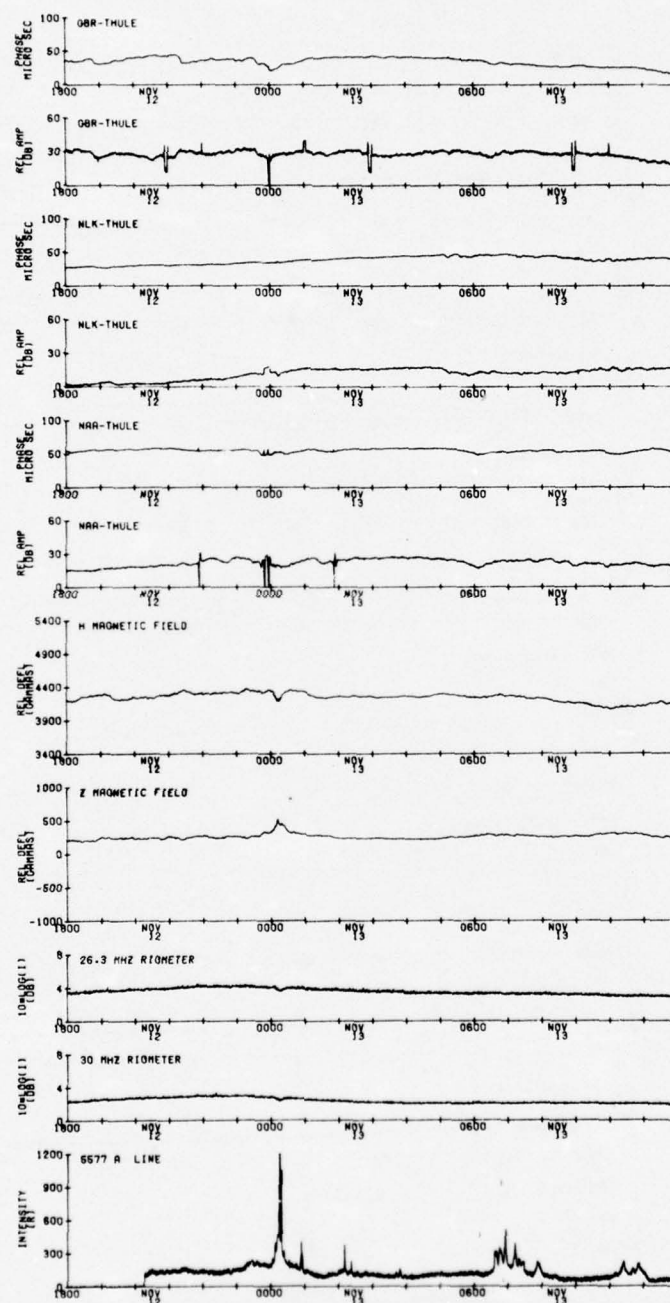


Figure 3.8. 30-second Thule VLF, magnetometer, riometer, and 5577Å photometer data: 1800 UT 12NOV74 - 1200 UT 13NOV74.



# ENERGETIC PARTICLE EVENT 13NOV74-14NOV74 THULE, GREENLAND

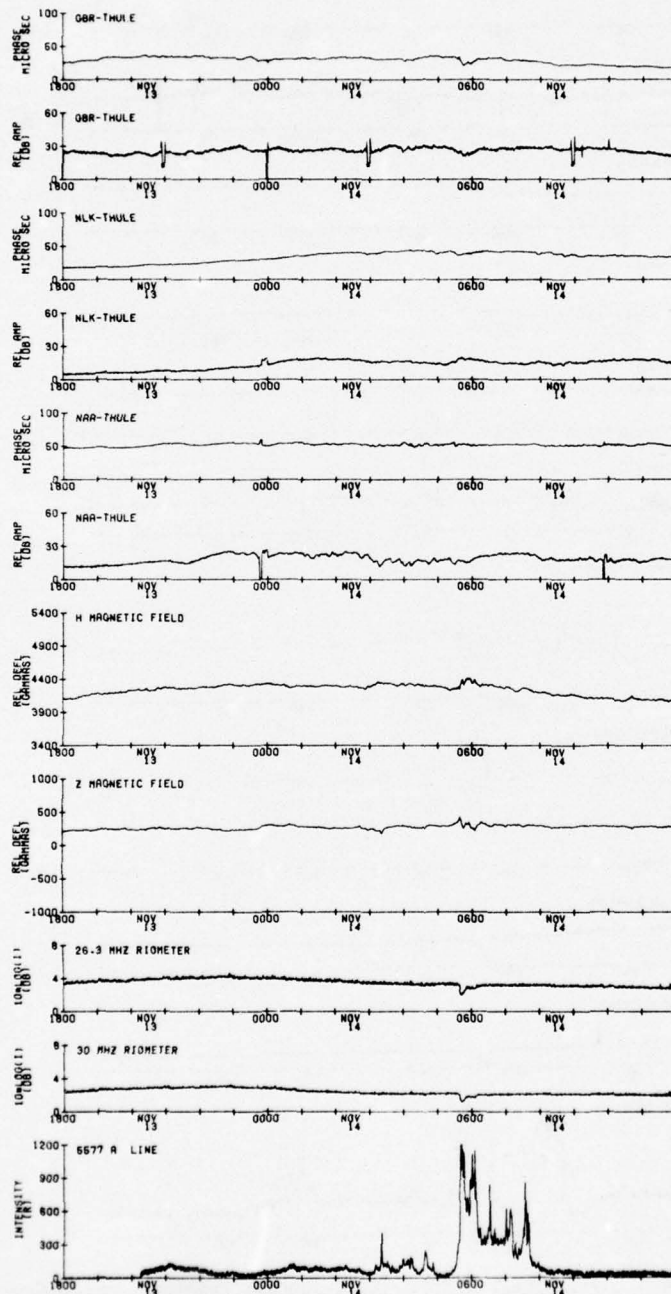


Figure 3.9. 30-second Thule VLF, magnetometer, riometer, and 5577A photometer data: 1800 UT 13NOV74 - 1200 UT 14NOV74.

ENERGETIC PARTICLE EVENT  
6 JAN 75 - 7 JAN 75  
THULE, GREENLAND

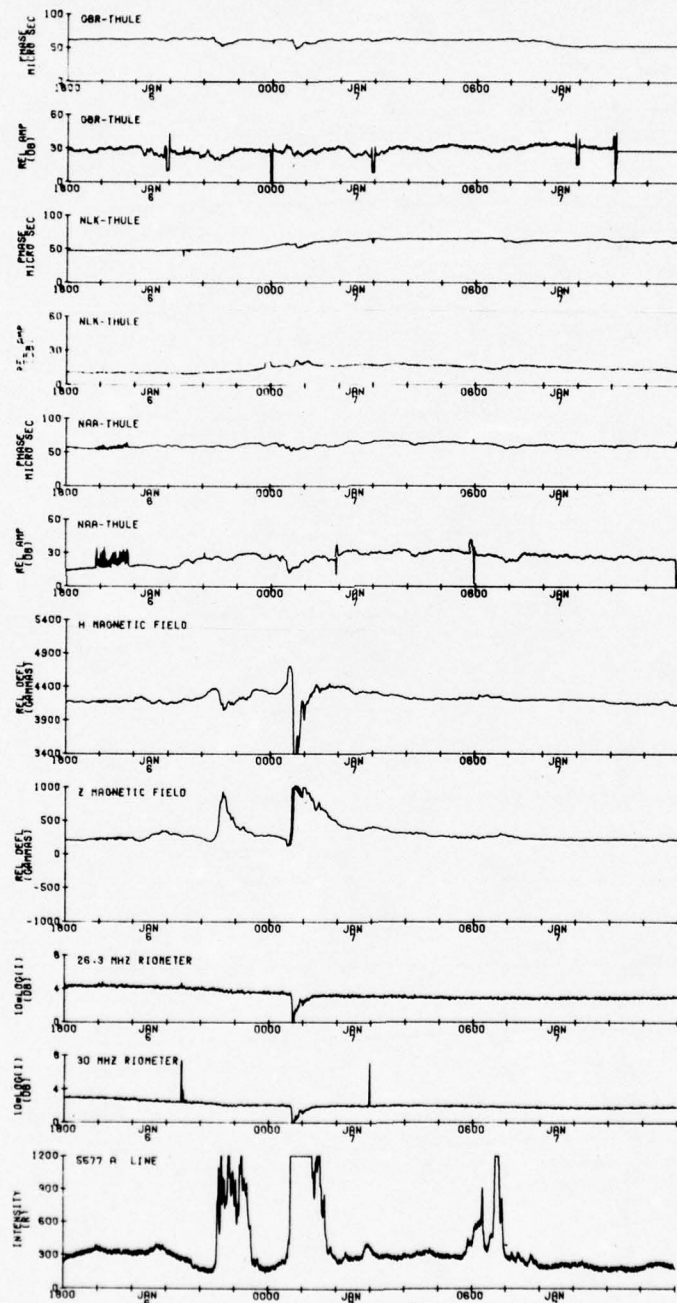


Figure 3.10. 30-second Thule VLF, magnetometer, riometer, and 5577 Å photometer data: 1800 UT 6 JAN 75 - 1200 UT 7 JAN 75.

# ENERGETIC PARTICLE EVENT 17JAN75-18JAN75 THULE, GREENLAND

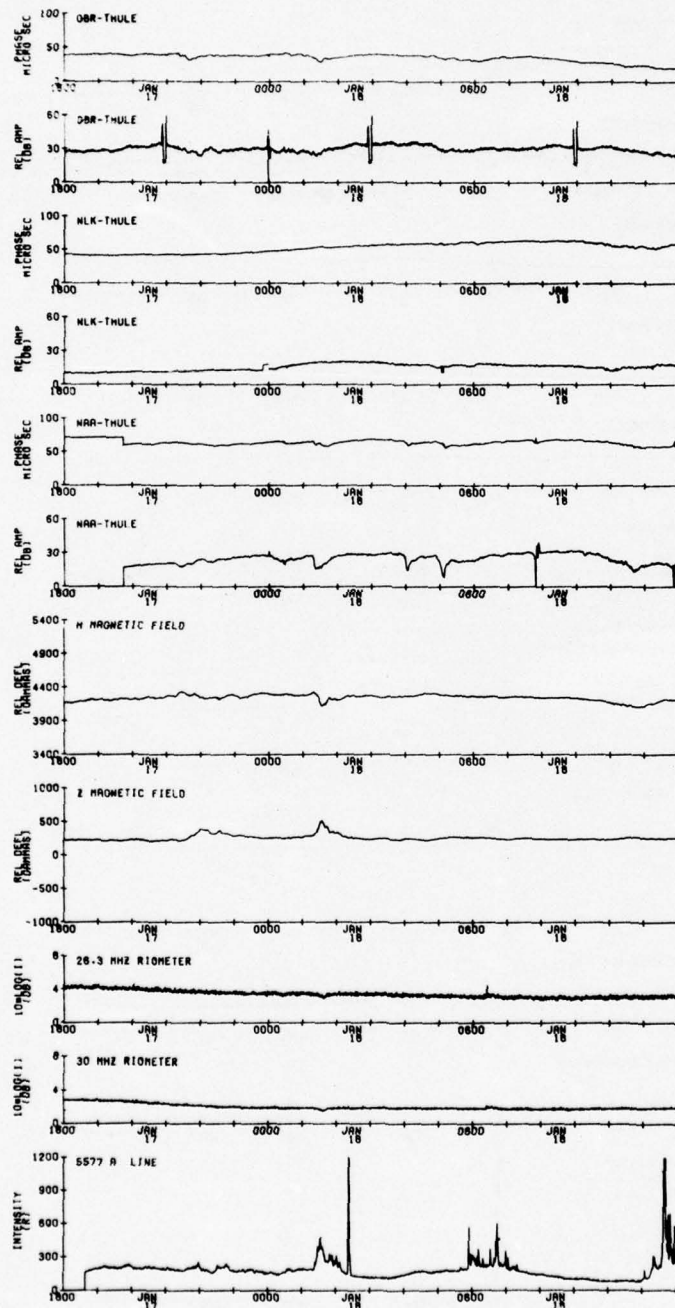


Figure 3.11. 30-second Thule VLF, magnetometer, riometer, and 5577Å photometer data: 1800 UT 17JAN75 - 1200 UT 18JAN75.



# ENERGETIC PARTICLE EVENT 1FEB75-2FEB75 THULE, GREENLAND

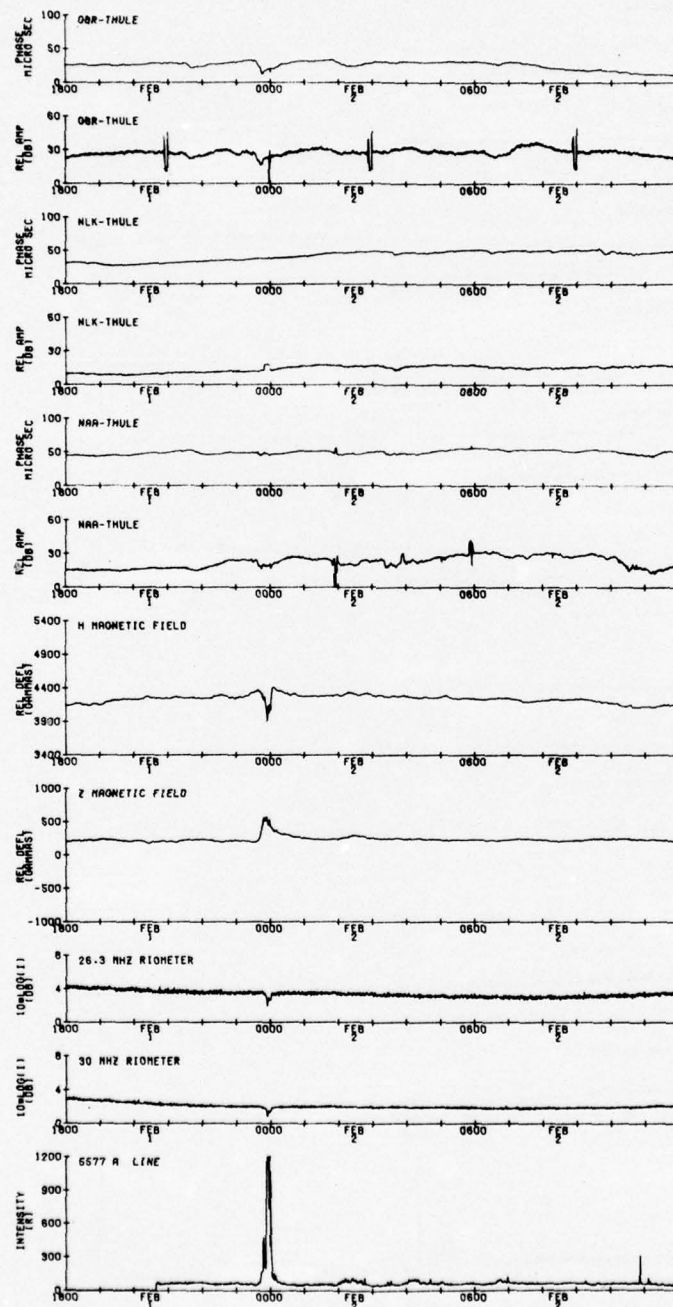


Figure 3.12. 30-second Thule VLF, magnetometer, riometer, and 5577A photometer data: 1800 UT 1FEB75 - 1200 UT 2FEB75.

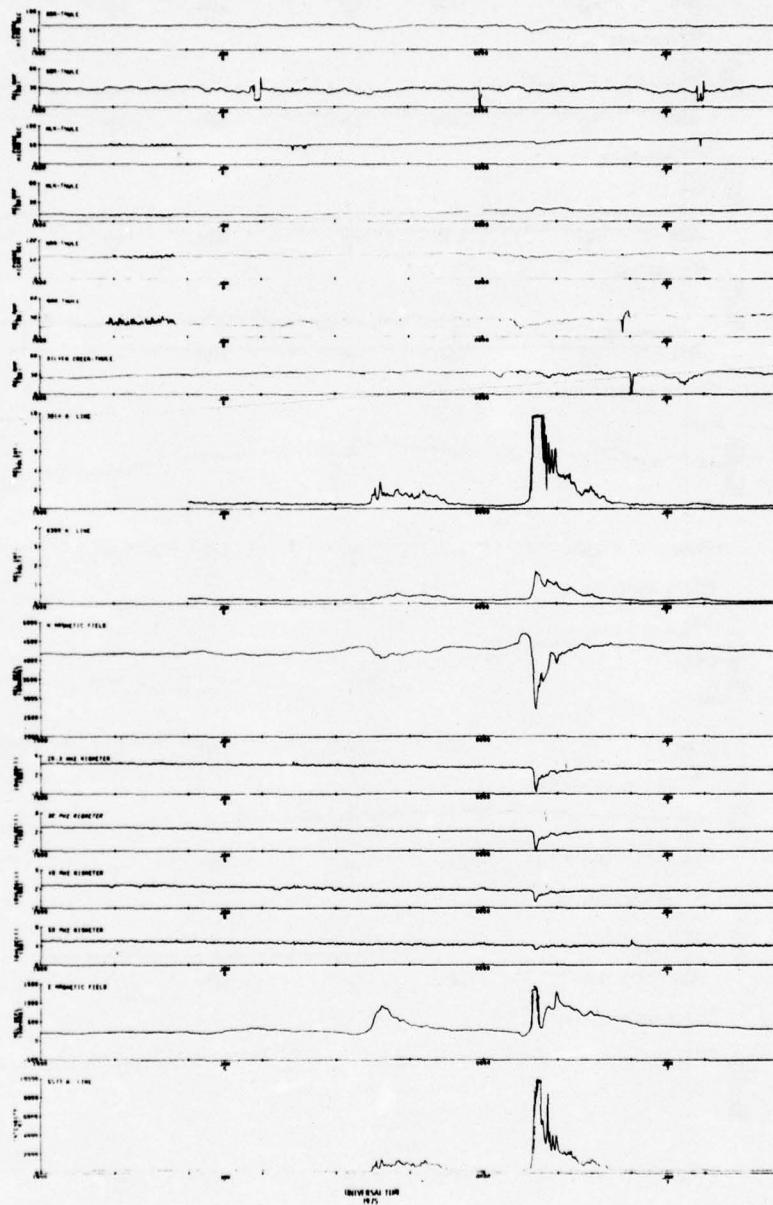


Figure 3.13. 30-second Thule VLF, magnetometer, riometer, and 5577Å photometer data: 1800 UT 6JAN75 - 0400 UT 7JAN75.

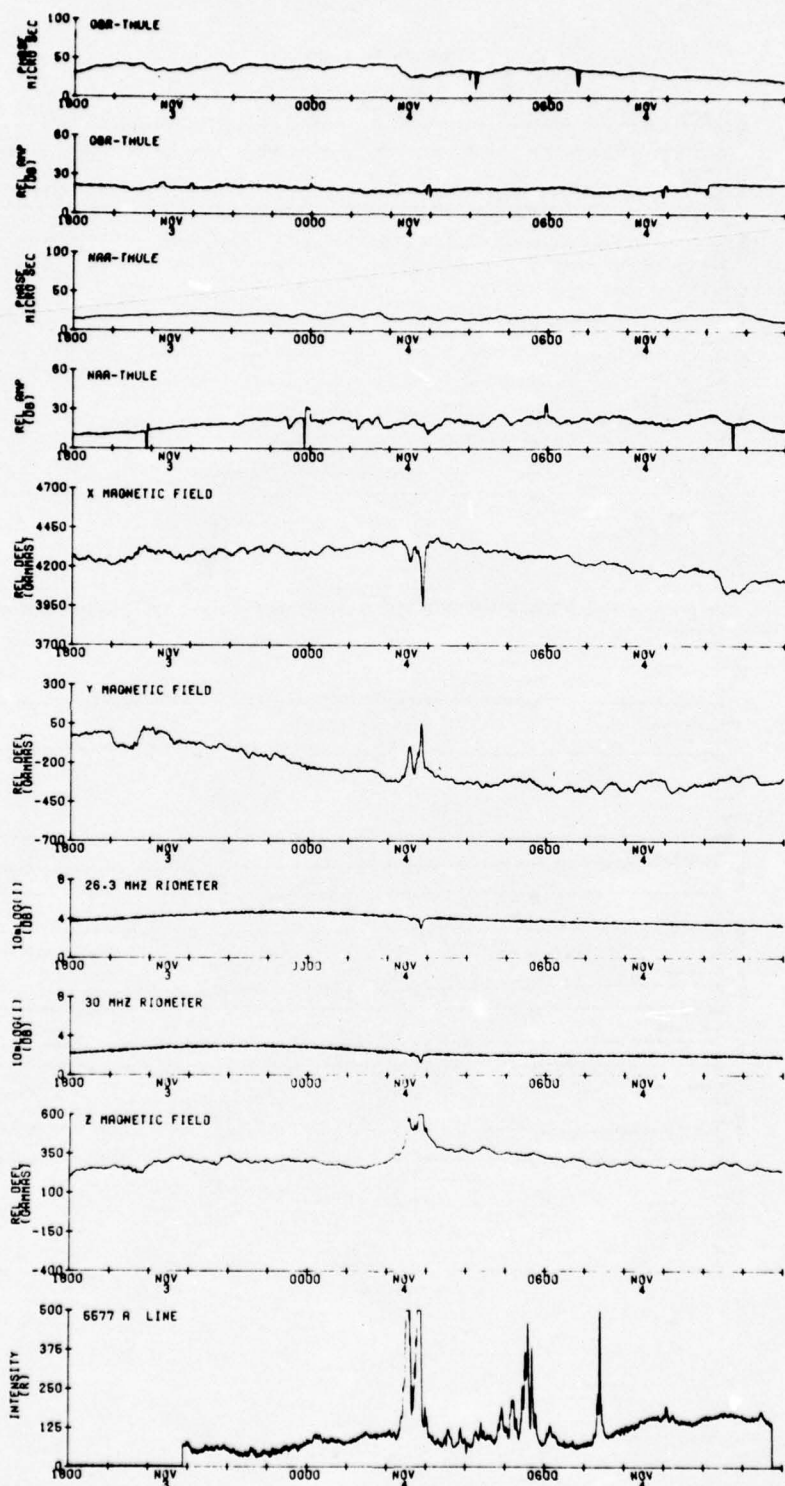


Figure 3.14. 30-second Thule VLF, magnetometer, riometer, and 5577Å photometer data: 1800 UT 3Nov75 - 1200 UT 4Nov75.



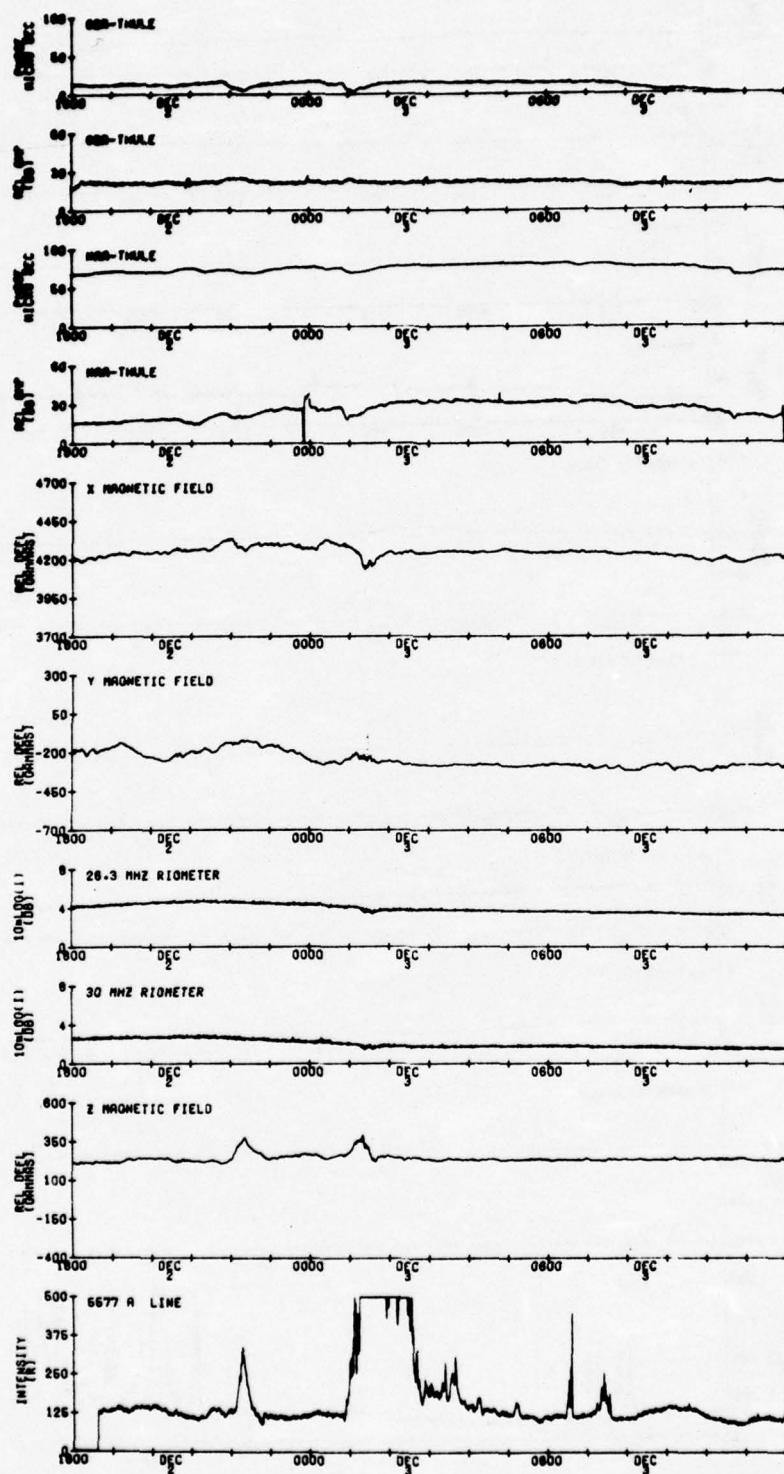


Figure 3.15. 30-second Thule VLF, magnetometer, riometer, and 5577Å photometer data: 1800 UT 2Dec75 - 1200 UT 3Dec75.

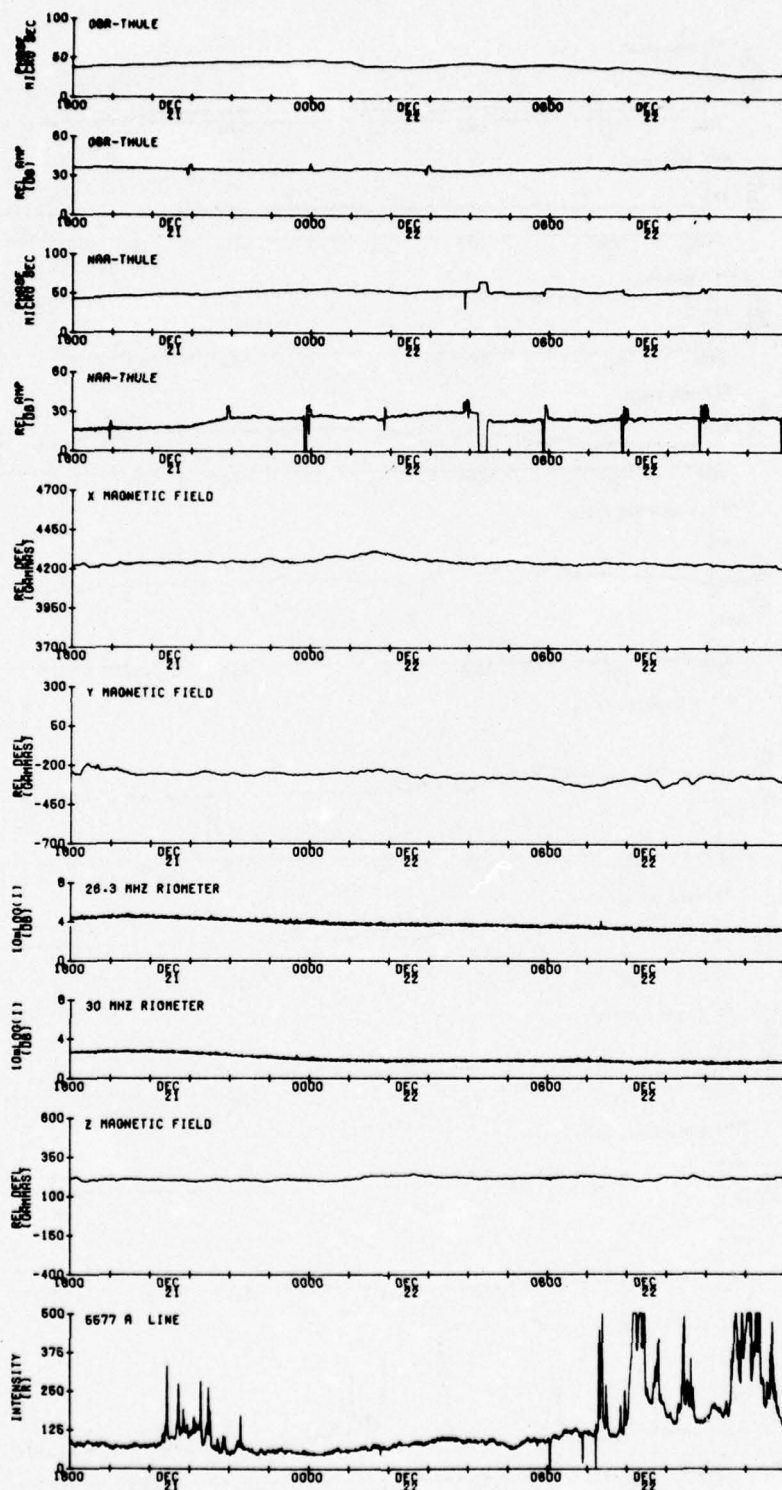


Figure 3.16. 30-second Thule VLF, magnetometer, riometer, and 5577A photometer data: 1800 UT 21Dec75 - 1200 UT 22Dec75.

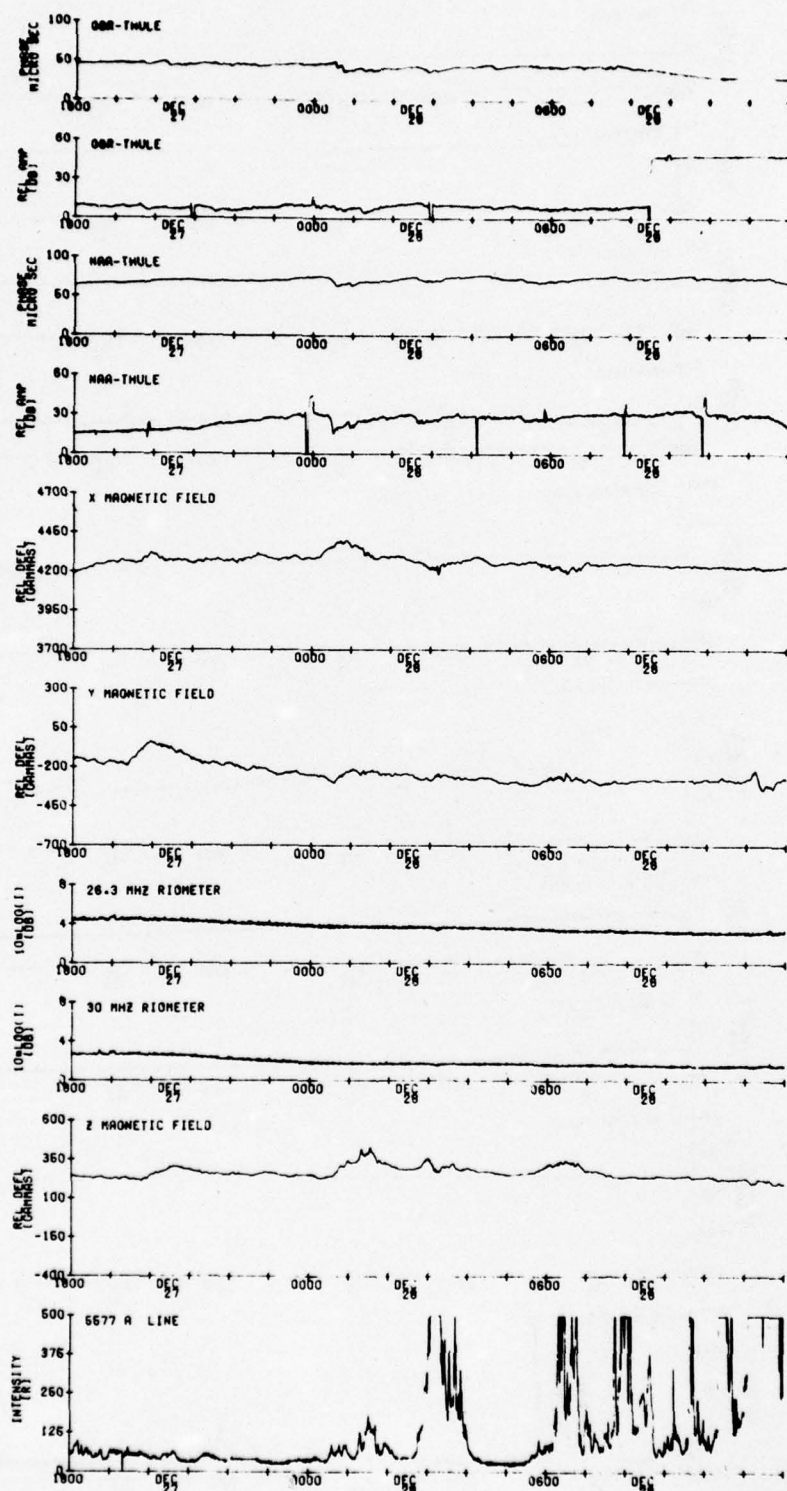


Figure 3.17. 30-second Thule VLF, magnetometer, riometer, and 5577Å photometer data: 1800 UT 27Dec75 - 1200 UT 28Dec75.



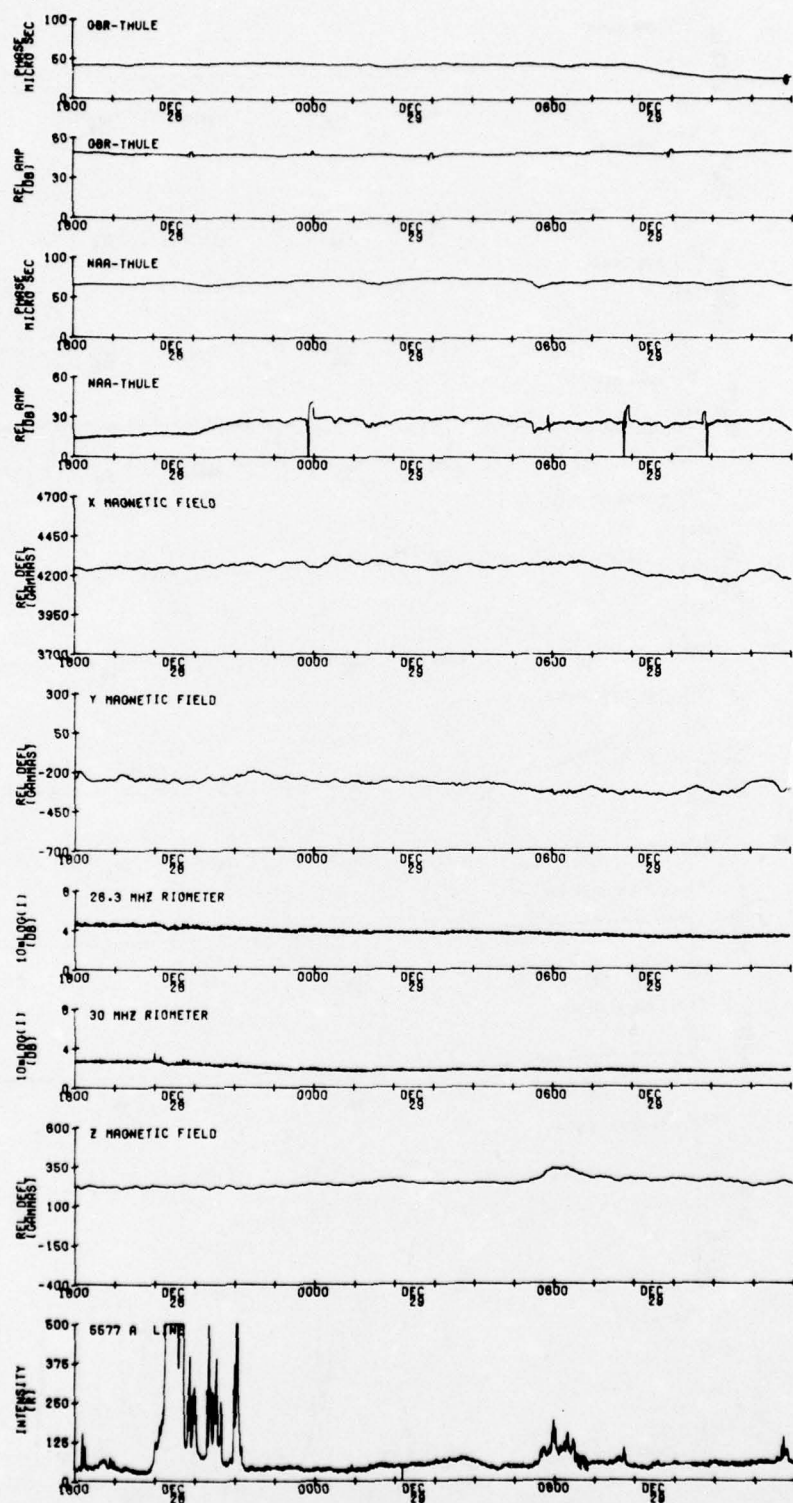


Figure 3.18. 30-second Thule VLF, magnetometer, riometer, and 5577Å photometer data: 1800 UT 28Dec75 - 1200 UT 29Dec75.

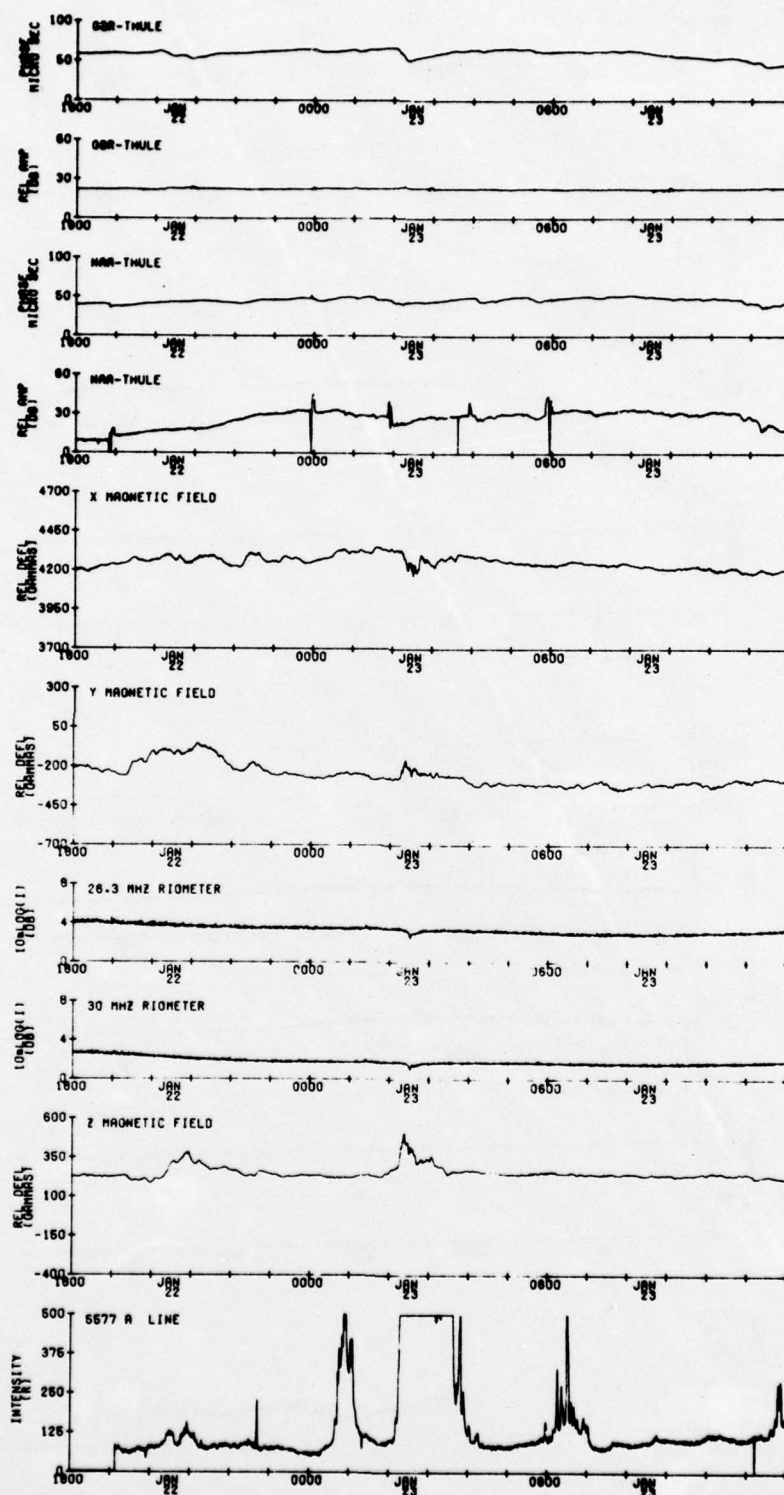


Figure 3.19. 30-second Thule VLF, magnetometer, riometer, and 5577Å photometer data: 1800 UT 22Jan76 - 1200 UT 23Jan76.

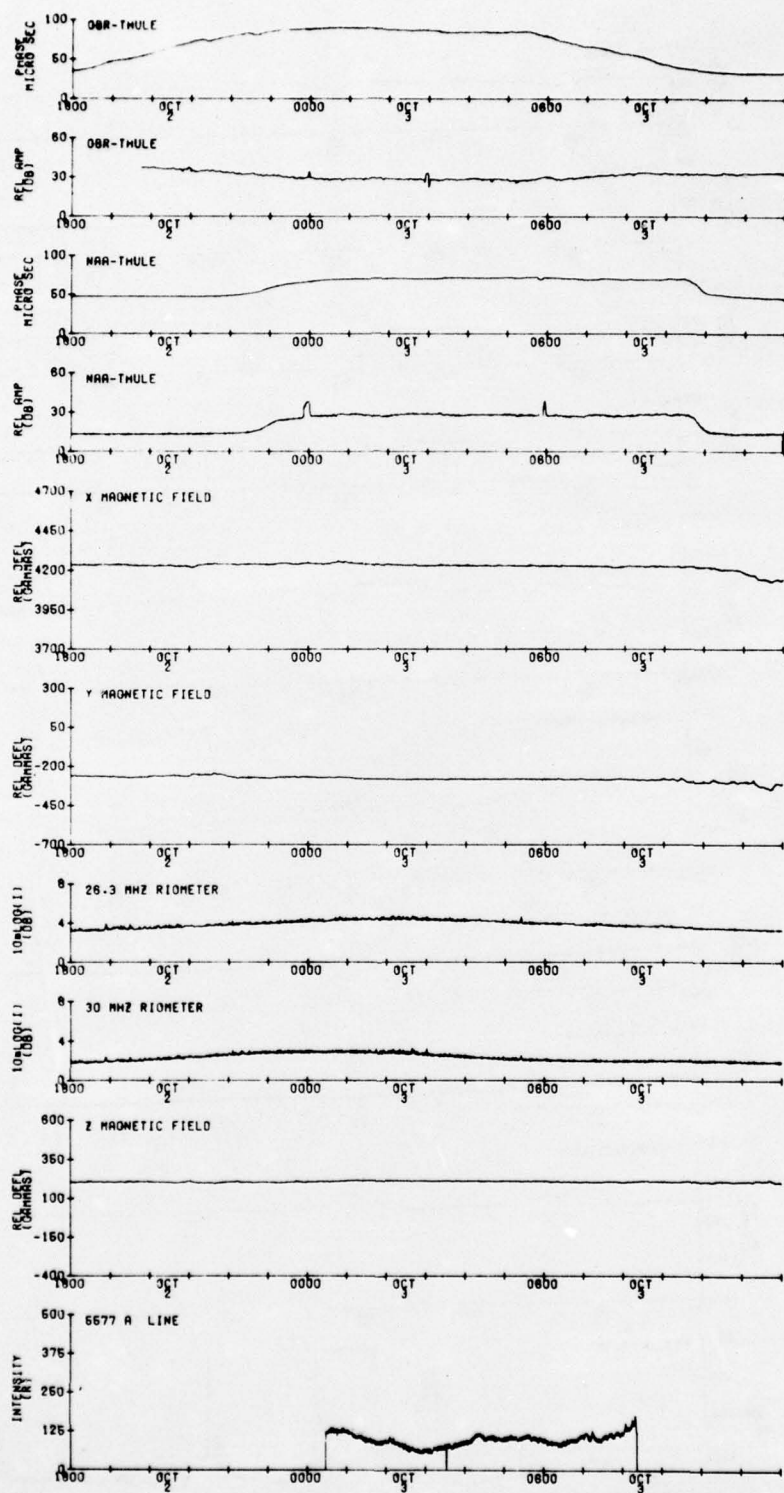


Figure 3.20. 30-second Thule VLF, magnetometer, riometer, and 5577Å photometer data: 1800 UT 20Oct75 - 1200 UT 30Oct75.



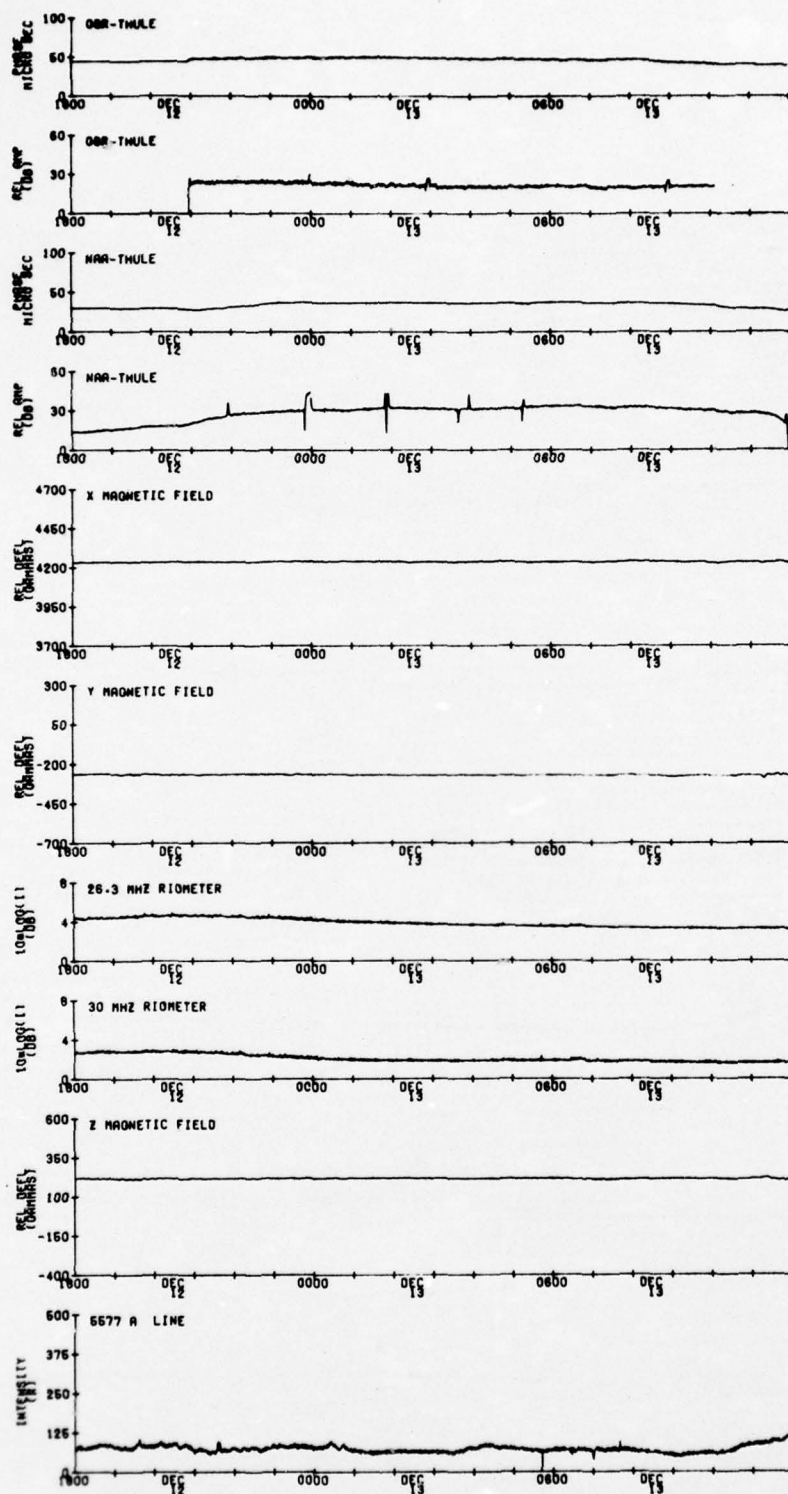


Figure 3.21. 30-second Thule VLF, magnetometer, riometer, and 5577 Å photometer data: 1800 UT 12Dec75 - 1200 UT 13Dec75.

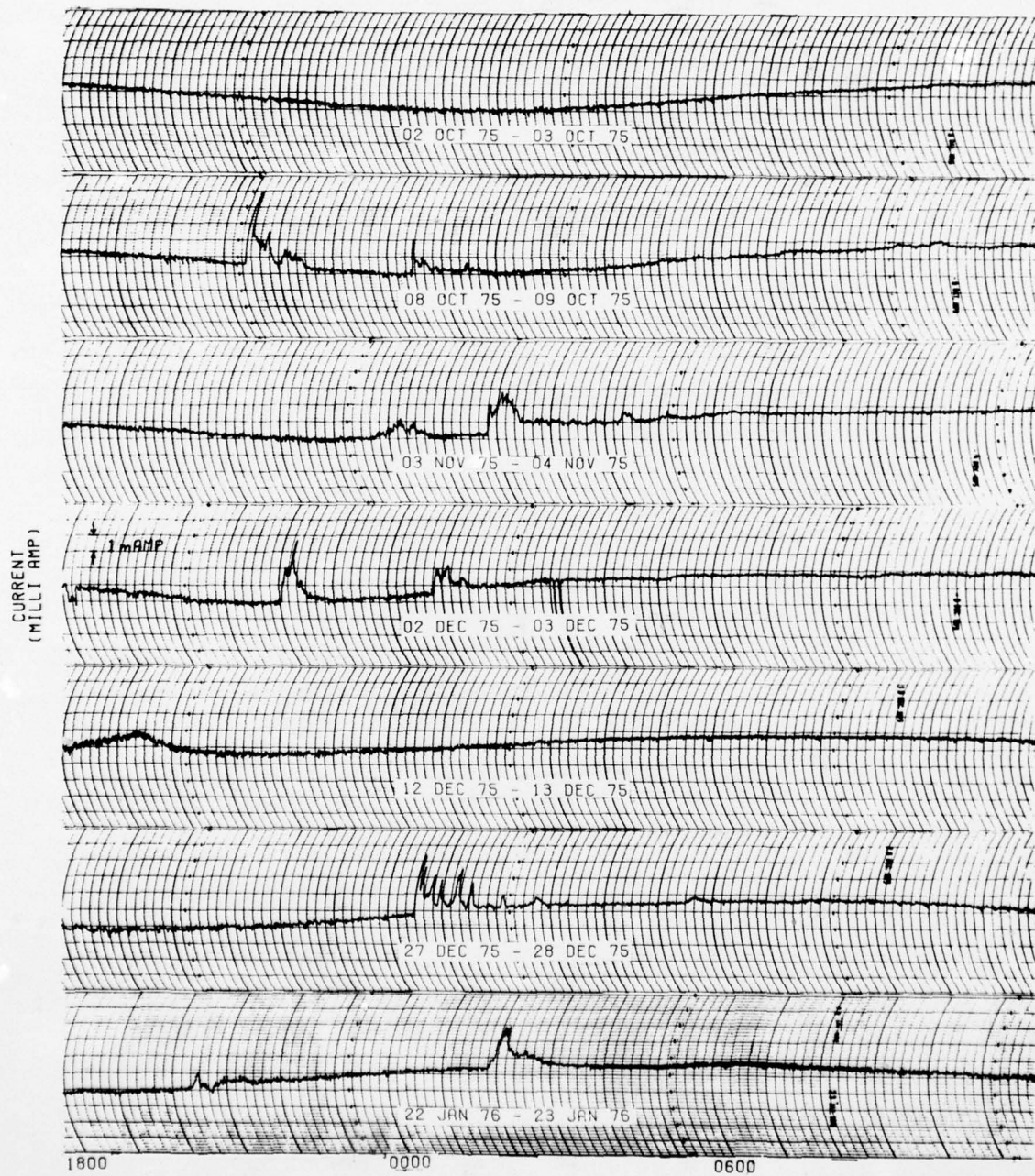


Figure 3.22. Godhavn 30MHz Riometer Charts, 1800 UT - 1200 UT.

FIGURES IN SECTION 4



# MAGNETIC DISTURBANCE 13FEB74-14FEB74 THULE, GREENLAND

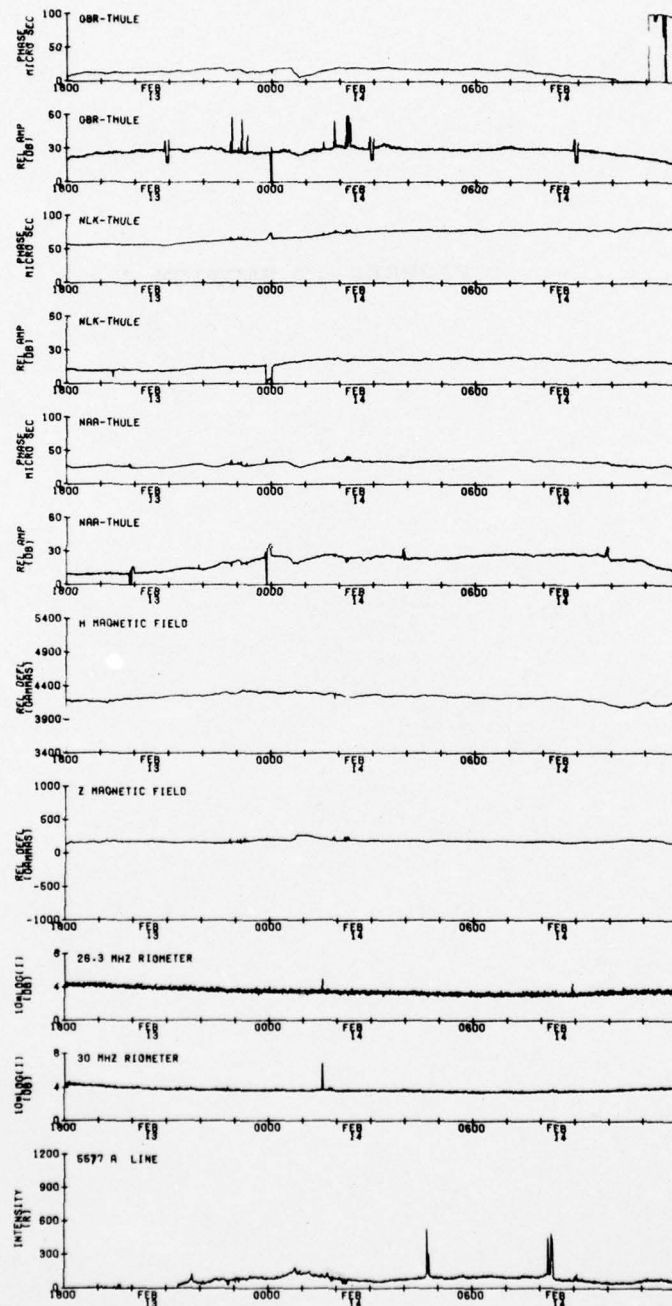


Figure 4.1. 30-second Thule VLF, magnetometer, riometer, and 5577A photometer data: 1800 UT 13FEB75 - 1200 UT 14FEB75.

# MAGNETIC DISTURBANCE 23FEB74-24FEB74 THULE, GREENLAND

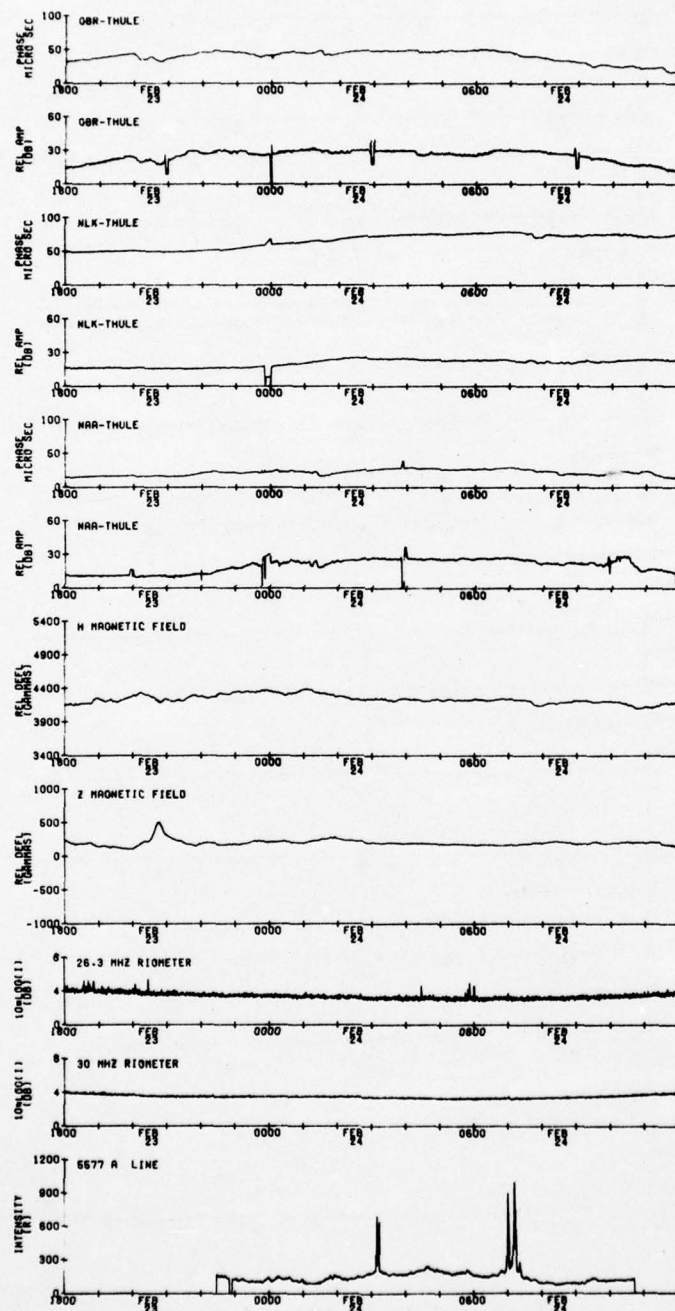


Figure 4.2. 30-second Thule VLF, magnetometer, riometer, and 5577 Å photometer data: 1800 UT 23FEB75 - 1200 UT 24FEB75.

# MAGNETIC DISTURBANCE 24NOV74-25NOV74 THULE, GREENLAND

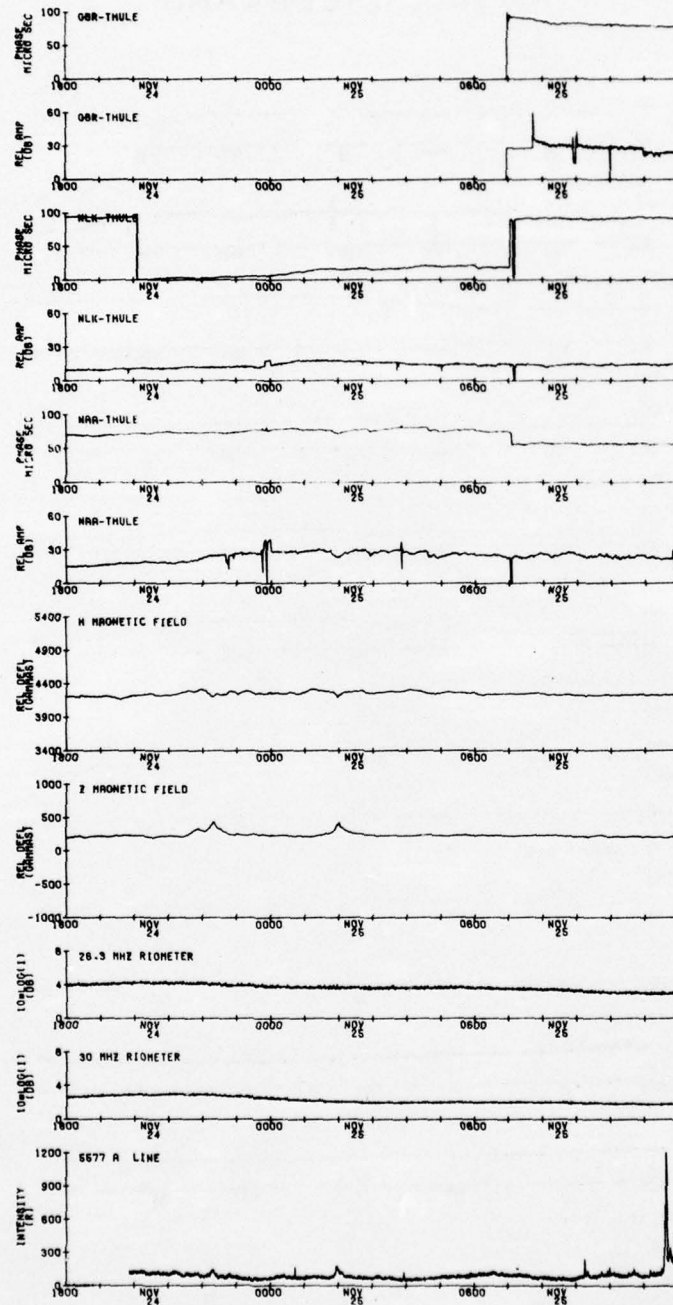


Figure 4.3. 30-second Thule VLF, magnetometer, riometer, and 5577Å photometer data: 1800 UT 24NOV74 - 1200 UT 25NOV74.



# MAGNETIC DISTURBANCE 9DEC 74 - 10DEC 74 THULE, GREENLAND

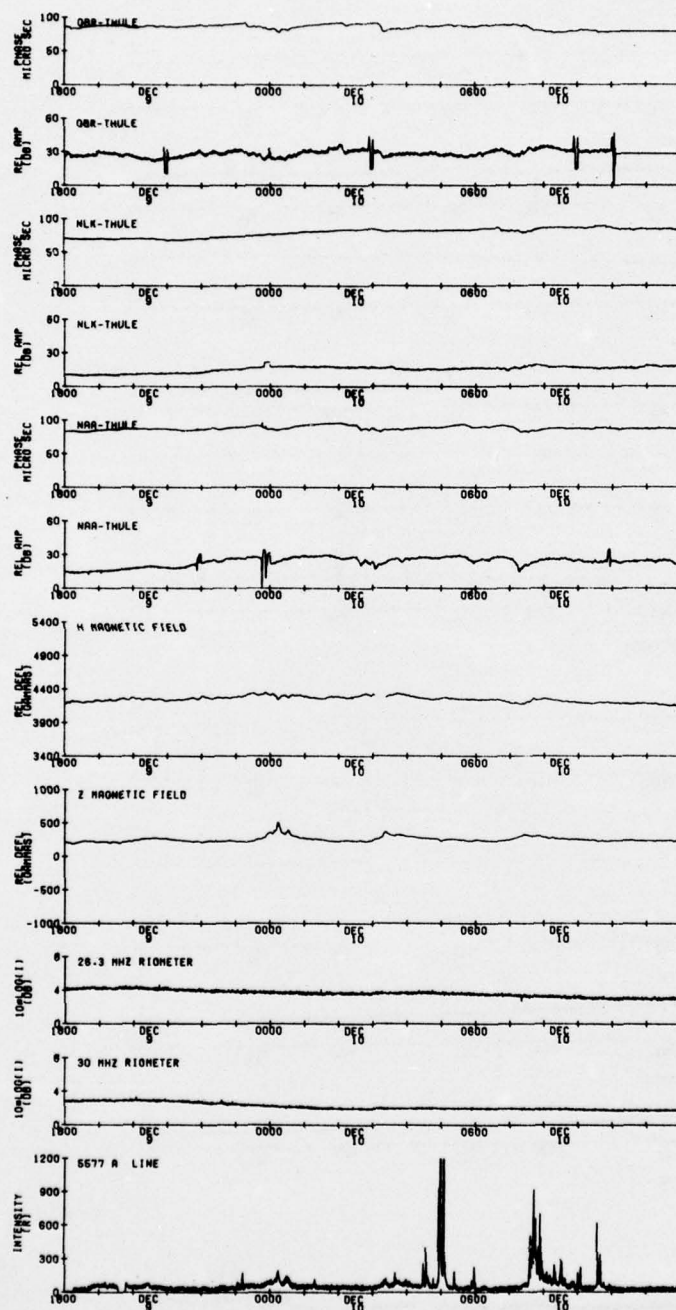


Figure 4.4. 30-second Thule VLF, magnetometer, riometer, and 5577Å photometer data: 1800 UT 9DEC74 - 1200 UT 10DEC74.

# MAGNETIC DISTURBANCE 20DEC 74-21DEC 74 THULE, GREENLAND

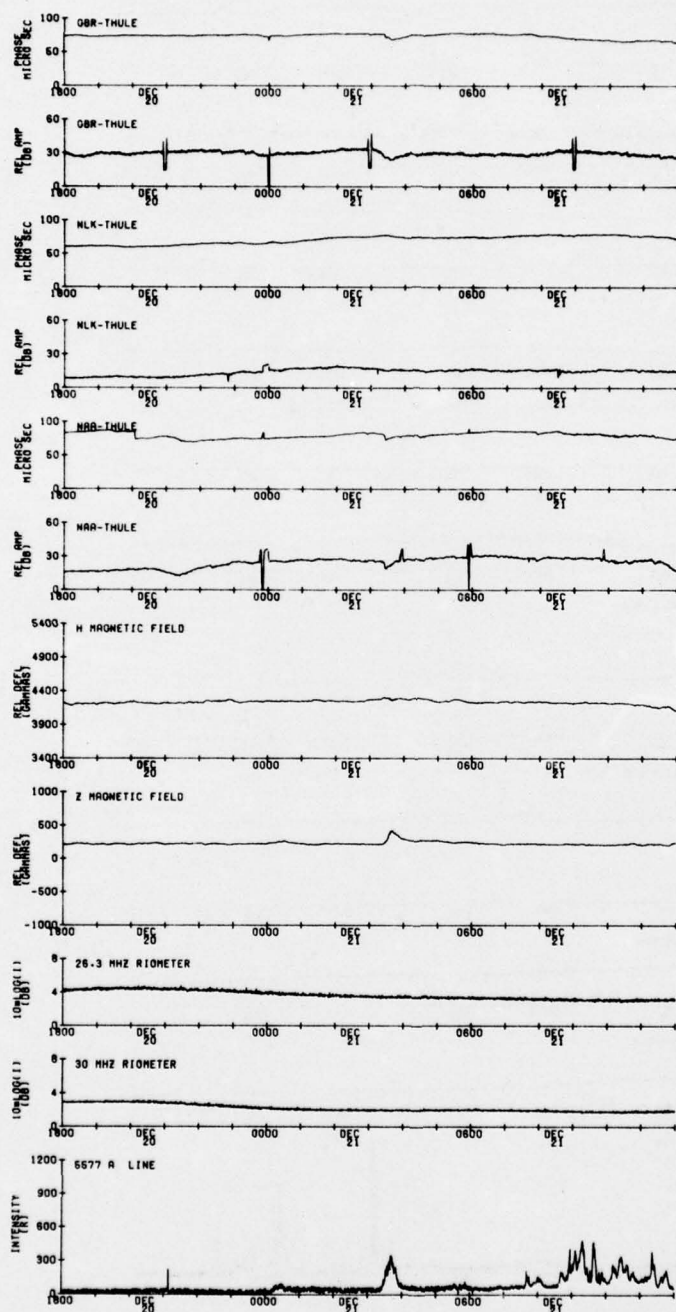


Figure 4.5. 30-second Thule VLF, magnetometer, riometer, and 5577A photometer data: 1800 UT 20DEC74 - 1200 UT 21DEC74.

MAGNETIC DISTURBANCE  
21 DEC 74 - 22 DEC 74  
THULE, GREENLAND

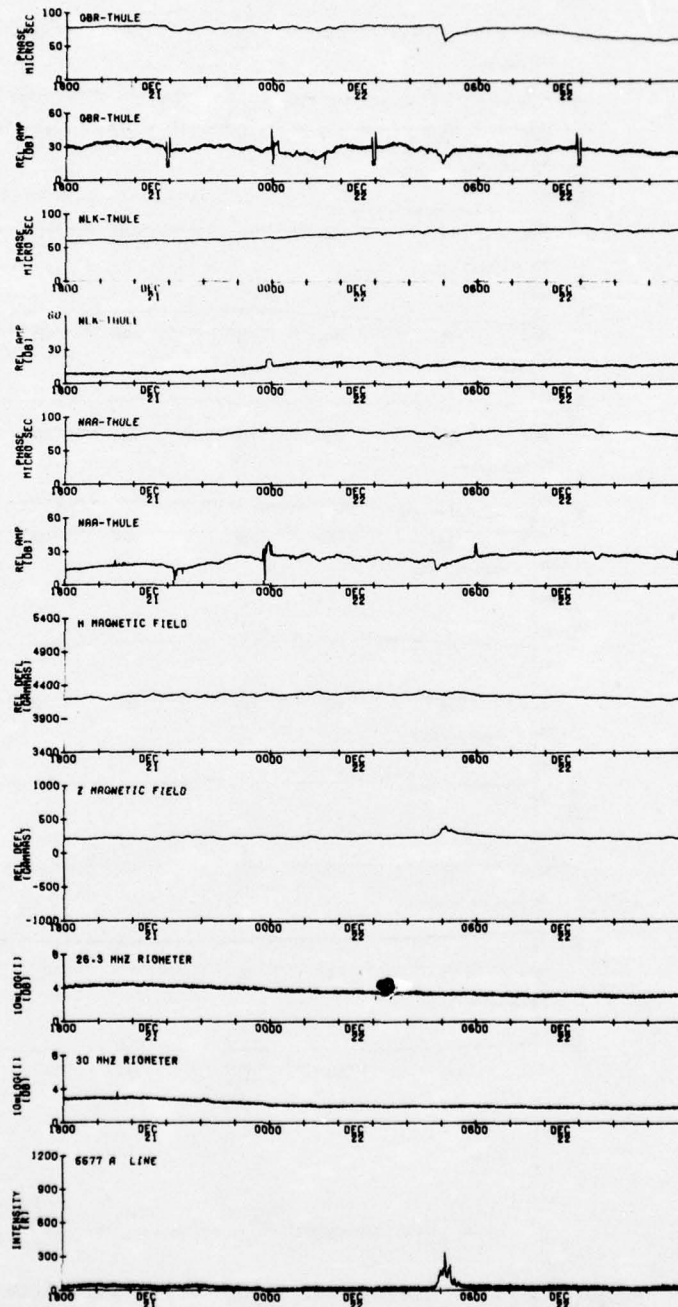


Figure 4.6. 30-second Thule VLF, magnetometer, riometer, and 5578 Å photometer data: 1800 UT 21DEC74 - 1200 UT 22DEC74.



# MAGNETIC DISTURBANCE 10FEB75 - 11FEB75 THULE, GREENLAND

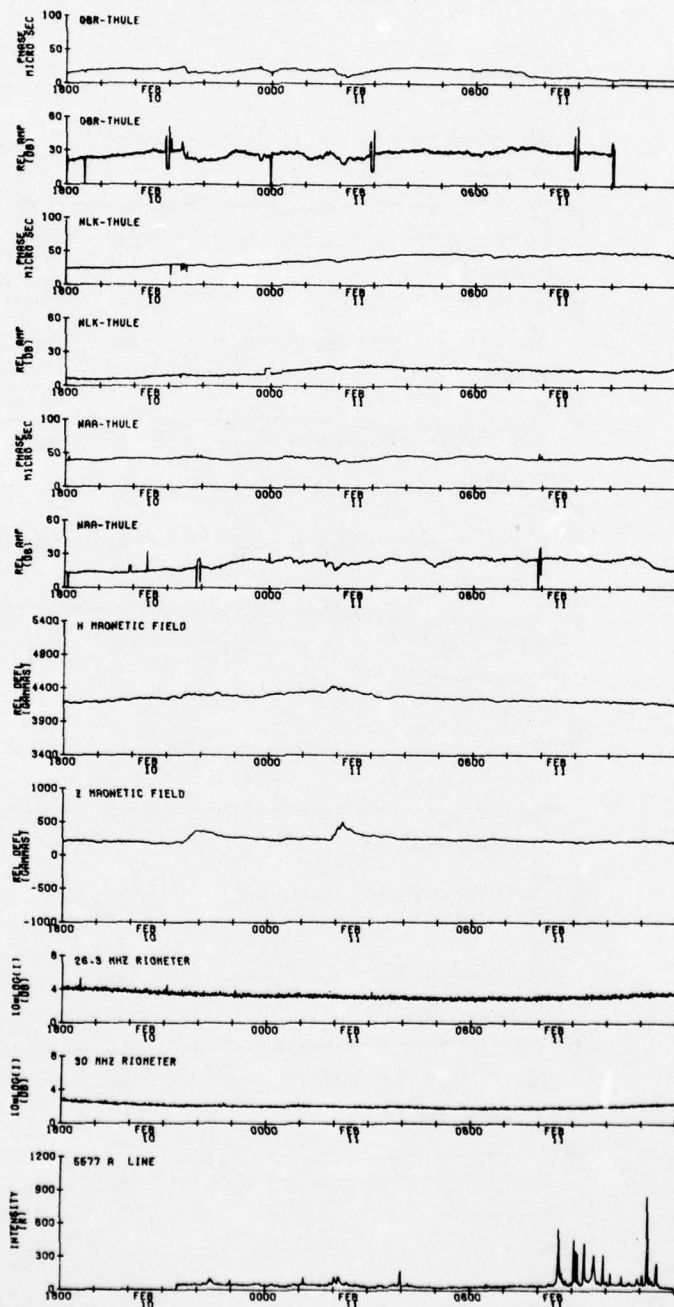


Figure 4.7. 30-second Thule VLF, magnetometer, riometer, and 5577Å photometer data: 1800 UT 10FEB75 -1200 UT 11FEB75.

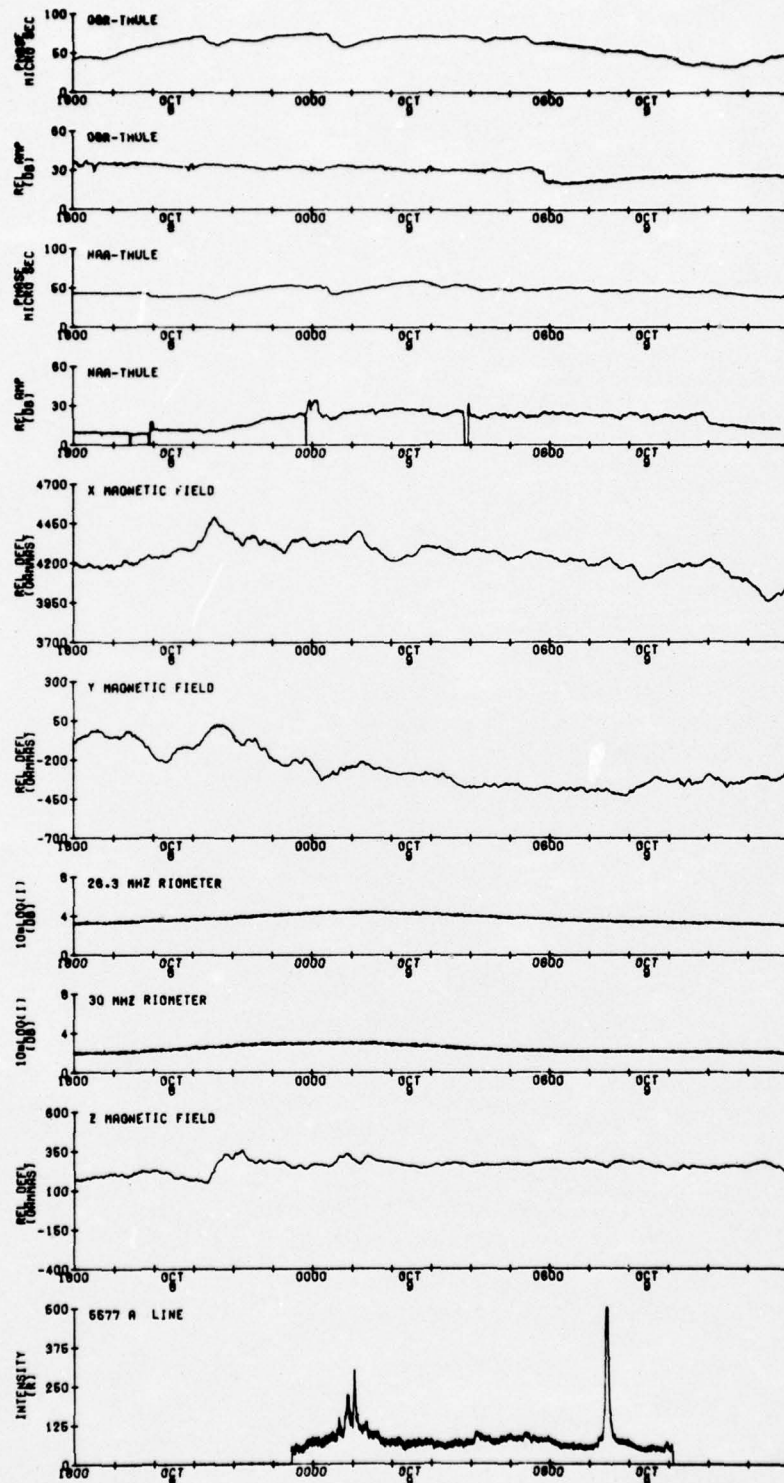


Figure 4.8. 30-second Thule VLF, magnetometer, riometer, and 5577Å photometer data: 1800 UT 8Oct75 - 1200 UT 9Oct75.